3. RESULTS AND DISCUSSION

SECTION (A)

The effect of some crown ethers on the corrosion rate of some types of stainless steel in 2M hydrochloric acid solution at different temperatures was investigated using weight loss method. The selected crown ethers are DB18C6, Kry-22DD, Kry-222 and DB24C8 while, the selected stainless steels are 430SS, 304SS and 316SS types. In the previous section, the effect of crown ethers concentrations on the corrosion rate was studied. The degree of surface coverage and percentage inhibition values were calculated. Different expressions of adsorption isotherms were applied to fit the type of adsorption isotherm. Moreover, the effect of temperature on the corrosion rate was studied and the thermodynamic parameters of activation were calculated and discussed.

3.1 Loss in mass technique.

3.1.1 Effect of crown ethers concentration on loss in mass values.

The corrosion behavior of a metal in an aqueous environment is characterized by the extent to which it dissolves in the solution. This can be quantified by using the simple relationship: [13-18]

$$\text{loss in mass } (\text{mg.cm}^{-2}) = \frac{M_B - M_A}{A} \qquad (3.1)$$

where, M_B: mass of metal before exposure to the corrosive solution (mg.).

M_A: mass of metal after exposure to the corrosive solution (mg.).

A : exposed surface area (cm^2).

The degree of dissolution, of course, is dependent on the surface area of the metal exposed and the time of exposure; hence the extent of corrosion is given with respect to area and time. The resulting quantity, corrosion rate, is thus a fundamental measurement in corrosion science. Corrosion rates can be evaluated by measuring either the concentration of the dissolved metal in solution by chemical analysis or by measuring weight of a specimen before and after exposure and applying equation (3.1). The later is the most common

method. The loss in mass technique is usually preferred because the quantity measured is directly related to the extent of corrosion and does not rely on any assumptions about reactions occurring during corrosion.

Figs. (3.1-3.12) represent the mass loss-time curves of different types of stainless steel (430, 304 and 316) in 2M HCl in absence and presence of different concentrations (ranging from $1x10^{-7}$ M to $1.1x10^{-6}$ M) of crown ethers (DB18C6, Kry-22DD, Kry-222 and DB24C8) at 303K. It is seen from all these figures that, by increasing the concentration of these compounds, the loss in mass values of different types of stainless steel were decreased. This means that the presence of these compounds retards the corrosion of these types of stainless steel in 2M HCl or in other words, these compounds act as corrosion inhibitors.

The linear variations of mass loss values with time in most cases of inhibited stainless steels (430, 304 and 316) in 2M HCl indicate the absence of insoluble surface films during corrosion [123]. In absence of any surface films, the inhibitors are first adsorbed on the metal surface and thereafter impede corrosion either by merely blocking the reaction sites (anodic and cathodic) or by altering the mechanism of the anodic and cathodic partial processes.

The dissolution of the three types of stainless steel on using these inhibitors might be interpreted on the basis of the interface inhibition mode [160], i.e., the inhibitors are effectively acting at the metal-solution interface. On using dilute solutions of crown ethers (ranging from $1x10^{-7}$ M to $1.1x10^{-6}$ M) in 2M HCl, an effective dimension of corrosion by the formation of an adsorbed monolayer could be brought through simple adsorption of these compounds at the metal-solution interface.

A comparative study on the dissolution of different types of stainless steel (430, 304 and 316) in absence and presence of the above mentioned crown ethers reflects some interesting features:

(1) In general, for all types of stainless steel, increasing the concentration of crown ethers (from $1x10^{-7}$ M to $1.1x10^{-6}$ M) remarkably decreases the rate of corrosion of stainless steels in 2M HCl solution as has been estimated from the loss in mass values, Figs. (3.1-3.12).

(2) The loss in mass values of different types of stainless steel in absence and presence of crown ethers obey the following order, [Figs. (3.13 - 3.16)].

$$430SS > 304SS > 316SS$$

(3) The effectiveness of crown ethers as corrosion inhibitors for all types of stainless steel varies according to the following order, [Fig. (3.17-3.19)]:

$$DB18C6 < Kry\text{-}22DD < Kry\text{-}222 < DB24C8$$

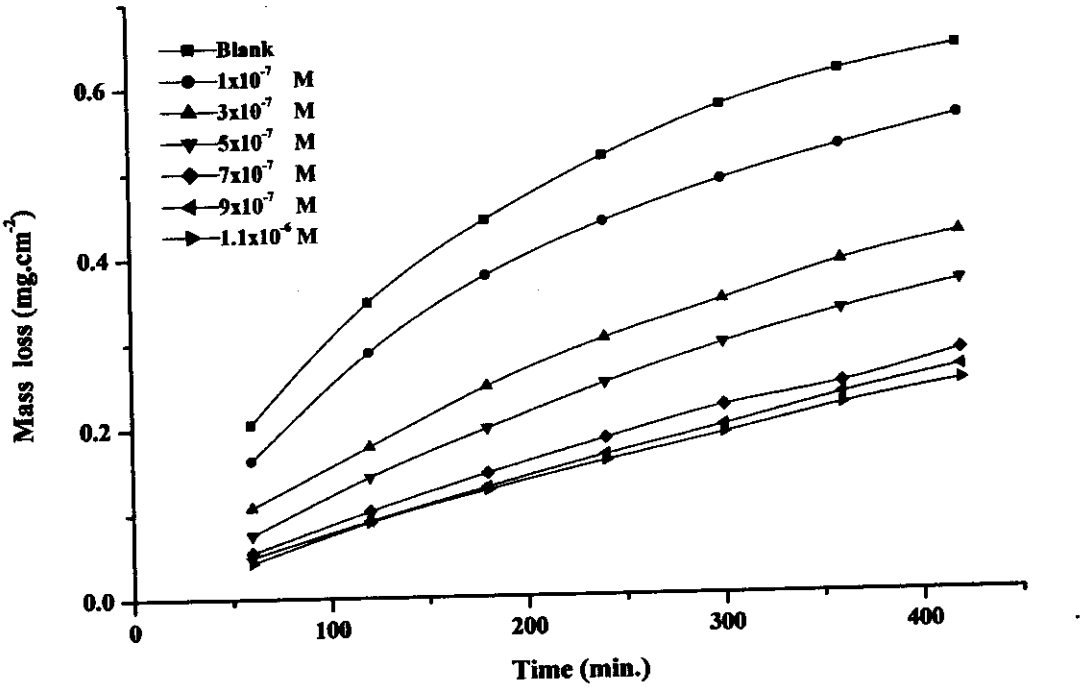

Fig. (3.1): Mass loss-time curves of 430SS in 2M HCl in absence and presence of different concentrations of DB18C6 at 303K.

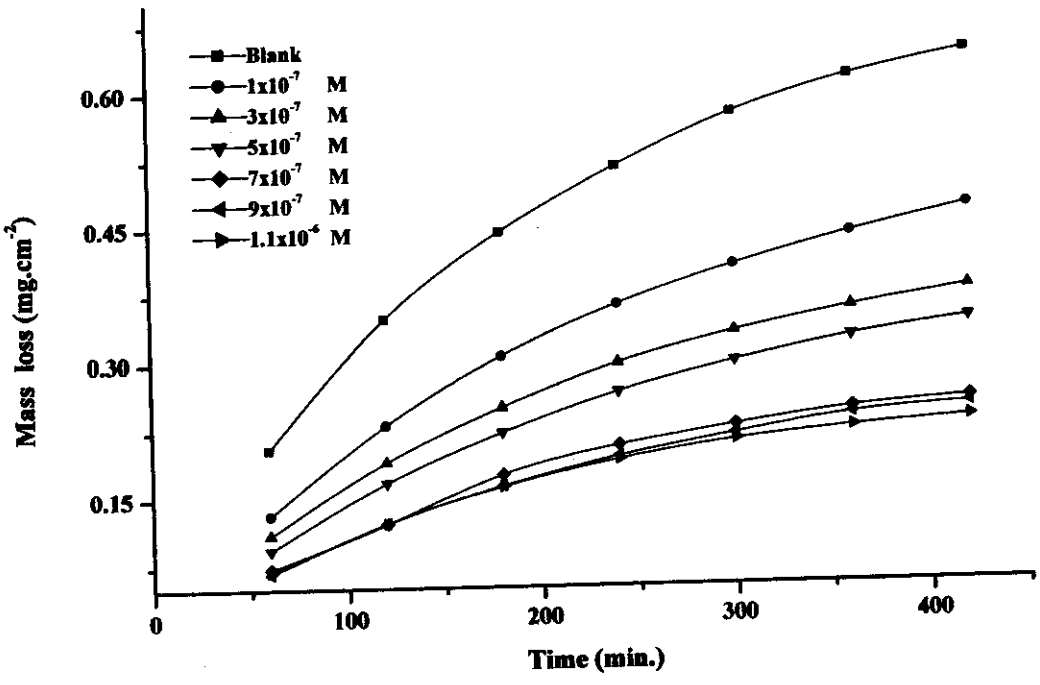

Fig. (3.2): Mass loss-time curves of 430SS in 2M HCl in absence and presence of different concentrations of Kry-22DD at 303K.

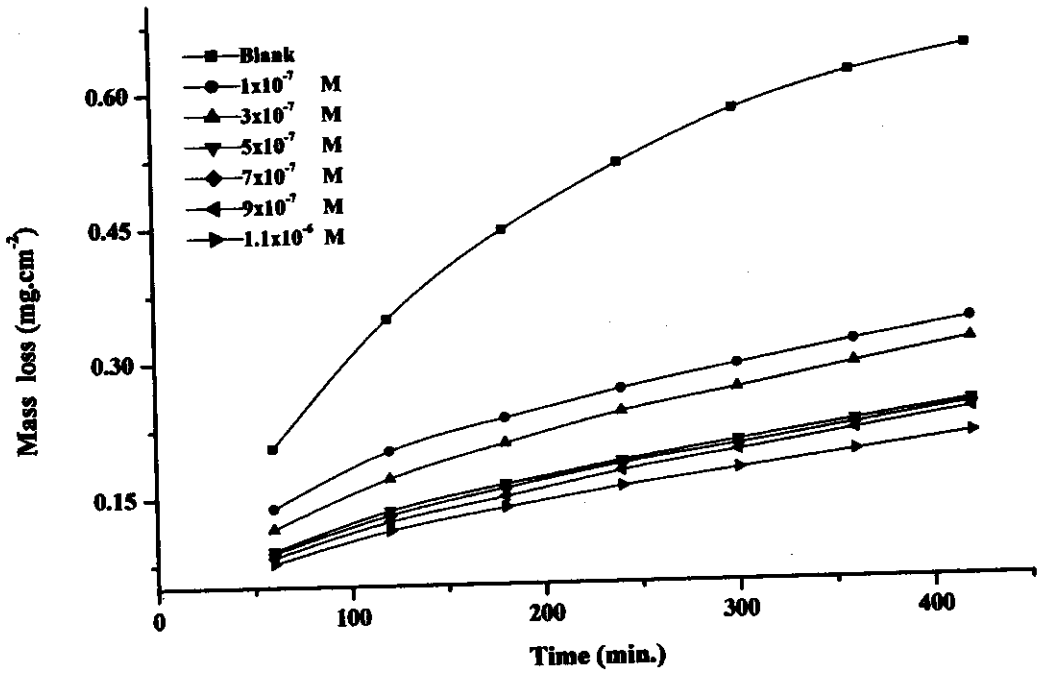

Fig. (3.3): Mass loss-time curves of 430SS in 2M HCl in absence and presence of different concentrations of Kry-222 at 303K.

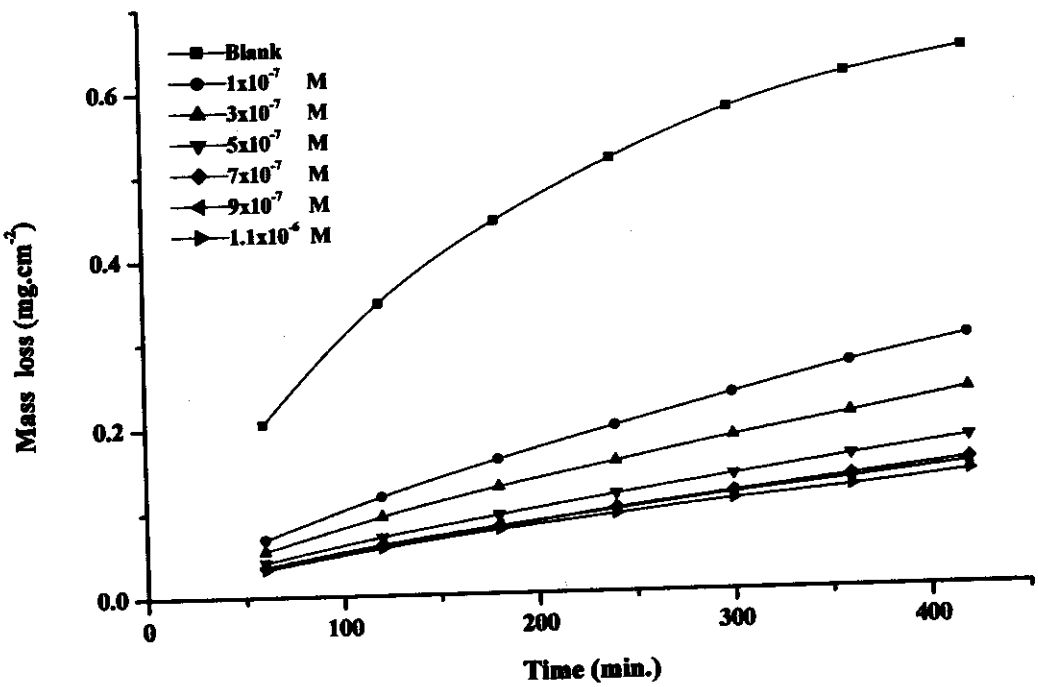

Fig. (3.4): Mass loss-time curves of 430SS in 2M HCl in absence and presence of different concentrations of DB24C8 at 303K.

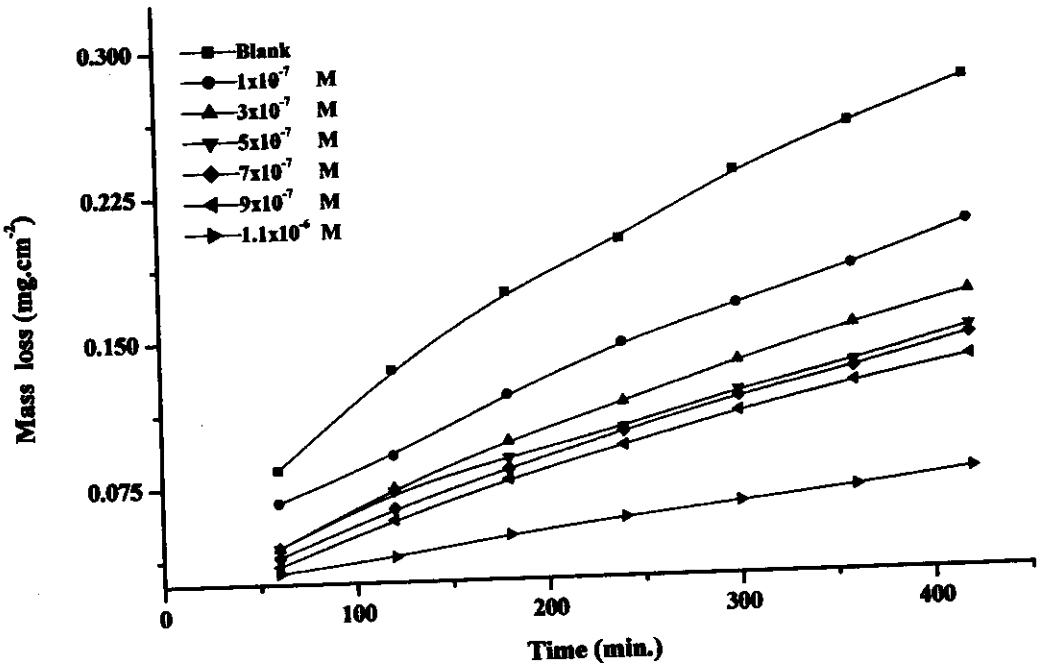

Fig. (3.5): Mass loss-time curves of 304SS in 2M HCl in absence and presence of different concentrations of DB18C6 at 303K.

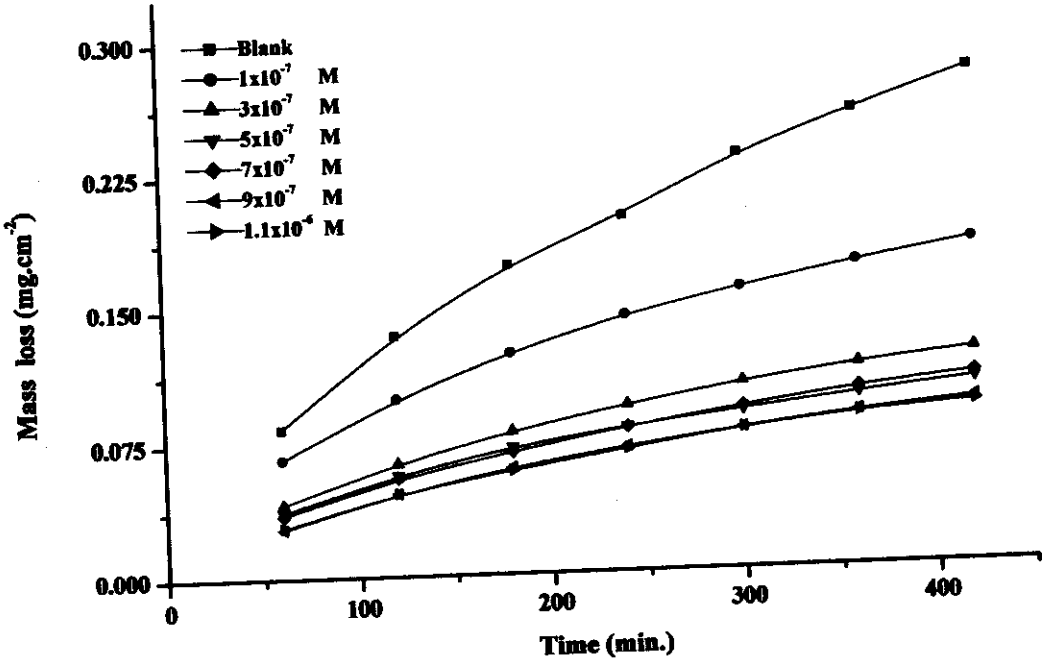

Fig. (3.6): Mass loss-time curves of 304SS in 2M HCl in absence and presence of different concentrations of Kry-22DD at 303K.

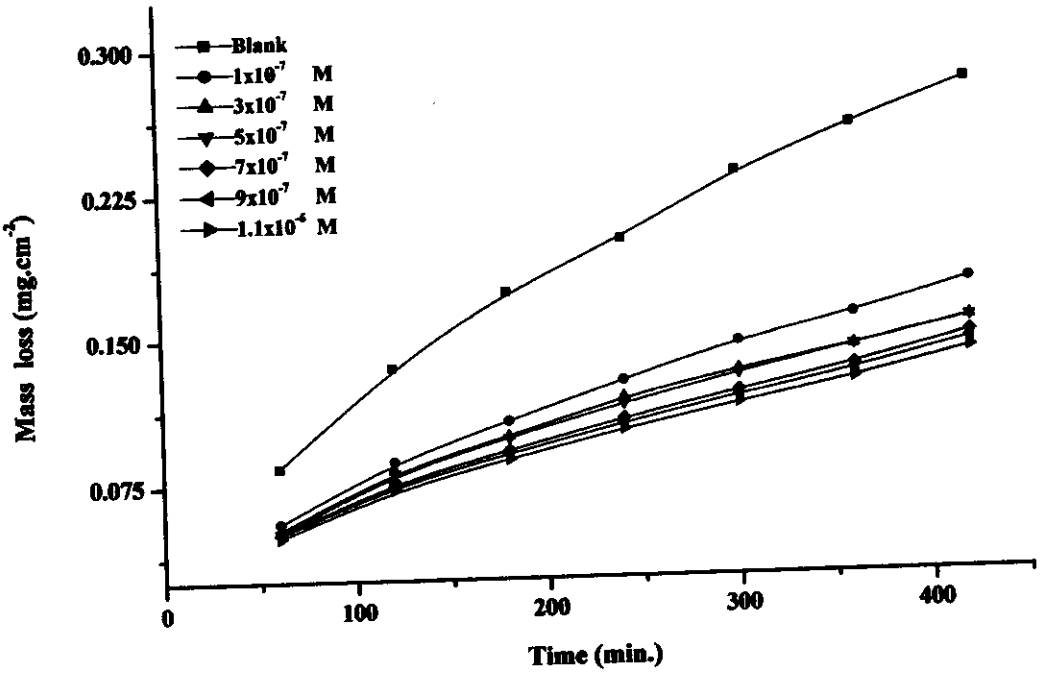

Fig. (3.7): Mass loss-time curves of 304SS in 2M HCl in absence and presence of different concentrations of Kry-222 at 303K.

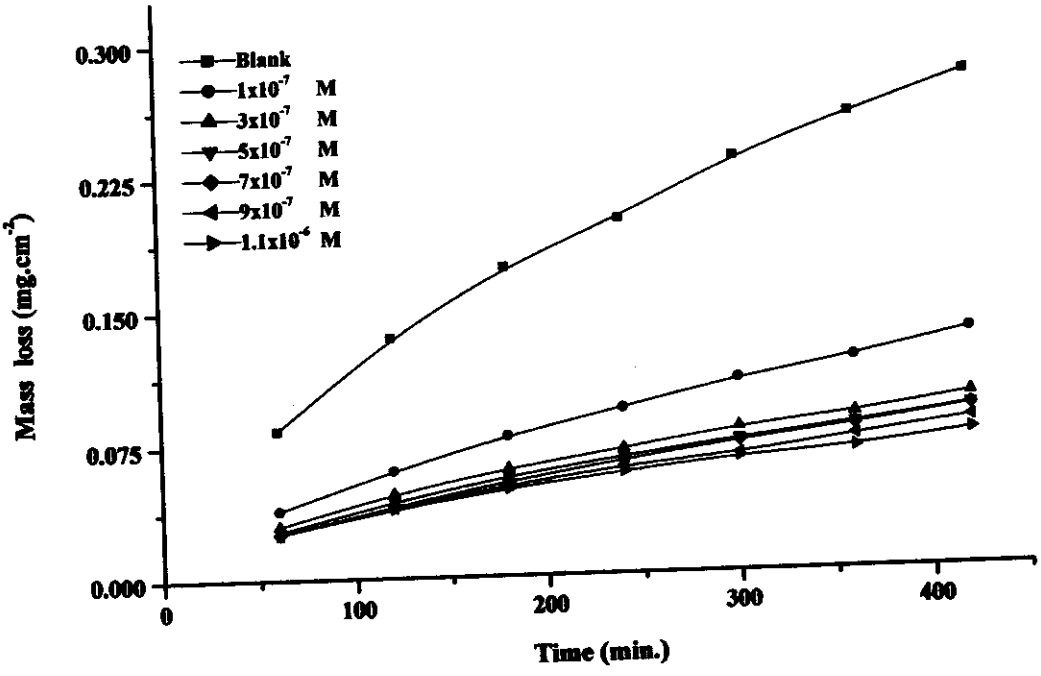

Fig. (3.8): Mass loss-time curves of 304SS in 2M HCl in absence and presence of different concentrations of DB24C8 at 303K.

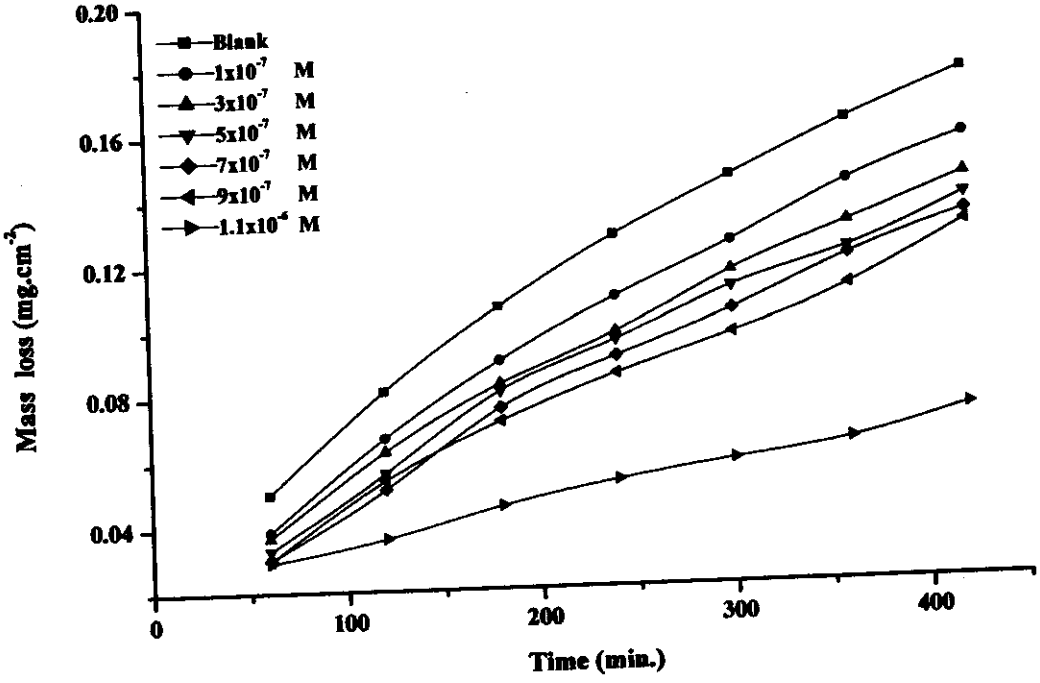

Fig. (3.9): Mass loss-time curves of 316SS in 2M HCl in absence and presence of different concentrations of DB18C6 at 303K.

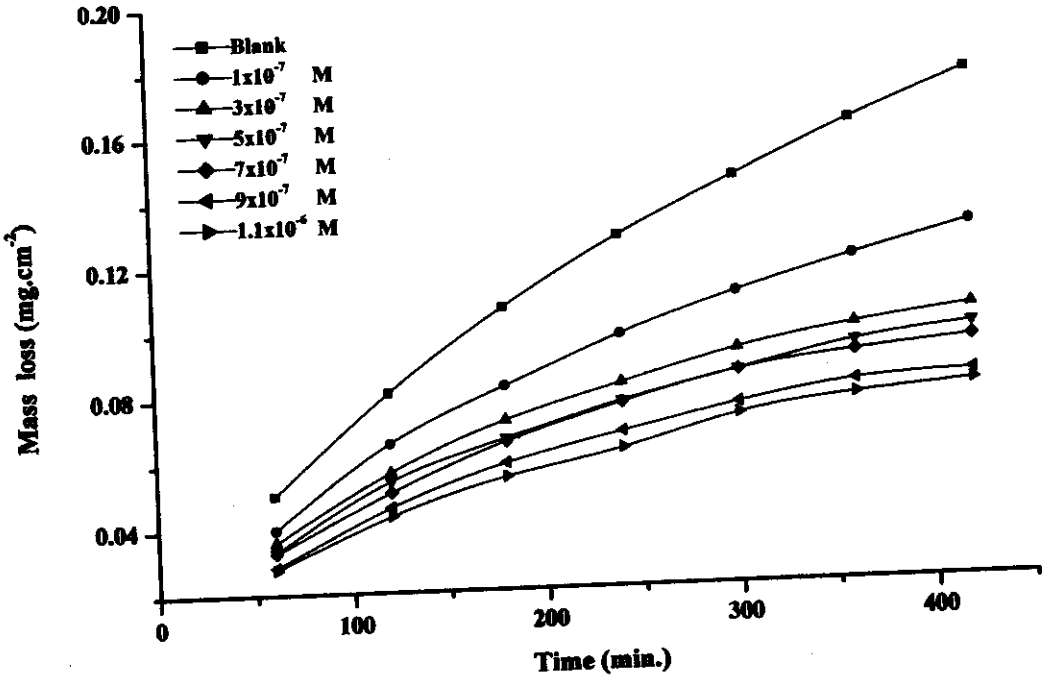

Fig. (3.10): Mass loss-time curves of 316SS in 2M HCl in absence and presence of different concentrations of Kry-22DD at 303K.

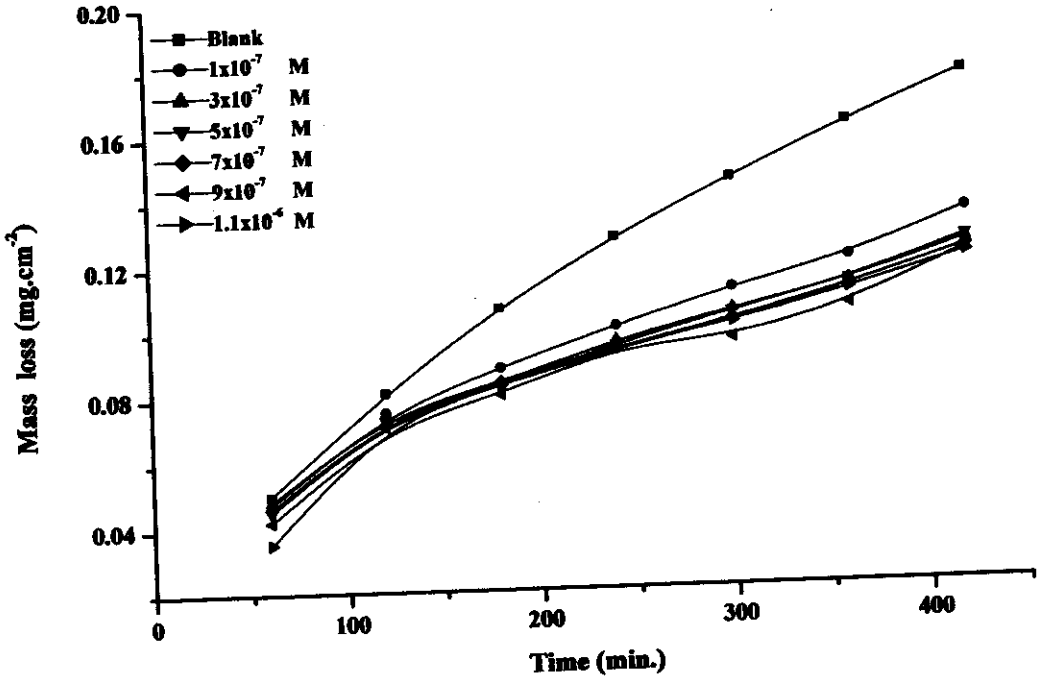

Fig. (3.11): Mass loss-time curves of 316SS in 2M HCl in absence and presence of different concentrations of Kry-222 at 303K.

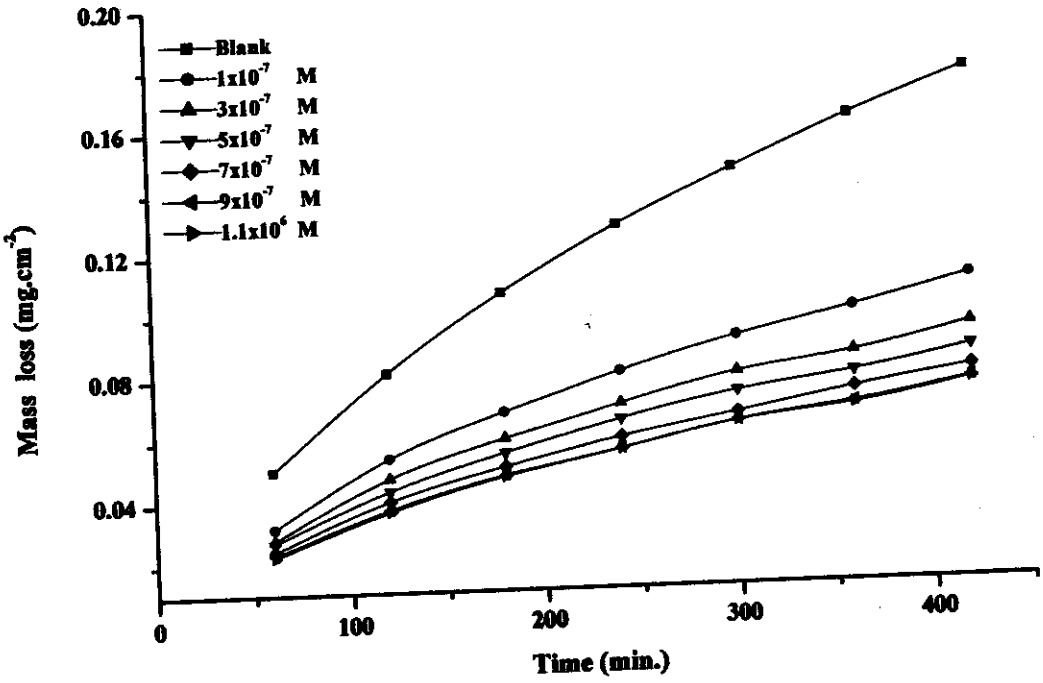

Fig. (3.12): Mass loss-time curves of 316SS in 2M HCl in absence and presence of different concentrations of DB24C8 at 303K.

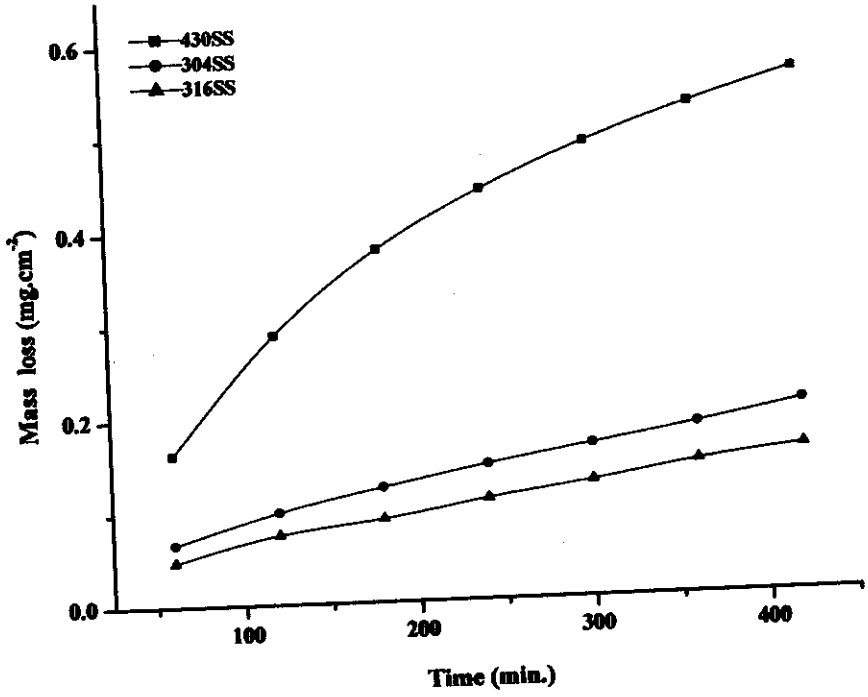

Fig. (3.13): Mass loss-time curves of 430, 304 and 316 stainless steels in presence of $1x10^{-7}$ M of DB18C6 for comparison.

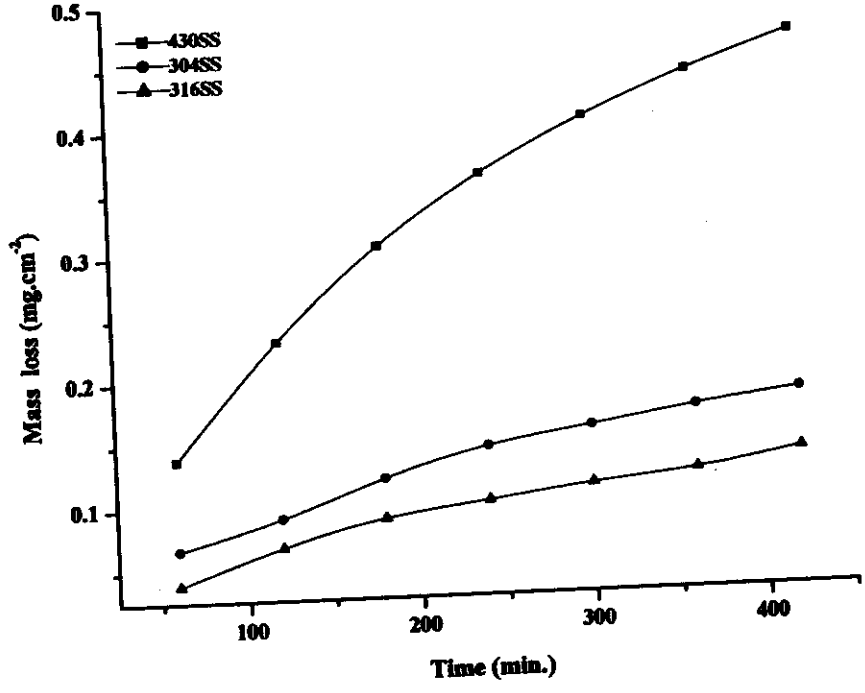

Fig. (3.14): Mass loss-time curves of 430, 304 and 316 stainless steels in presence of $1x10^{-7}$ M of Kry-22DD for comparison.

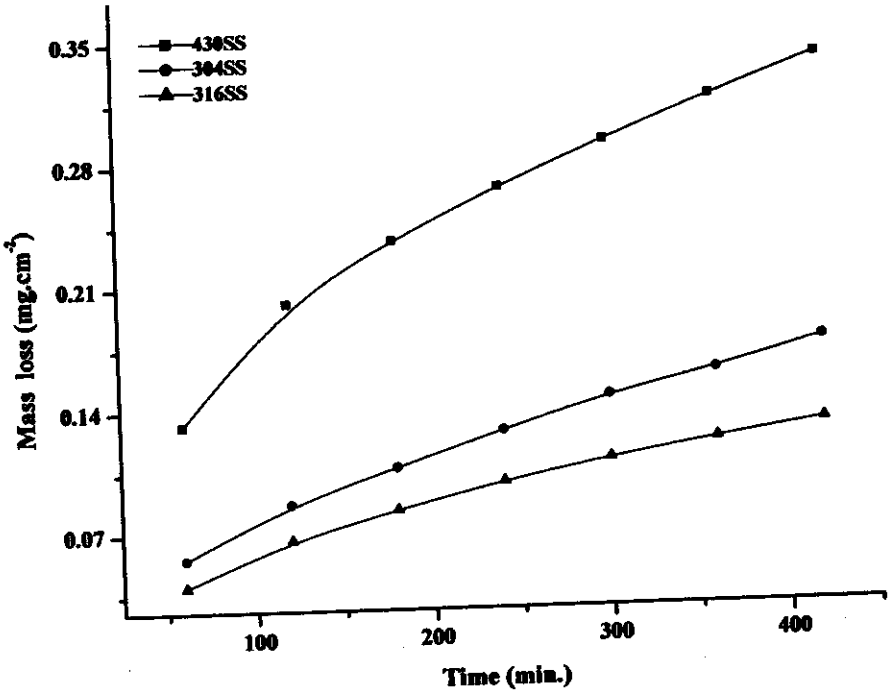

Fig. (3.15): Mass loss-time curves of 430, 304 and 316 stainless steels in presence of $1x10^{-7}$ M of Kry-222 for comparison.

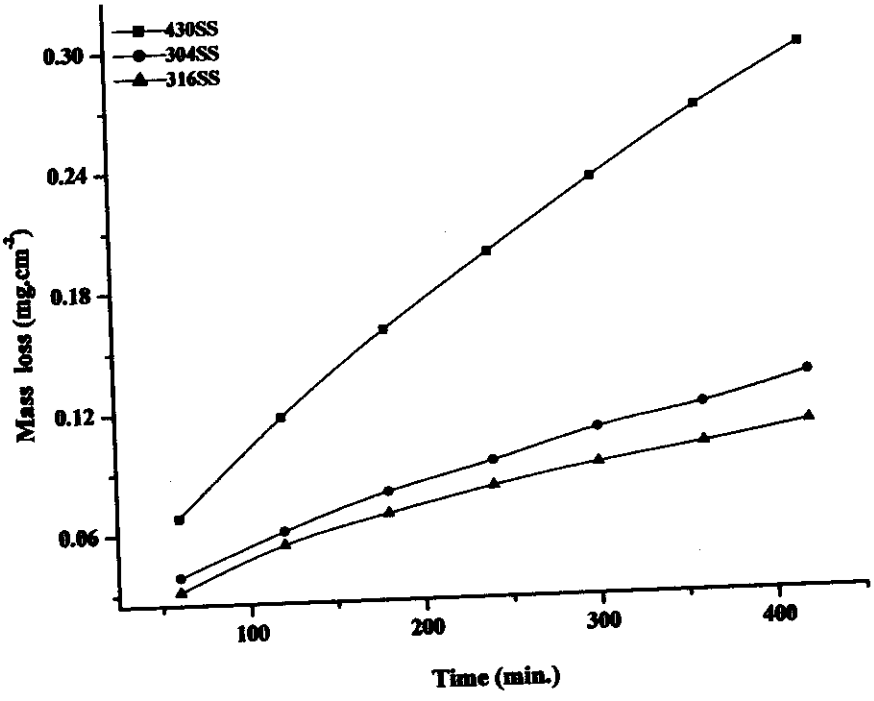

Fig. (3.16): Mass loss-time curves of 430, 304 and 316 stainless steels in presence of $1x10^{-7}$ M of DB24C8 for comparison.

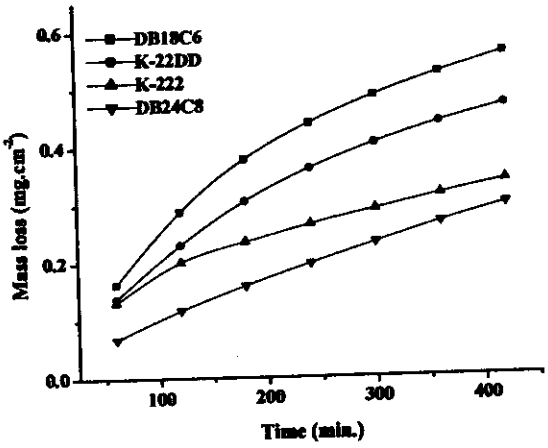

Fig. (3.17): Mass loss-time curves of 430 stainless steels in presence of $1x10^{-7}$ M of different types of crown ethers for comparison.

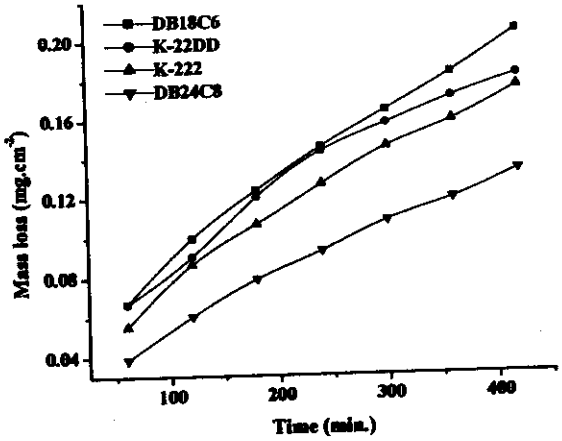

Fig. (3.18): Mass loss- time curves of 304 stainless steels in presence of $1x10^{-7}$ M of different types of crown ethers for comparison.

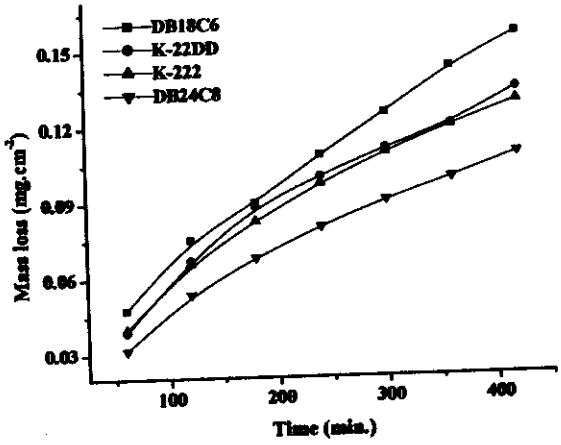

Fig. (3.19): Mass loss- time curves of 316 stainless steels in presence of $1x10^{-7}$ M of different types of crown ethers for comparison.

3.1.2 Effect of crown ethers on the corrosion rate of stainless steels.

To confirm the effect of crown ethers on the corrosion rate (k) of stainless steels, the relations between the corrosion rate (k) values of 430SS (Fig. 3.20), 304SS (Fig. 3.21) and 316SS (Fig. 3.22) with the concentration of different types of crown ethers were studied.

The corrosion rate values ($mg.cm^{-2}.min^{-1}$.) were calculated from this equation:

$$\text{Corrosion rate (k)} = \frac{\text{loss in mass (mg.cm}^{-2})}{\text{time (min.)}} \qquad (3.2)$$

It is clear that the corrosion rate (k) values of all types of stainless steel were decreased by increasing the concentration of crown ethers obeyed the given trend:

DB18C6 < Kry-22DD < Kry-222 < DB24C8

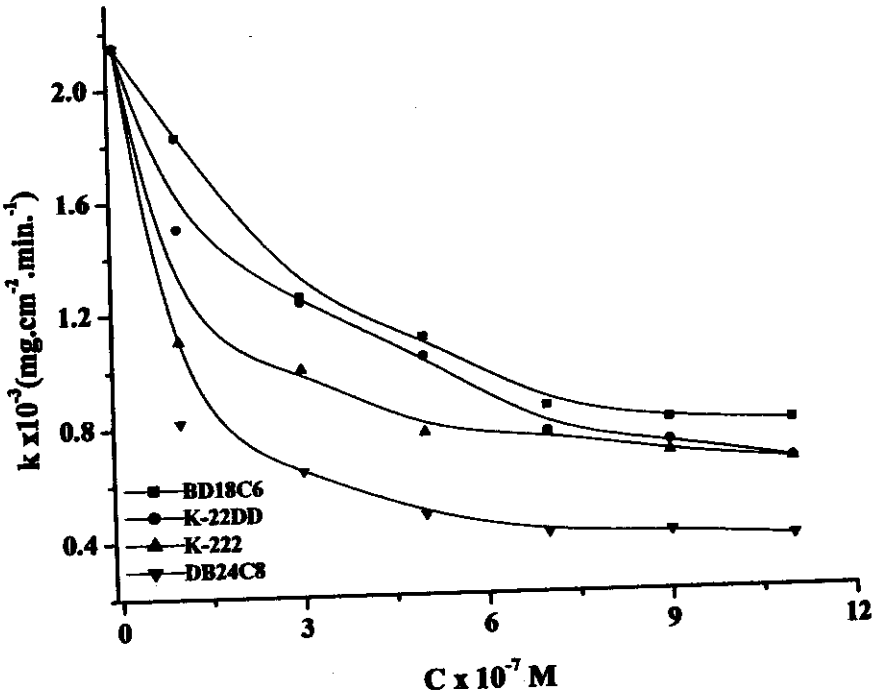

Fig. (3.20): Effect of crown ethers concentration on the corrosion rate (k) of 430 stainless steel.

3.1.3 Degree of surface coverage and percentage inhibition efficiency.

To clear up the effect of crown ethers on the inhibition mechanism of different types of stainless steel, the degree of surface coverage (θ) values were calculated from the equation [11-14]:

$$\theta = 1 - \frac{M_{add}}{M_{free}} \qquad (3.3)$$

where: M_{free} and M_{add} are loss in mass values in the corrosive medium, and in the inhibited medium at given time values and temperature, each of them are in ($mg.cm^{-2}$) respectively.

Also, the percentage inhibition efficiency (%IE) values were calculated using the following equation:

$$\% IE = \frac{M_{free} - M_{add}}{M_{free}} x100 \qquad (3.4)$$

Table (3.1), represents the variation of degree of surface coverage (θ) and the percentage inhibition efficiency (%IE) values of the different types of stainless steel in presence of different concentrations of crown ethers at 303K. It is clear that all the values of the degree of a surface coverage (θ) and consequently, the percentage inhibition efficiency (%IE) increase by increasing the concentration of different types of crown ethers.

Figs. (3.23-3.24), represent the relation between the percentage inhibition efficiency (%IE) and the immersion time (minute) for 304 and 316 stainless steels in presence of different types and concentrations of the investigated crown ethers. It is obviously that the percentage inhibition efficiencies (%IE) were increased by increasing the immersion time. This is attributed to the formation of a barrier film which prevents the attack of acid on the metal surface.

Table (3.1): Variation of degree of surface coverage (θ) and percentage inhibition efficiency* (%IE) of different types of stainless steel in presence of different concentrations of crown ethers at 303K.

Concn..	DB18C6			Kry-22DD			Kry-222			DB24C8		
(M)	430SS	304SS	316SS	430SS	304SS	316SS	430SS	304SS	316SS	430SS	304SS	316SS
$1x10^{-7}$	0.148 [14.83]	0.270 [27.04]	0.148 [14.77]	0.300 [30.00]	0.281 [28.14]	0.237 [23.68]	0.486 [48.58]	0.366 [36.58]	0.215 [21.47]	0.618 [61.84]	0.535 [53.46]	0.372 [37.19]
$3x10^{-7}$	0.514 [51.40]	0.424 [42.36]	0.234 [23.35]	0.425 [42.49]	0.533 [53.29]	0.353 [35.33]	0.534 [53.38]	0.411 [41.11]	0.250 [25.00]	0.700 [70.00]	0.648 [64.83]	0.455 [45.45]
$5x10^{-7}$	0.517 [51.67]	0.488 [48.84]	0.251 [25.14]	0.486 [48.58]	0.593 [59.30]	0.397 [39.69]	0.640 [64.04]	0.426 [42.61]	0.260 [25.98]	0.776 [77.57]	0.670 [67.02]	0.493 [49.32]
$7x10^{-7}$	0.642 [64.23]	0.500 [49.95]	0.291 [29.07]	0.601 [60.08]	0.595 [59.50]	0.401 [40.08]	0.647 [64.66]	0.464 [46.43]	0.266 [26.60]	0.809 [80.89]	0.681 [68.08]	0.538 [53.80]
$9x10^{-7}$	0.680 [67.98]	0.535 [53.52]	0.332 [33.24]	0.625 [62.47]	0.650 [64.97]	0.470 [47.02]	0.622 [66.19]	0.476 [47.59]	0.269 [26.90]	0.811 [81.07]	0.698 [69.79]	0.560 [56.04]
$1.1x10^{-6}$	0.694 [69.40]	0.722 [72.16]	0.587 [58.66]	0.631 [63.13]	0.656 [65.64]	0.510 [51.04]	0.695 [69.53]	0.493 [49.25]	0.270 [26.94]	0.822 [82.20]	0.714 [71.36]	0.568 [56.84]

* The values between brackets refer to percentage inhibition efficiency (%IE).

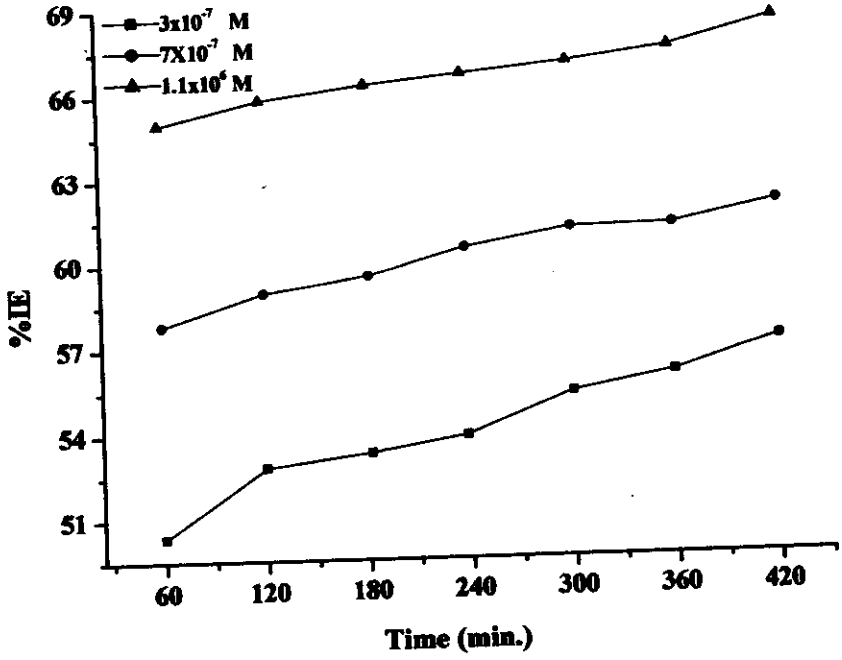

(I)

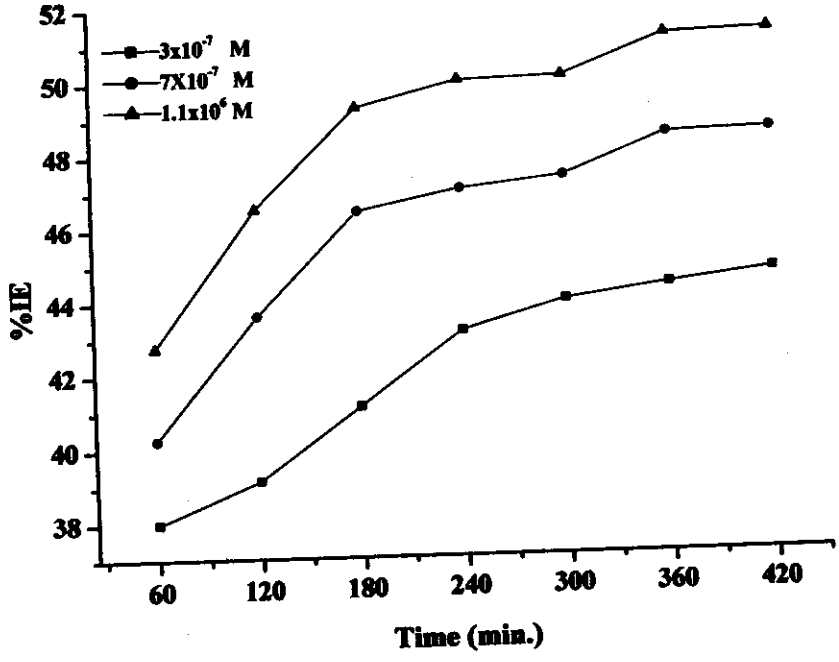

(II)

Fig. (3.23) : Relation between the percentage inhibition values (%IE) with the immersion time for 304SS in 2M HCl in presence of different concentrations of Kry.22DD (I) and Kry.222 (II) at 303K.

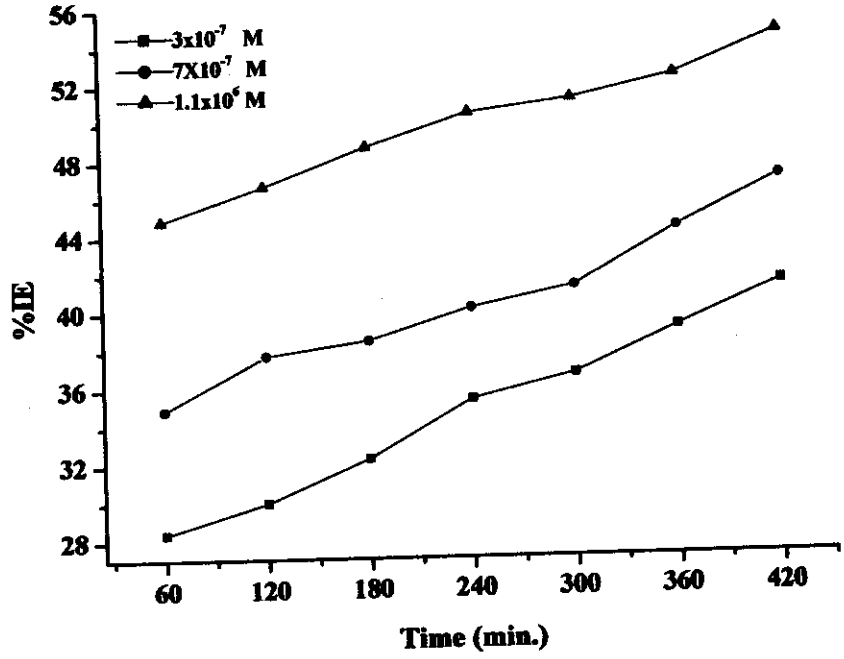

(I)

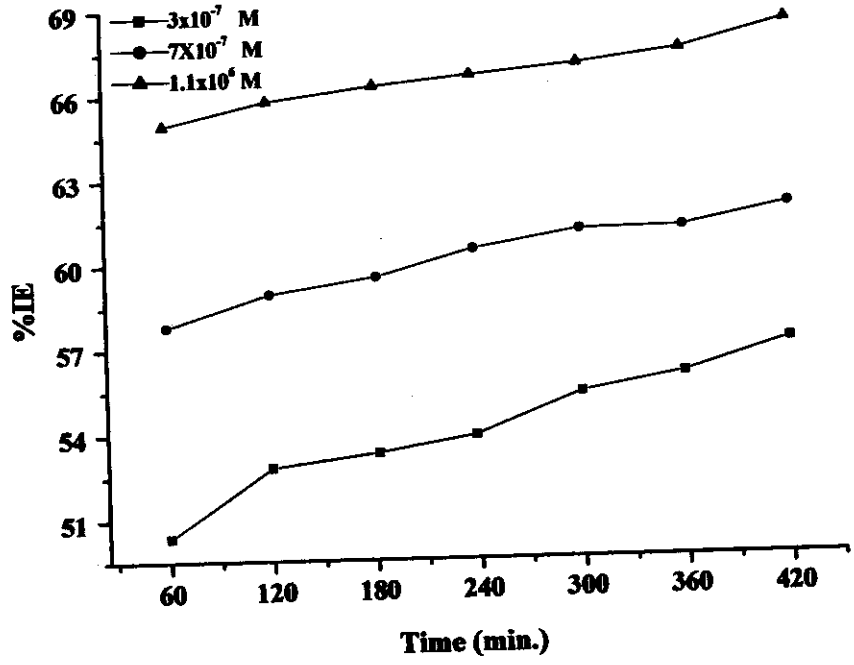

(II)

Fig. (3.24) : Relation between the percentage inhibition values (%IE) with the immersion time for 316SS in 2M HCl in presence of different concentrations of Kry.22DD (I) and DB24C8 (II) at 303K.

3.1.4 Adsorption isotherms.

As far as the inhibition process is concerned, it is generally assumed that the adsorption of the crown ethers at the metal solution interface is the first step in the reaction mechanism of the inhibitors in the aggressive acid media [161]. Four types of adsorption may take place in the inhibiting phenomena involving organic molecules (crown ethers) at the metal solution interface namely:

(i) Electrostatic attraction between charged molecules and charged metals.
(ii) Interaction of electron pairs in the oxygen and/or nitrogen atoms in crown ether molecules with the metal.
(iii) Interaction of JI-electrons with the metals.
(iv) A combination of the above.

Chemisorption involves charge sharing or charge transfer from the inhibitor molecules to the surface in order to form a coordinate bond. In fact electron transfer is typical for a transition metal having a low energy electron orbital. Concerning inhibitors, electron transfer can be expected with compounds having relatively loosely bound electrons [162]. The situation may arise because of the presence of multiple bonds or aromatic rings, having a π bond character in the adsorbed inhibitor [163-170]. The inhibition efficiency of a homogenous series of organic substances, differing only in the hetero atoms, is usually in the following sequence:

$$P > Se > S > N > O$$

Interpretation may be found in the easier polarizability and lower electronegativity of the elements on the left of the above sequence [171]. The adsorption of an organic adsorbate on the surface of a metal is regarded as a substitutional adsorption process between the organic compounds in the aqueous phase (Org_{aq}) and the water molecules adsorbed on the electrode surface (H_2O_s), [172].

$$Org_{aq} + XH_2O_s = Org_s + H_2O_{aq} \qquad (3.5)$$

where, X is the ratio of the number of water molecules replaced by one molecules of organic adsorbate. The adsorption process depends on the structure of the inhibitor, the type of the metal and the nature of its surface, the nature of the corrosion medium and its pH value, the temperature and the electrochemical potential of the metal-solution interface [173]. Also, the type of

adsorption provides information about the interaction among the adsorbed molecules themselves as well as their interaction with the metal surface. Actually an adsorbed molecule may make the surface more or less difficult for another molecule to become attached to a neighboring site and multilayer adsorption may take place. There may be more or less than one inhibitor molecule per surface site. Finally, various surface sites could have varying degrees of activation. For these reasons a number of mathematical adsorption isotherm expressions have been developed to take into consideration some of non-ideal effects. The above process reaches equilibrium in which the chemical potential (μ) in the left side is equal to that of right side. Now, depending on the expression of (μ) as related to the physical model adopted to describe adsorption, one may obtain different expressions of the adsorption isotherm such as Temkin, Frumkin, Frundich and Langmuir isotherms (see appendix). In the present work the adsorption process obeys the Temkin's adsorption isotherm [174], which obeys the following equation:

$$\ln K C = a \theta \qquad (3.6)$$

where,

θ: s the degree of surface coverage

a: is the molecule interaction parameter depending upon molecular interactions in the adsorption layer and the degree of heterogeneity of the metal surface. It can possess both positive and negative values and it is a measure of the steepness of the adsorption isotherm. The more positive the value of (a), the steeper is the adsorption isotherm. This is interpreted [175] to imply that the interactions between molecules with positive (a) value cause an increase in the adsorption energy with the increase of (θ).

C: is the inhibitor concentration in the bulk solution.

K: is the equilibrium constant of the adsorption reaction and it is related to the standard free energy of adsorption ($\Delta G^{\circ}_{ads.}$) by:

$$K = \frac{1}{55.5} \exp\left[\frac{-\Delta G^{o}_{ads}}{RT} \right] \qquad (3.7)$$

where, R is the universal gas constant and T is the absolute temperature.

The variation of the degree of surface coverge (θ), with (log C) for different types of stainless steel in the presence of different types of crown

ethers are shown in Figs. (3.25-3.27). It is clearly that the relation between (θ) and (log C) gives a straight lines. This means that the adsorption of crown ethers obeys the Temkin's adsorption isotherm. This suggests that the used crown ethers block the reaction sites on the surface of stainless steel samples by adsorption [176], and reduces the available area for further corrosion reaction.

On the other hand, it is found that the kinetic-thermodynamic model of El Awady et. al. [177]:

$$\log \theta / (1-\theta) = \log K' + y \log C \qquad (3.8)$$

is valid to operate the present adsorption data. The equilibrium constant of adsorption $K=K'^{(1/y)}$, where 1/y is the number of the surface active sites occupied by only one crown ether molecule and (C) is the bulk concentration of the inhibitor. The relation between $\log\theta/(1-\theta)$ against logC at 303K are given in Figs. (3.28 - 3.30) where straight line relationships were obtained suggesting the validity of this model for all cases studied. The calculated values of 1/y, K and $\Delta G°_{ads.}$ are given in Table (3.2). Inspection of the data of this Table shows that the values of ($\Delta G°_{ads.}$) and its negative sign indicate that the adsorption of crown ethers on the surface of different types of stainless steel is proceeding spontaneously and is accompanied by a highly-efficient adsorption. It is worth noting that the value of 1/y is less than unity. This means that the given inhibitor molecules will not occupy more than one active site. In general, the values of ($\Delta G°_{ads.}$) obtained from El-Awady model are very close to the values obtained from Temkin's adsorption isotherms.

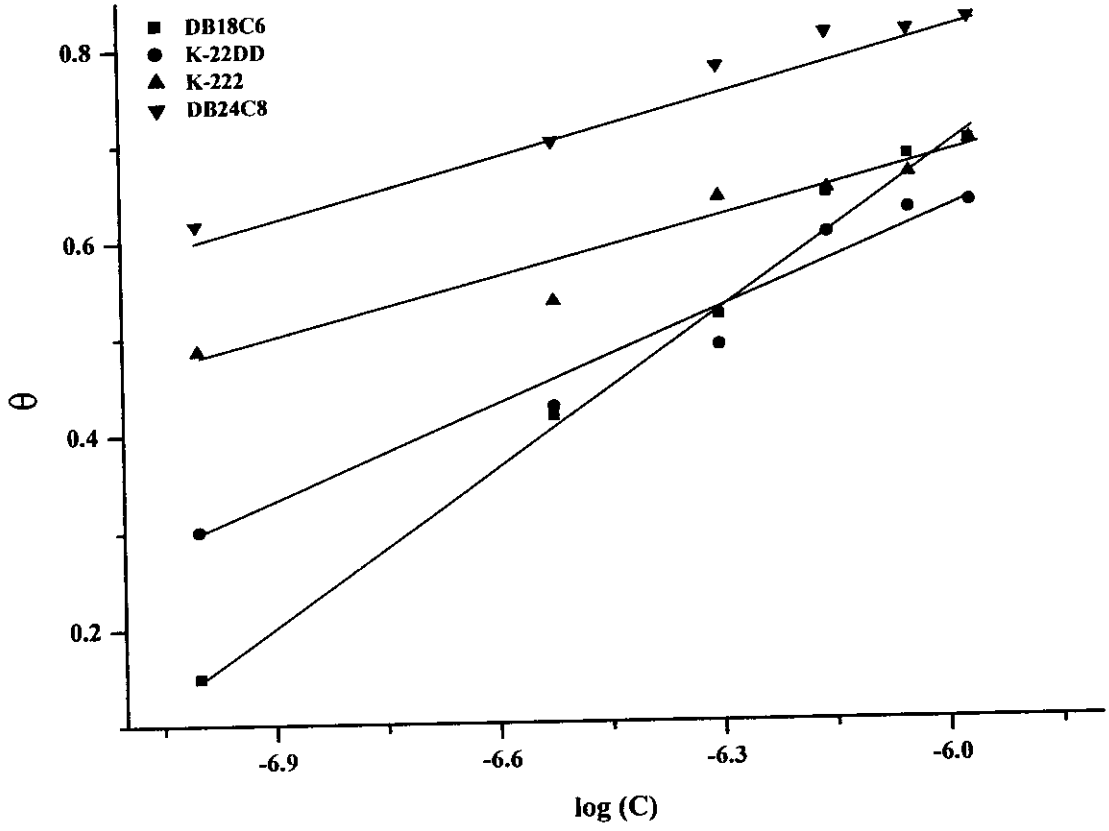

Fig. (3.25): Curve fitting of corrosion data for 430SS in 2M HCl in presence of different concentrations of crown ethers to the Temkin's adsorption isotherm at 303K.

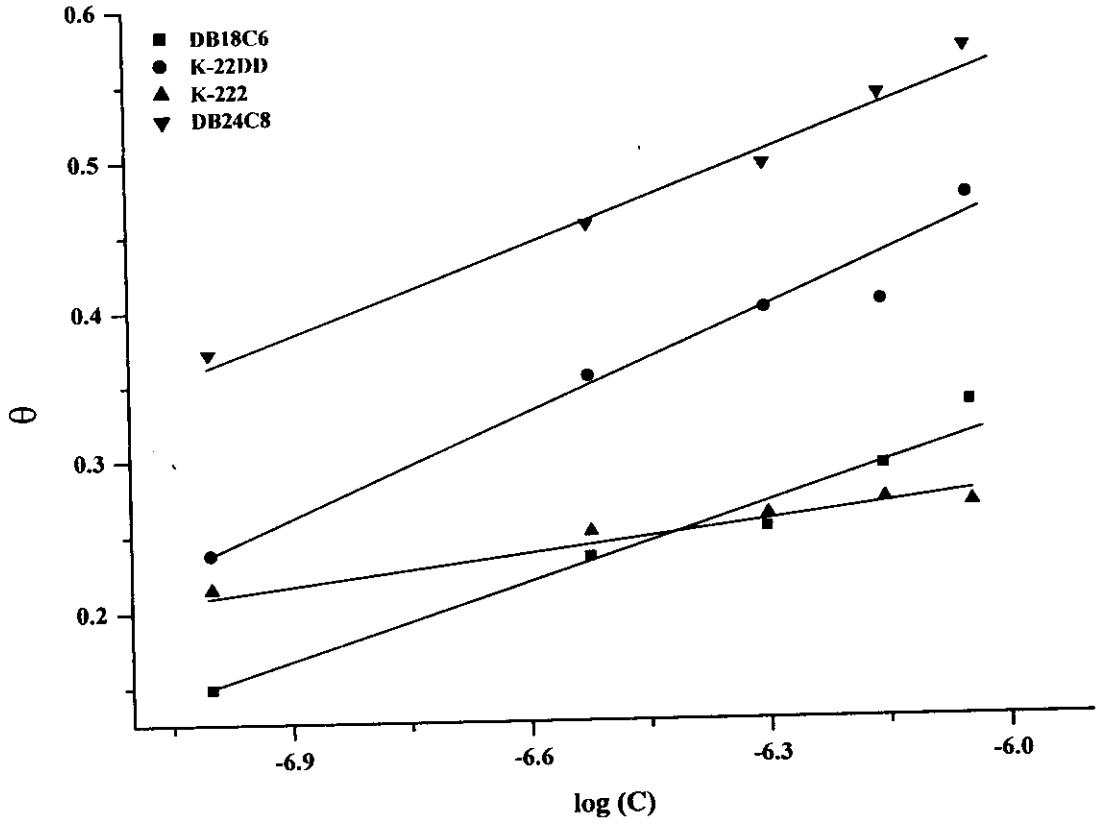

Fig. (3.27): Curve fitting of corrosion data for 316SS in 2M HCl in presence of different concentrations of crown ethers to the Temkin's adsorption isotherm at 303K.

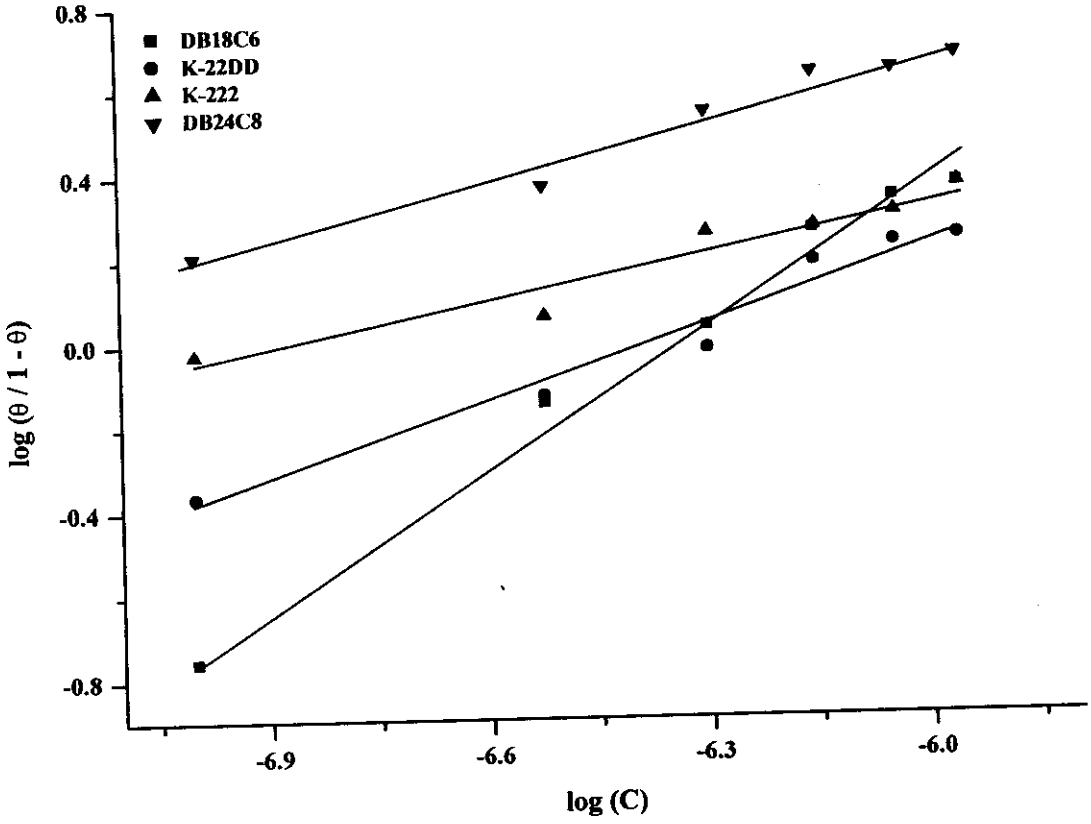

Fig. (3.28): Curve fitting of corrosion data for 430SS in 2M HCl in presence of different concentrations of crown ethers to the kinetic model.

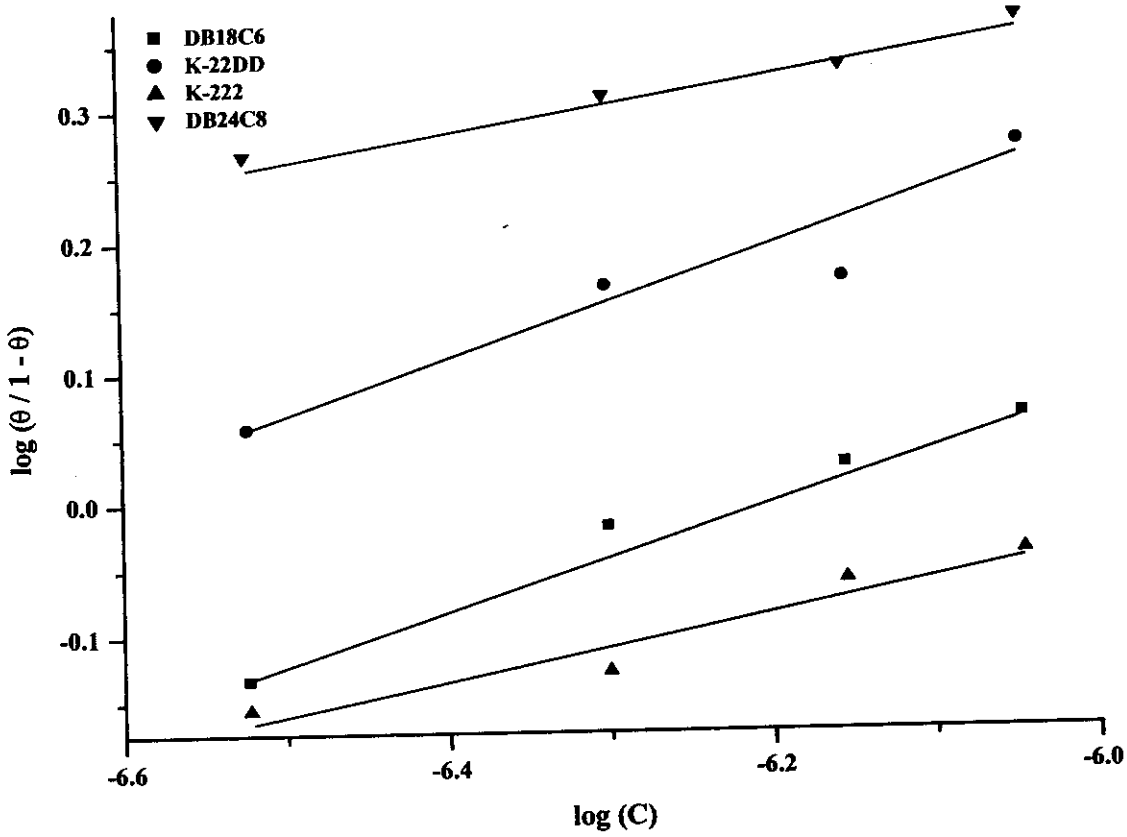

Fig. (3.29): Curve fitting of corrosion data for 304SS in 2M HCl in presence of different concentrations of crown ethers to the kinetic model.

3.1.5 Effect of temperature and thermodynamic parameters of activation.

In this part the effect of temperature on the corrosion rate of different types of stainless steel in 2M HCl in absence and presence of different concentrations of crown ethers was studied. The behavior at the different temperatures (303, 313, 323 and 333K) was investigated by weight loss measurements [Figs. (3.31-3.66)]. It is clear from all these figures that the weight loss values increase at all concentrations with raising the temperature from 303K to 333K. This is attributed to the desorption of some crown ether molecules from the surface at higher temperatures. The increase in weight loss values with increasing temperature is suggestive of physical adsorption of the crown ethers on the surface of the different types of stainless steel.

The values of corrosion rate (k) which obtained at the above mentioned temperatures permit the calculation of the Arrhenius activation energy (E_a^*) according to the following equation [4]:

$$\log k = \frac{-E_a^*}{RT} + A \qquad (3.9)$$

where, (A) is a constant depends on the metal type and the electrolyte. The form of Arrhenius equation is applicable in the present study. Arrhenius plot of logarithmic values of corrosion rate (mg cm^{-2} min^{-1}) against the reciprocal values of absolute temperature (I/T), is shown graphically in Figs. (3.67-3.69). The values of activation energy (E_a^*) were calculated from the slopes of the straight lines.

The values of activation energy (E_a^*) of dissolution of the different types of stainless steel in absence and presence of different types of crown ethers are given in Table (3.3). It is obvious that the activation energy values (E_a^*) were increased by increasing the concentration of crown ethers. This indicates that the dissolution of these types of stainless steel under these conditions is activation controlled. The activation energy (E_a^*) of the dissolution of 304SS type in 2M HCl from Fig. (3.68) is equal 28.97 kJ mol^{-1} which is in good agreement with the work of Singh, who found that the activation energy is 34.8 kJ mol^{-1}, for the corrosion of AISI 304SS in1.0M H_2SO_4 [178], and by El Hashemy, 31.23 kJ mol^{-1}, for the corrosion of 304SS in 1.0M HCl solution [123]. Also, the activation

energies (E_a^*) of the dissolution of 430SS and 316SS types in 2M HCl from Figs. (3.67 & 3.69) are 27.77 kJ mol^{-1} and 50.12 kJ mol^{-1}, respectively, which are in agreement with the work of Sanad et. al. [179], where they found that the activation energies (E_a^*) of the dissolution of 430SS and 316SS types in 1.0M HCl are 16.12 kcal mol^{-1} and 16.58 kcal mol^{-1}, respectively.

Generally, one can say that the nature and concentration of electrolyte affect greatly the activation energy of the corrosion process. The addition of any type of the investigated crown ethers to the solution increases the activation energy values (E_a^*) as shown in Table (3.3), and the extent of the increase is proportional to the inhibition efficiency of the inhibitor. This indicates that the energy barrier of the corrosion reaction increases in the presence of these additives. This means that by the addition of crown ethers in the corrosive media, the corrosion reaction will be further pushed to the surface sites that are characterized by higher values of activation energies (E_a^*). This means that stainless steel corrosion occurs at the uncovered part of the surface. Thus, adsorption of crown ethers was assumed to occur on the higher energy sites [180]. The presence of crown ethers which result in the blocking of the active sites, must be associated with an increase in the activation energy (E_a^*) of stainless steels in the inhibited sites [6].

Free energies of activation (ΔG^*) were calculated by applying the transition state equation [6]:

$$\Delta G^* = RT\left[\ln\frac{kT}{h} - \ln(\text{rate})\right] \qquad (3.10)$$

where, h = Plank's constant

k = Boltzman's constant

R = gas constant

T = absolute temperature

The enthalpy of activation (ΔH^*) and the entropy of activation (ΔS^*) were calculated by applying the following equations:

$$\Delta H^* = E_a^* - RT \qquad (3.11)$$

$$\Delta S^* = \frac{\Delta H^* - \Delta G^*}{T} \qquad (3.12)$$

The values of the thermodynamic parameter for the dissolution of different types of stainless steel are listed in Tables (3.4-3.6). Inspection of these data reveals that the values of (ΔH^*) and (ΔG^*) in the presence of crown ethers increase over that the uninhibited solution. This implies that energy barrier of the corrosion reaction in the presence of crown ethers increases. On the other hand, (ΔS^*) values are lower and have negative values in presence of crown ethers. This means that addition of these compounds causes a decrease in the disordering in going from reactants to the activated complexes [180-181]. Also, from Tables (3.4-3.6), it is evident that the values of (ΔG^*) increase with increasing temperature where the constantly values of (ΔH^*) indicated that the mechanism of the corrosion reaction was not changed by raising the temperatures from 303K to 333K. On the other hand, the low values of (ΔH^*) suggested that the crown ethers are physically adsorbed on the surface of stainless steels [180].

The order of the inhibition efficiencies of crown ethers as gathered from the increase in (E_a^*) and (ΔH^*) values and decrease in (ΔS^*) values for all types of stainless steels obey this sequence:

DB18C6 < Kry-22DD < Kry-222 < DB24C8

This order agrees with that obtained from the values of corrosion rate.

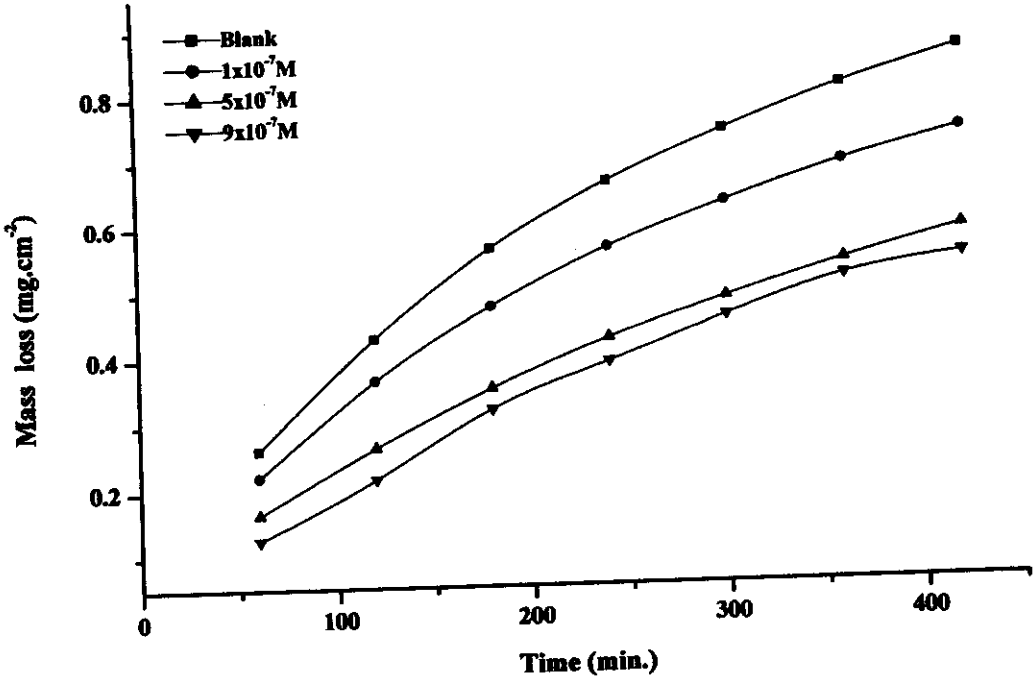

Fig. (3.31): Mass loss-time curves of 430SS in 2M HCl in absence and presence of different concentrations of DB18C6 at 313K.

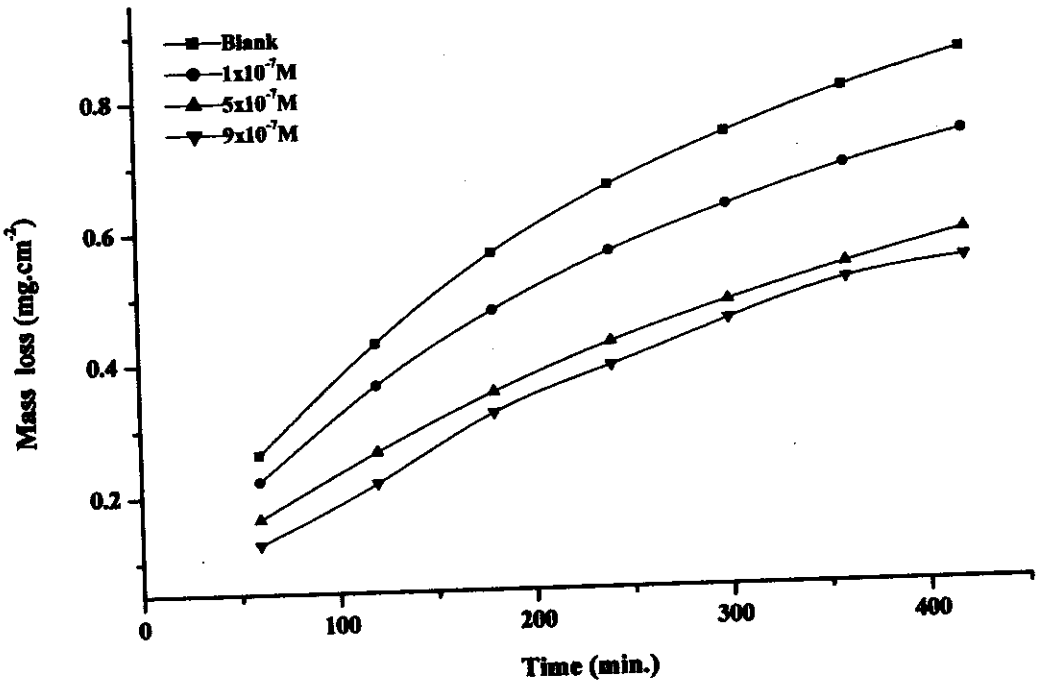

Fig. (3.32): Mass loss-time curves of 430SS in 2M HCl in absence and presence of different concentrations of Kry-22DD at 313K.

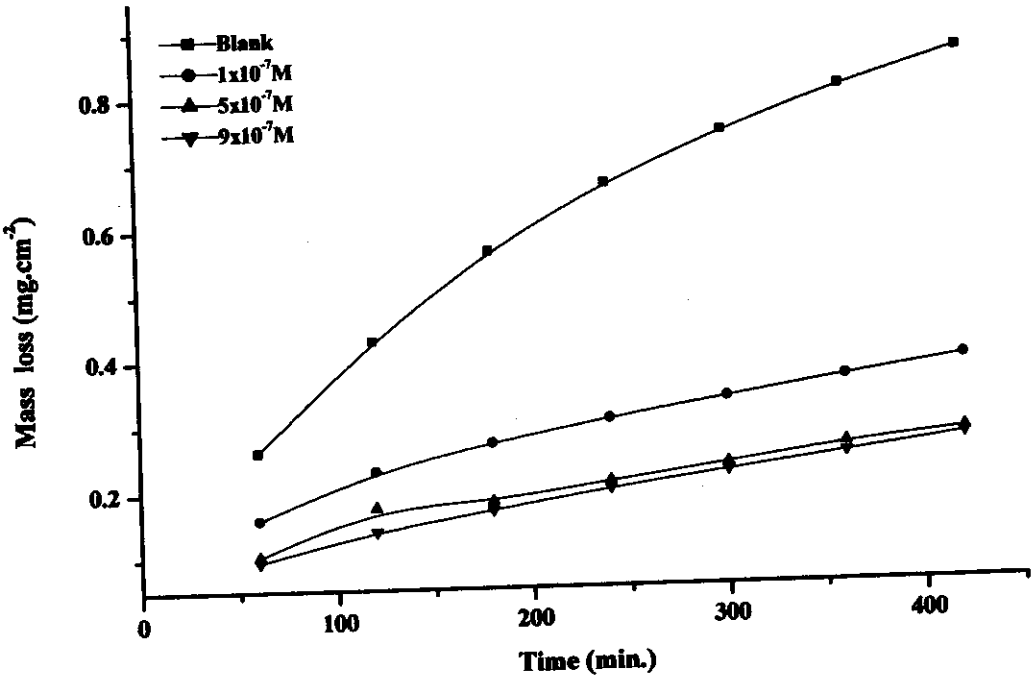

Fig. (3.33): Mass loss-time curves of 430SS in 2M HCl in absence and presence of different concentrations of Kry-222 at 313K.

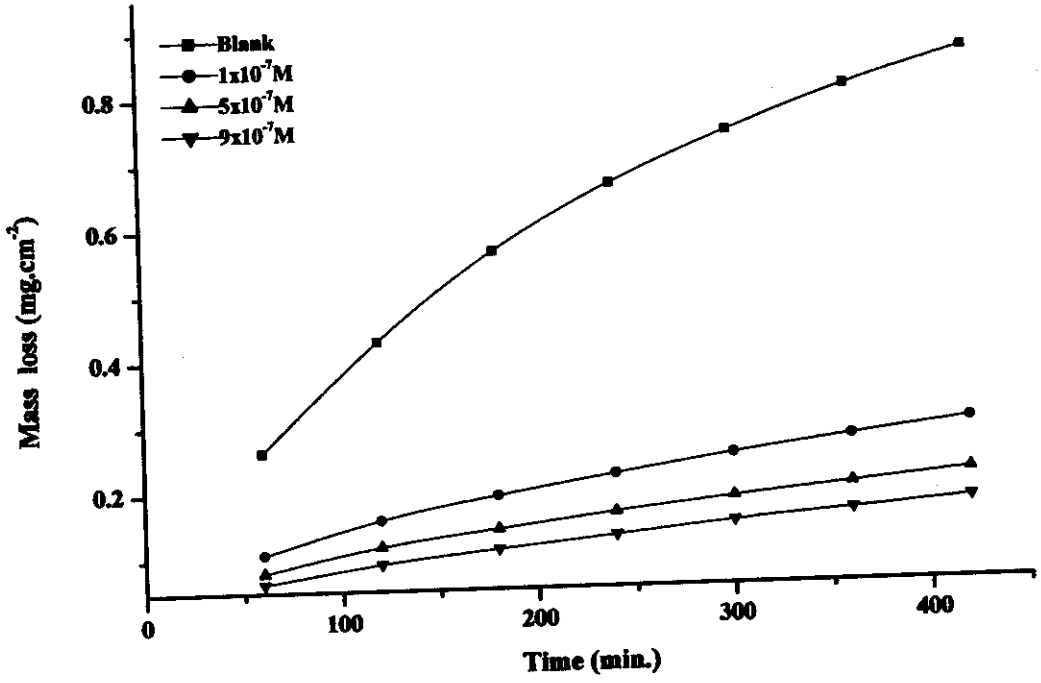

Fig. (3.34): Mass loss-time curves of 430SS in 2M HCl in absence and presence of different concentrations of DB24C8 at 313K.

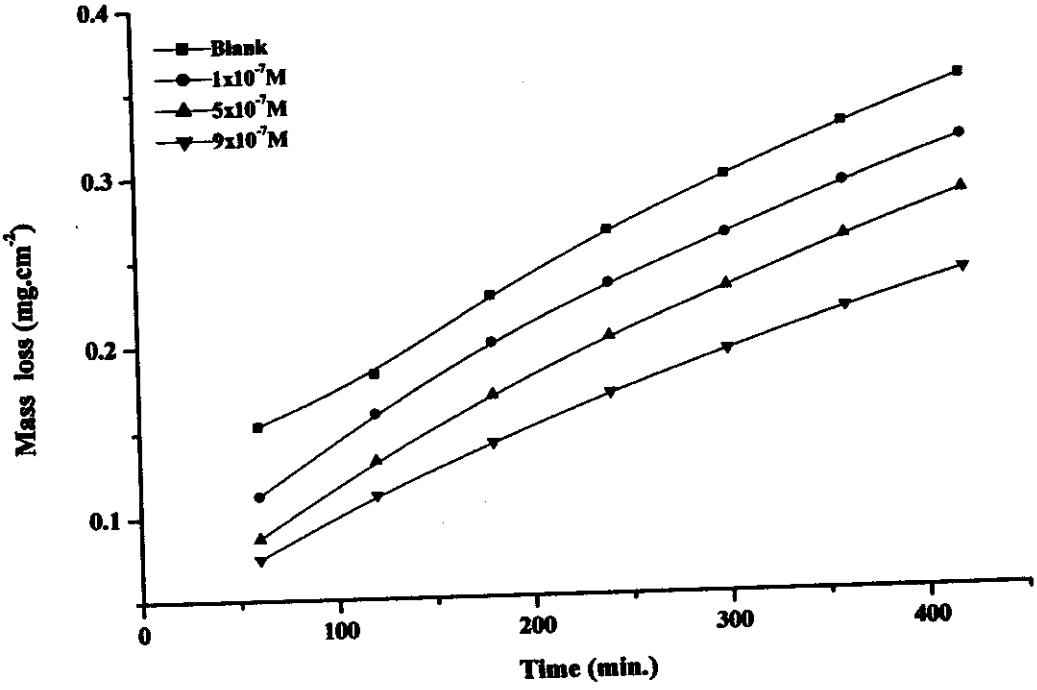

Fig. (3.35): Mass loss-time curves of 304SS in 2M HCl in absence and presence of different concentrations of DB18C6 at 313K.

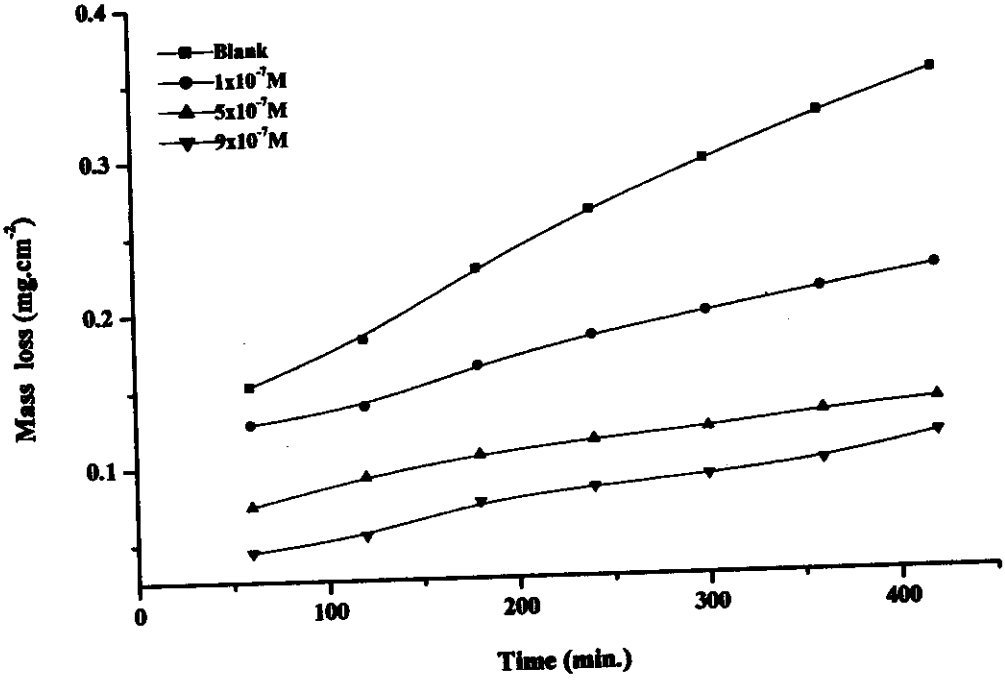

Fig. (3.36): Mass loss-time curves of 304SS in 2M HCl in absence and presence of different concentrations of Kry-22DD at 313K.

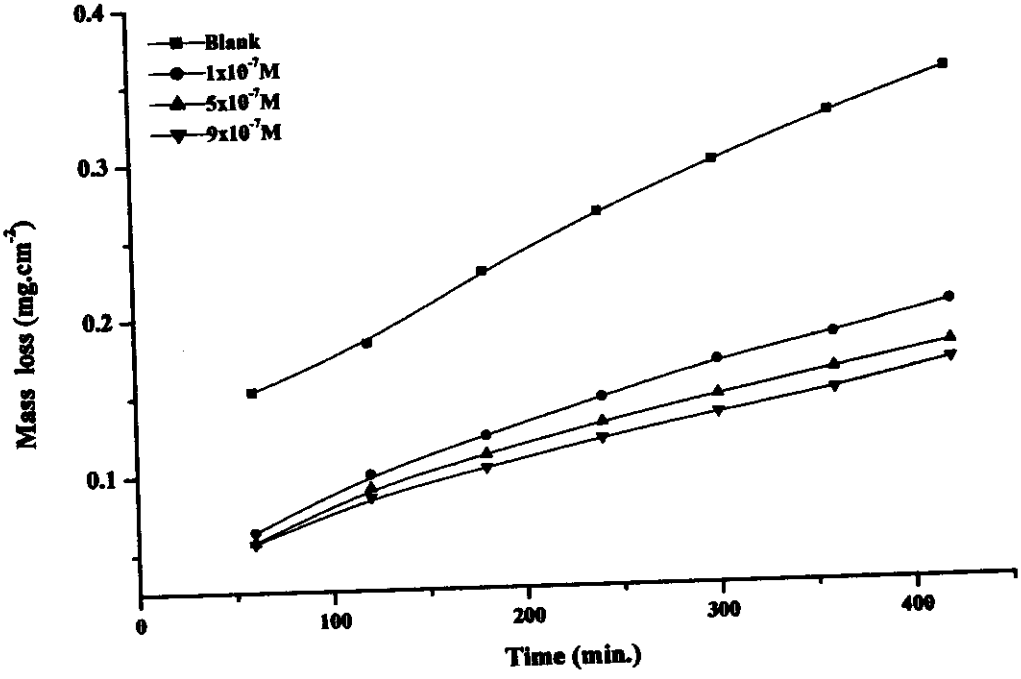

Fig. (3.37): Mass loss-time curves of 304SS in 2M HCl in absence and presence of different concentrations of Kry-222 at 313K.

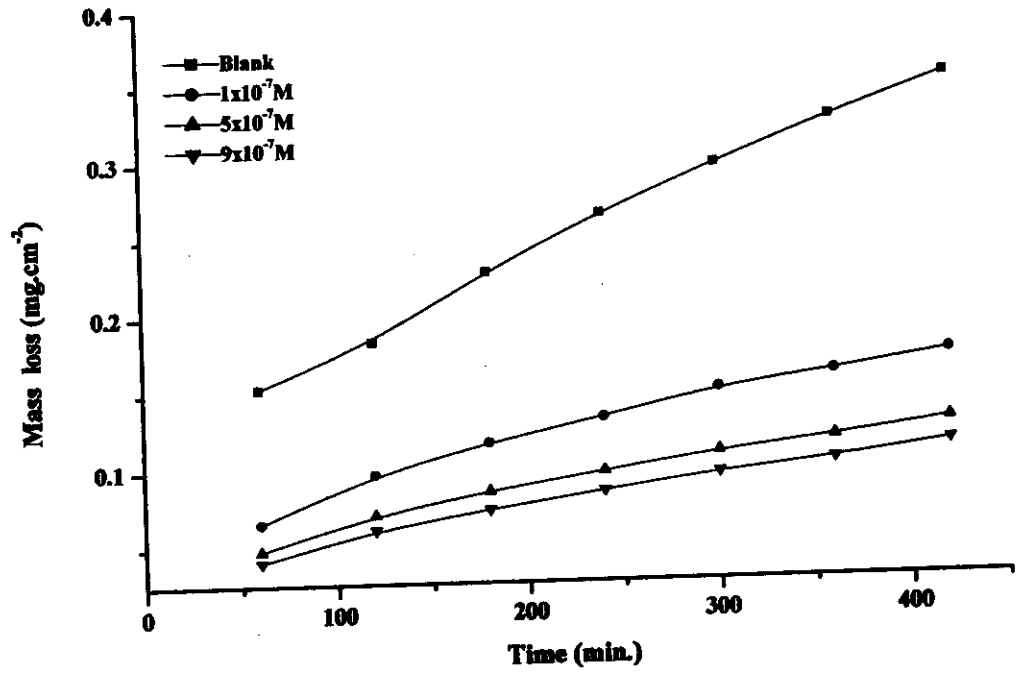

Fig. (3.38): Mass loss-time curves of 304SS in 2M HCl in absence and presence of different concentrations of DB24C8 at 313K.

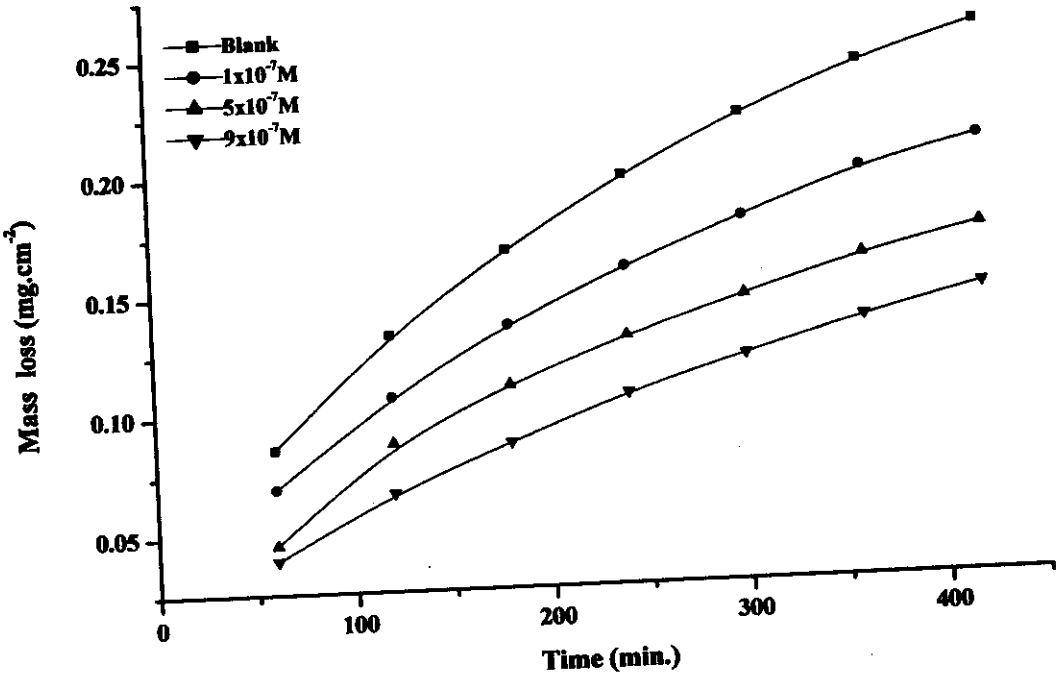

Fig. (3.39): Mass loss-time curves of 316SS in 2M HCl in absence and presence of different concentrations of DB18C6 at 313K.

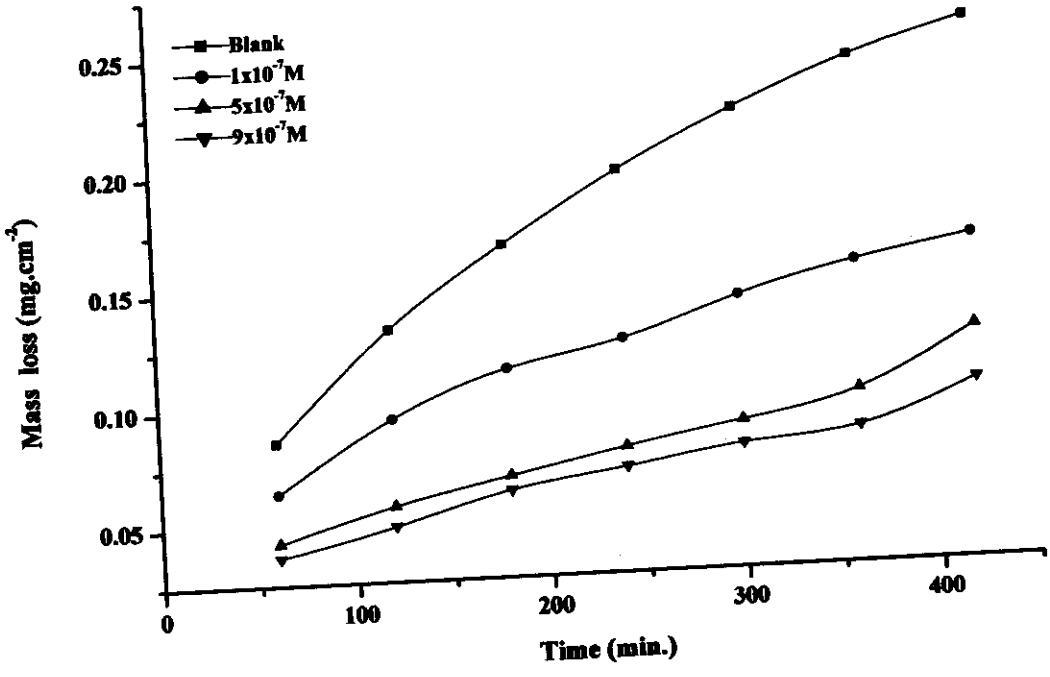

Fig. (3.40): Mass loss-time curves of 316SS in 2M HCl in absence and presence of different concentrations of Kry-22DD at 313K.

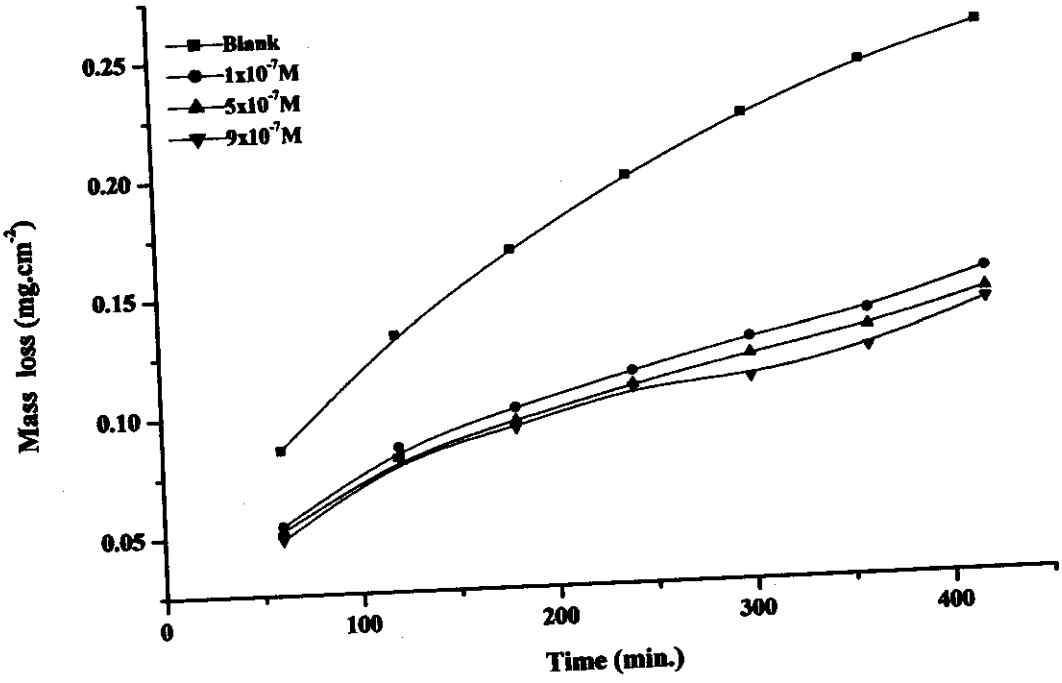

Fig. (3.41): Mass loss-time curves of 316SS in 2M HCl in absence and presence of different concentrations of Kry-222 at 313K.

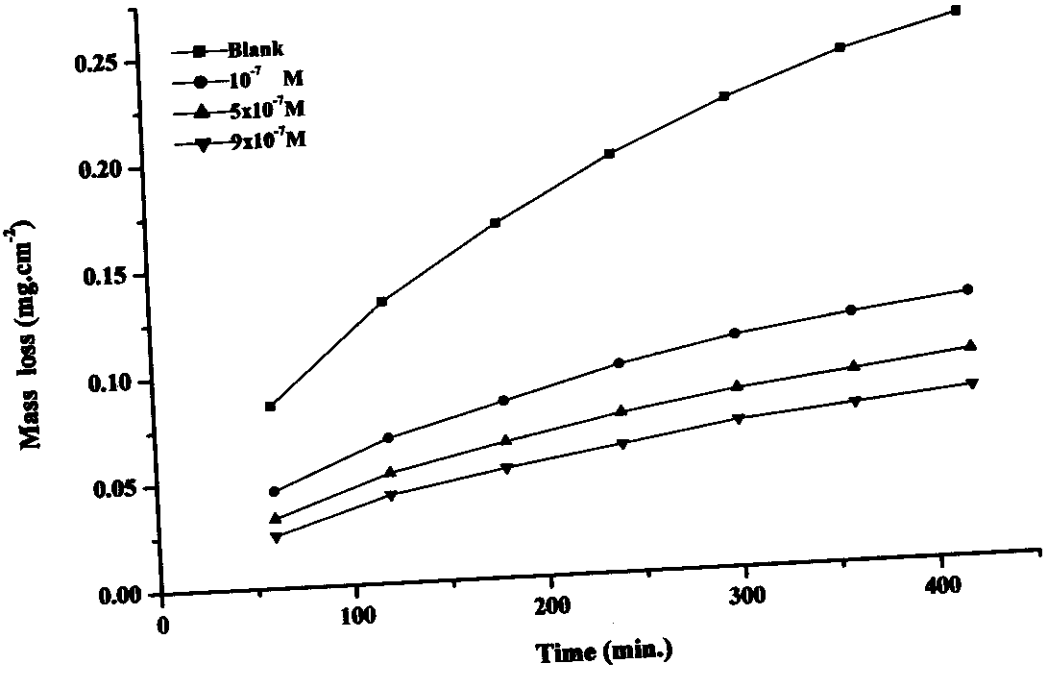

Fig. (3.42): Mass loss-time curves of 316SS in 2M HCl in absence and presence of different concentrations of DB24C8 at 313K.

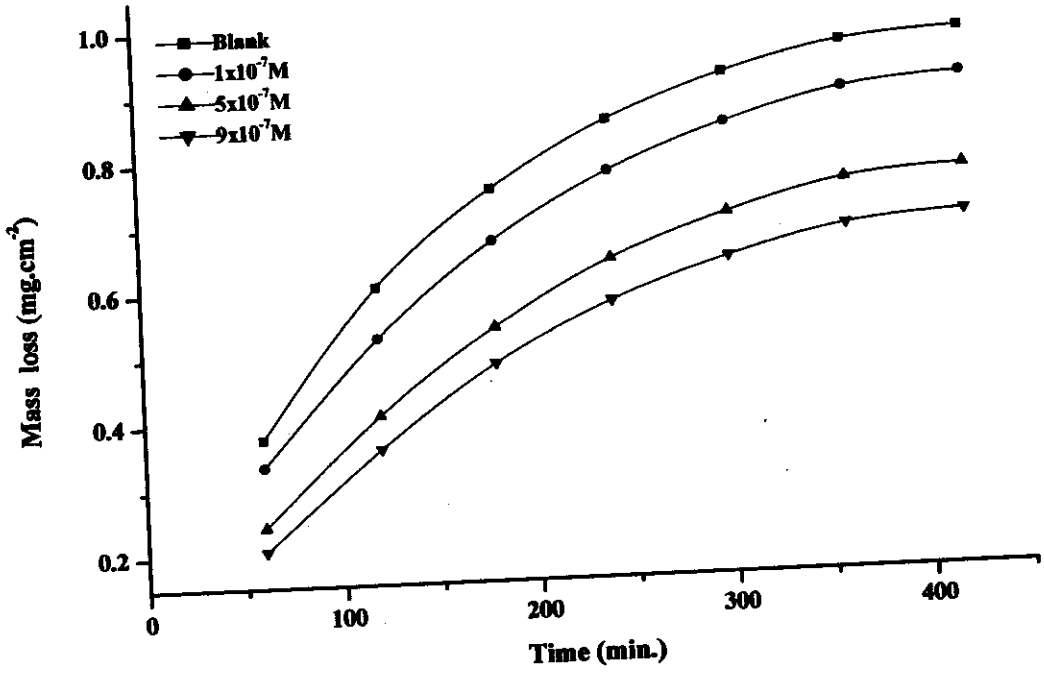

Fig. (3.43): Mass loss-time curves of 430SS in 2M HCl in absence and presence of different concentrations of DB18C6 323K.

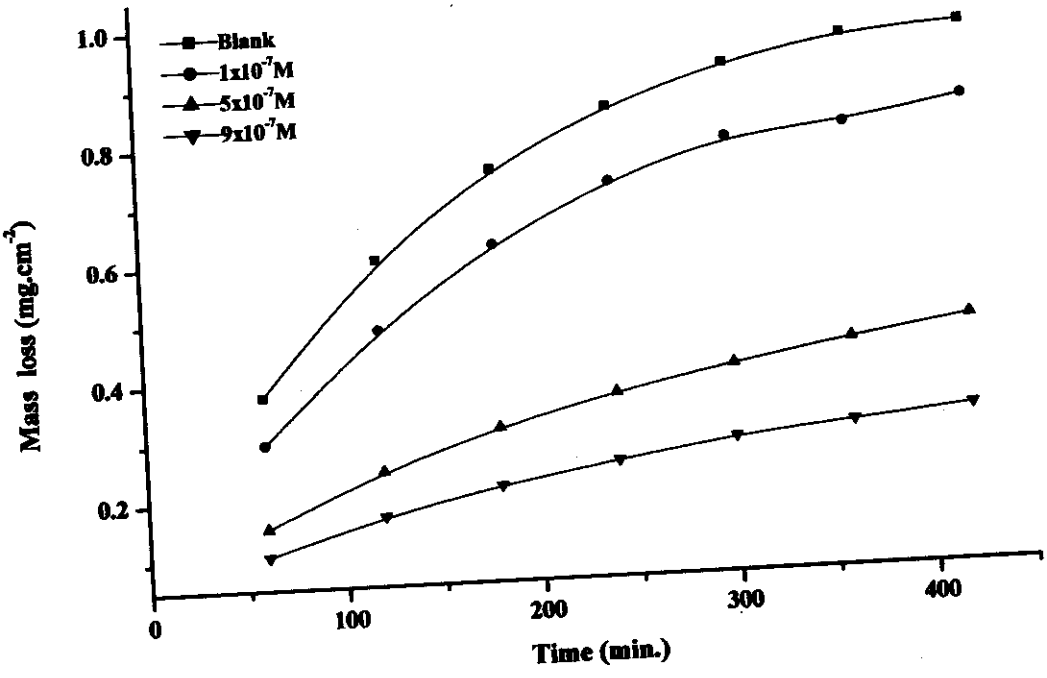

Fig. (3.44): Mass loss-time curves of 430SS in 2M HCl in absence and presence of different concentrations of Kry-22DD 323K.

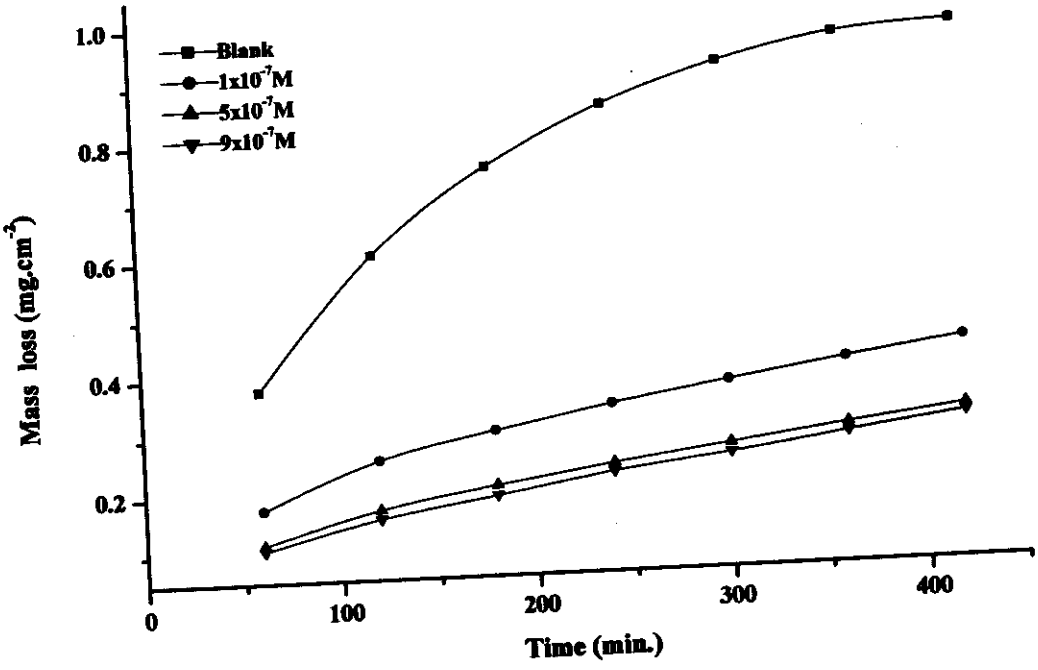

Fig. (3.45): Mass loss-time curves of 430SS in 2M HCl in absence and presence of different concentrations of Kry-222 323K.

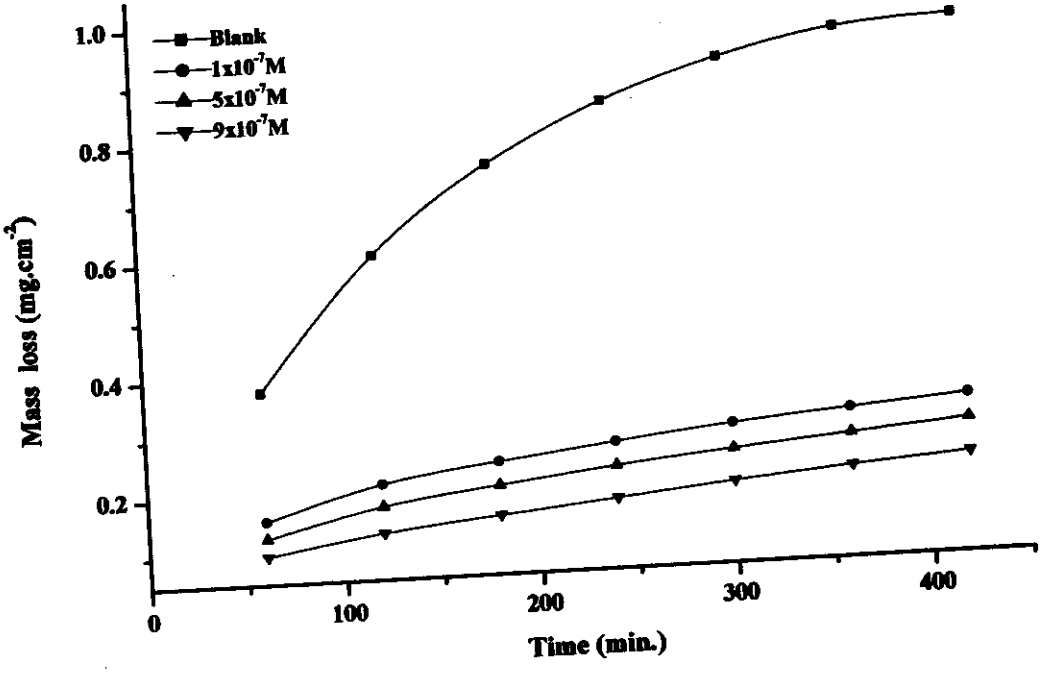

Fig. (3.46): Mass loss-time curves of 430SS in 2M HCl in absence and presence of different concentrations of DB24C8 323K.

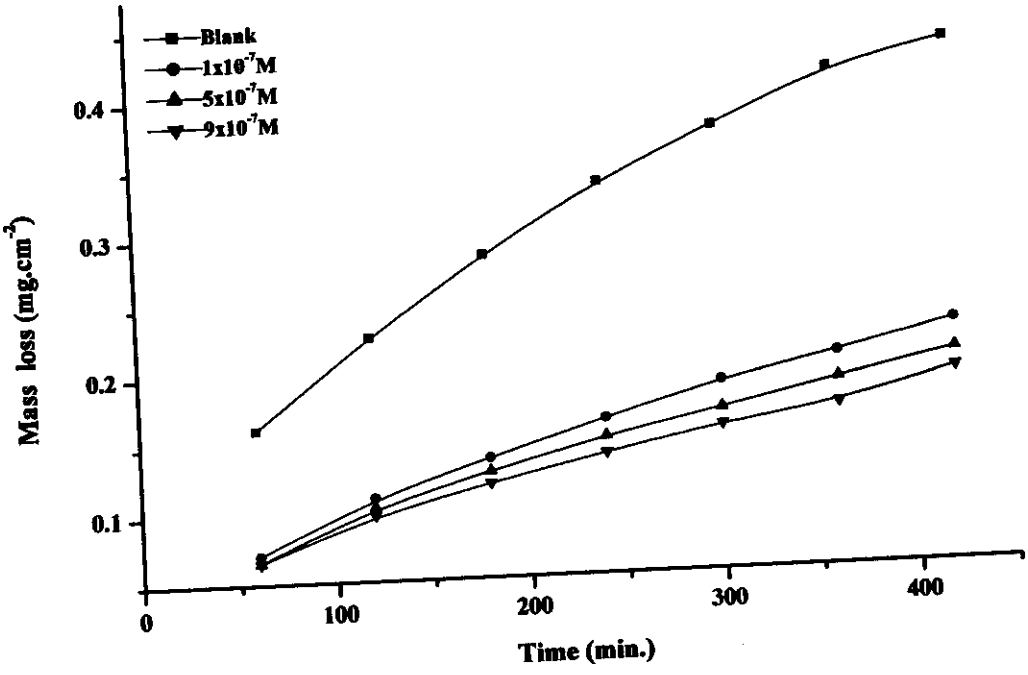

Fig. (3.49): Mass loss-time curves of 304SS in 2M HCl in absence and presence of different concentrations of Kry-222 at 323K.

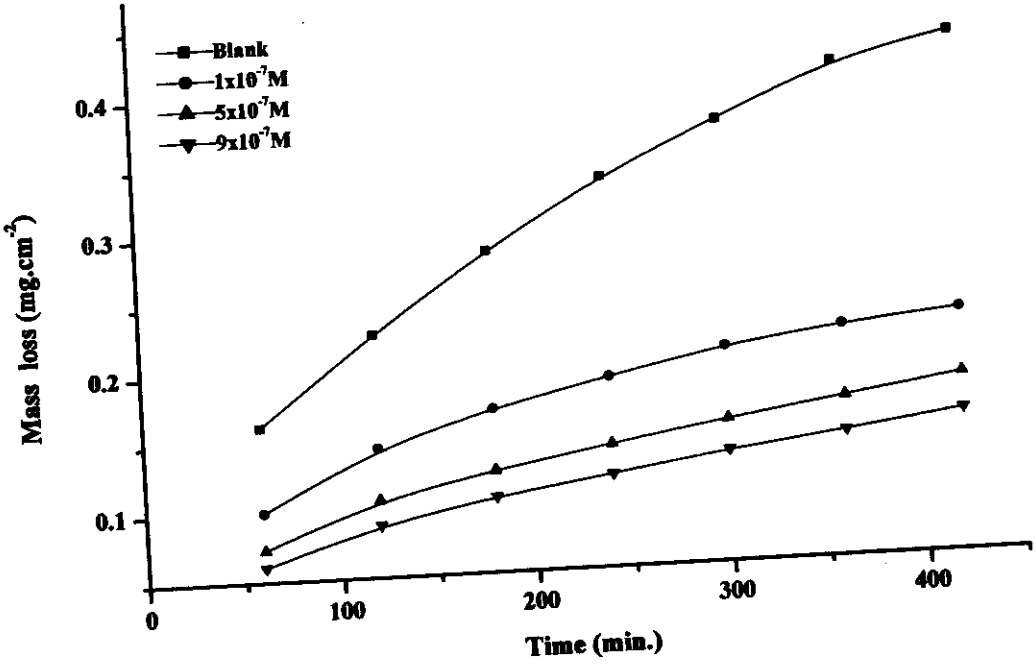

Fig. (3.50): Mass loss-time curves of 304SS in 2M HCl in absence and presence of different concentrations of DB24C8 at 323K.

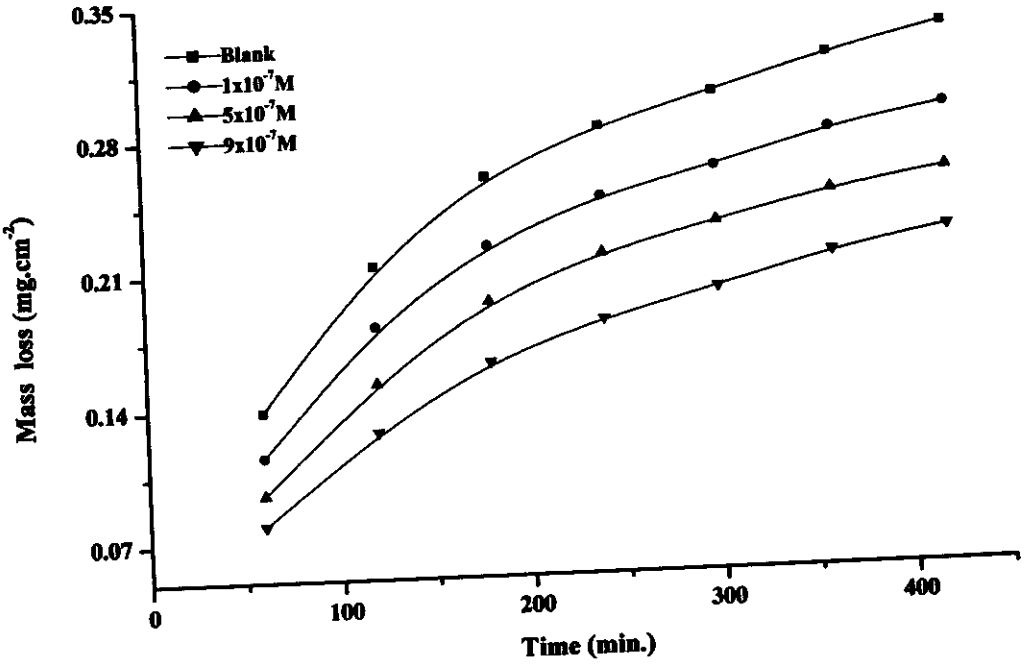

Fig. (3.51): Mass loss-time curves of 316SS in 2M HCl in absence and presence of different concentrations of DB18C6 at 323K.

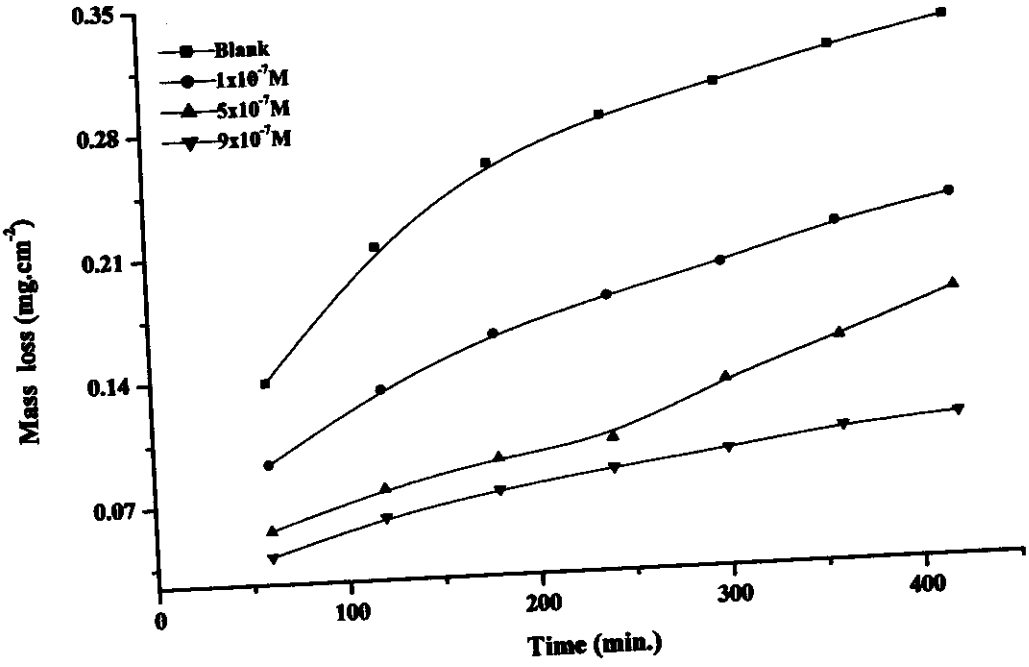

Fig. (3.52): Mass loss-time curves of 316SS in 2M HCl in absence and presence of different concentrations of Kry-22DD at 323K.

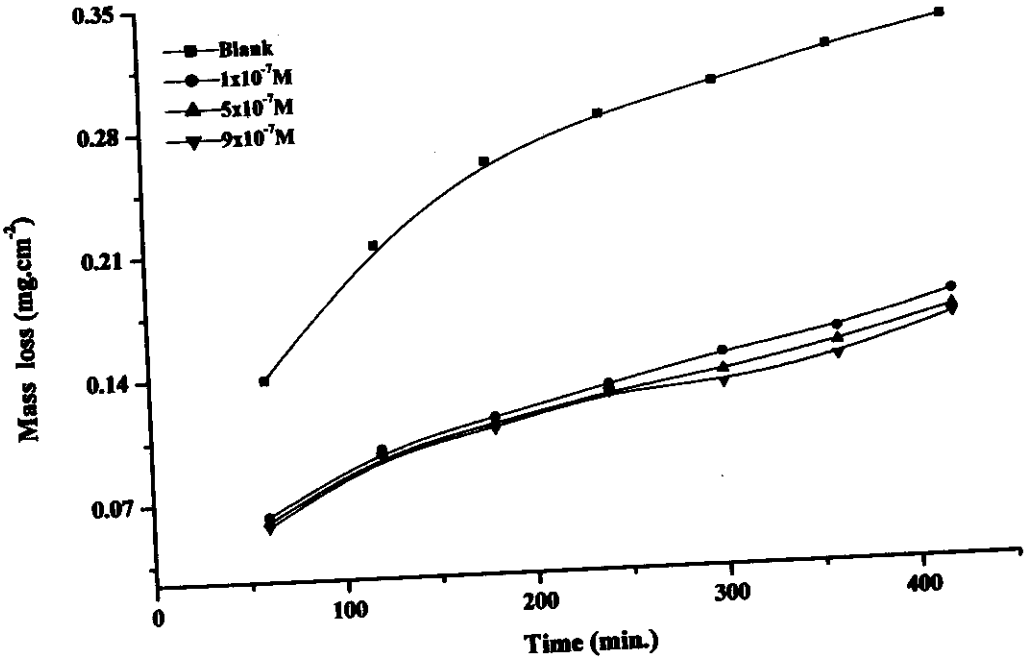

Fig. (3.53): Mass loss-time curves of 316SS in 2M HCl in absence and presence of different concentrations of Kry-222 at 323K.

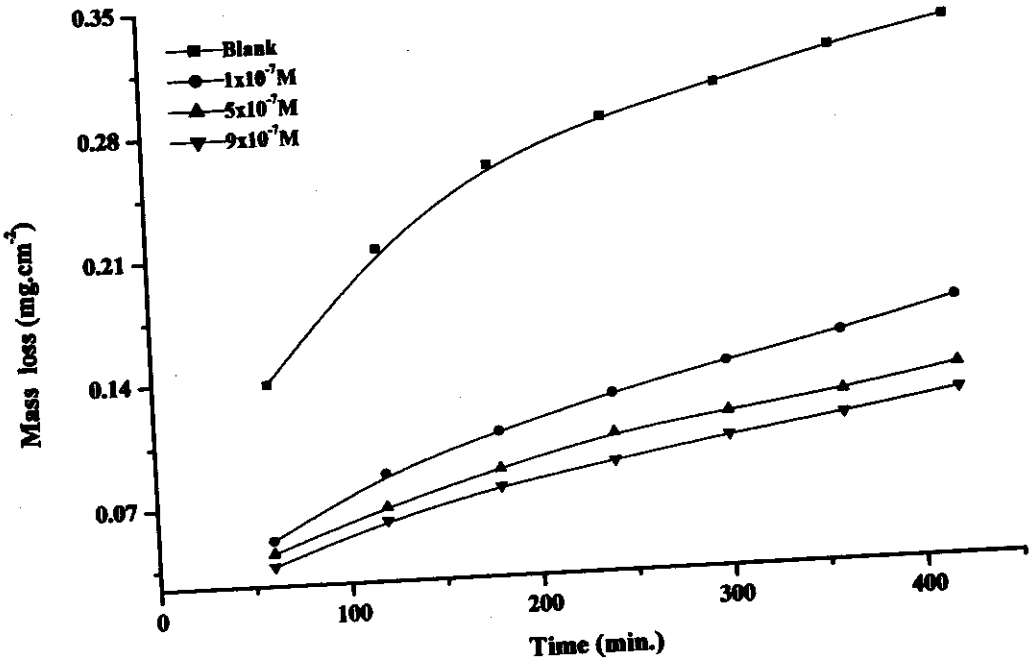

Fig. (3.54): Mass loss-time curves of 316SS in 2M HCl in absence and presence of different concentrations of DB24C8 at 323K.

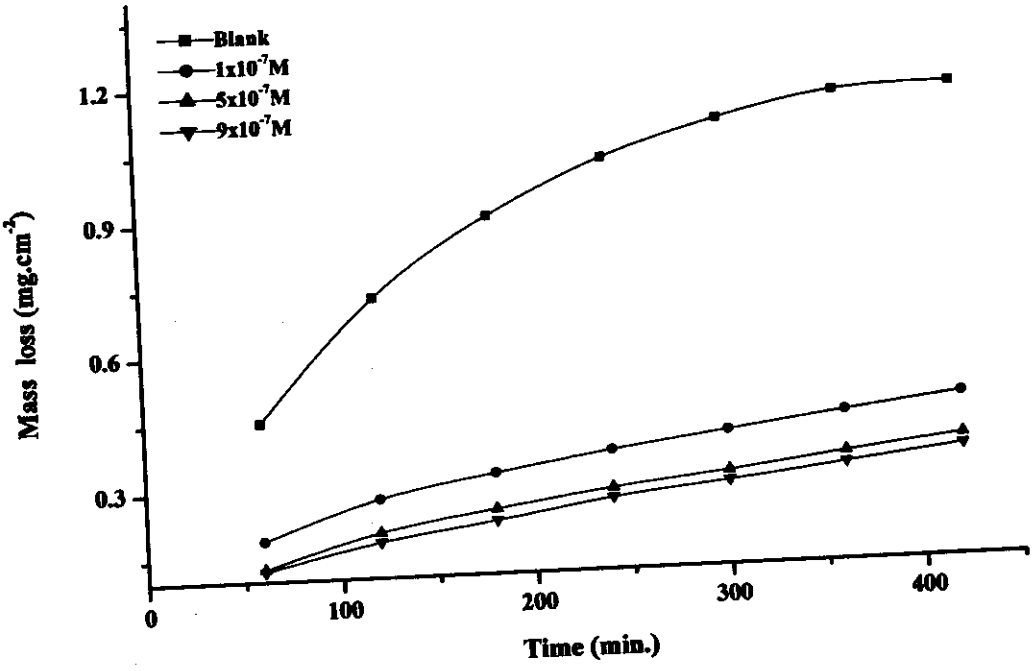

Fig. (3.57): Mass loss-time curves of 430SS in 2M HCl in absence and presence of different concentrations of Kry-222 at 333K.

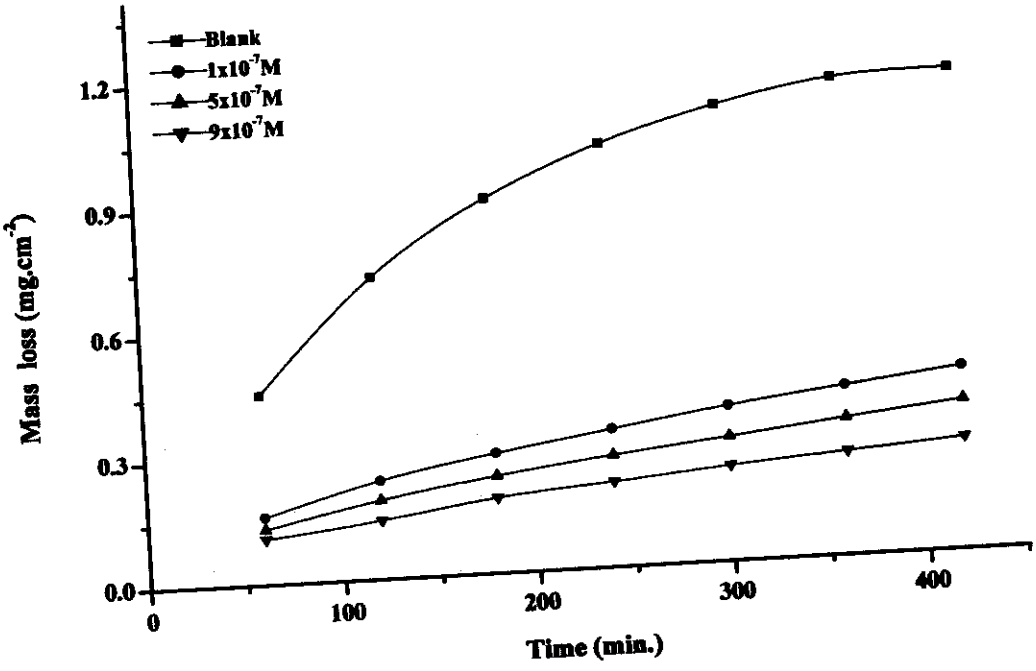

Fig. (3.58): Mass loss-time curves of 430SS in 2M HCl in absence and presence of different concentrations of DB24C8 at 333K.

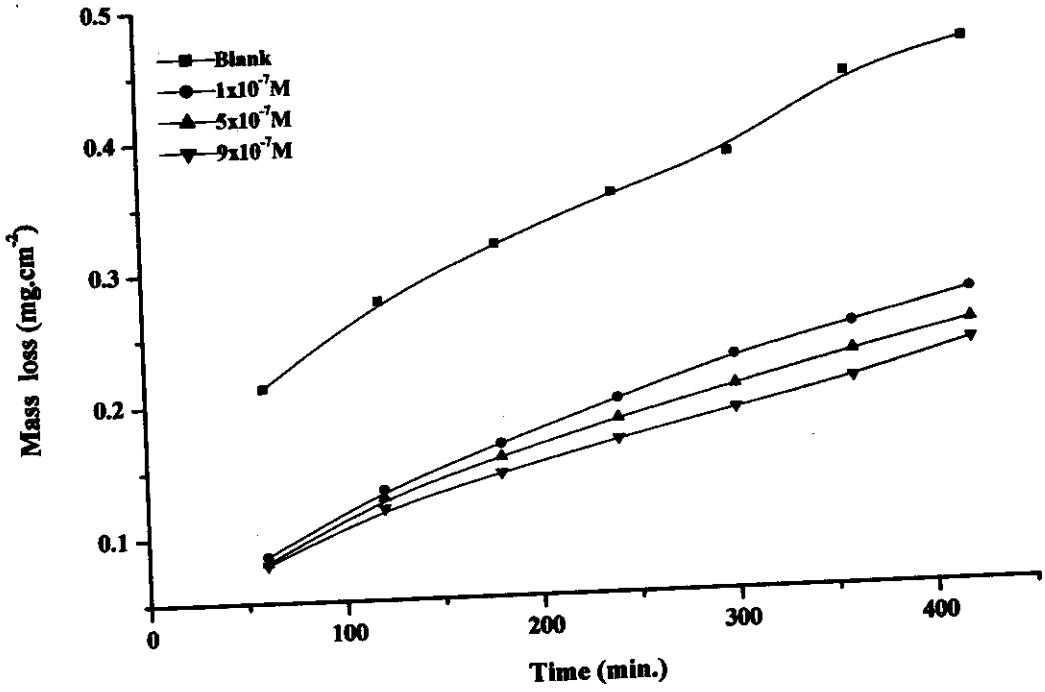

Fig. (3.61): Mass loss-time curves of 304SS in 2M HCl in absence and presence of different concentrations of Kry-222 at 333K.

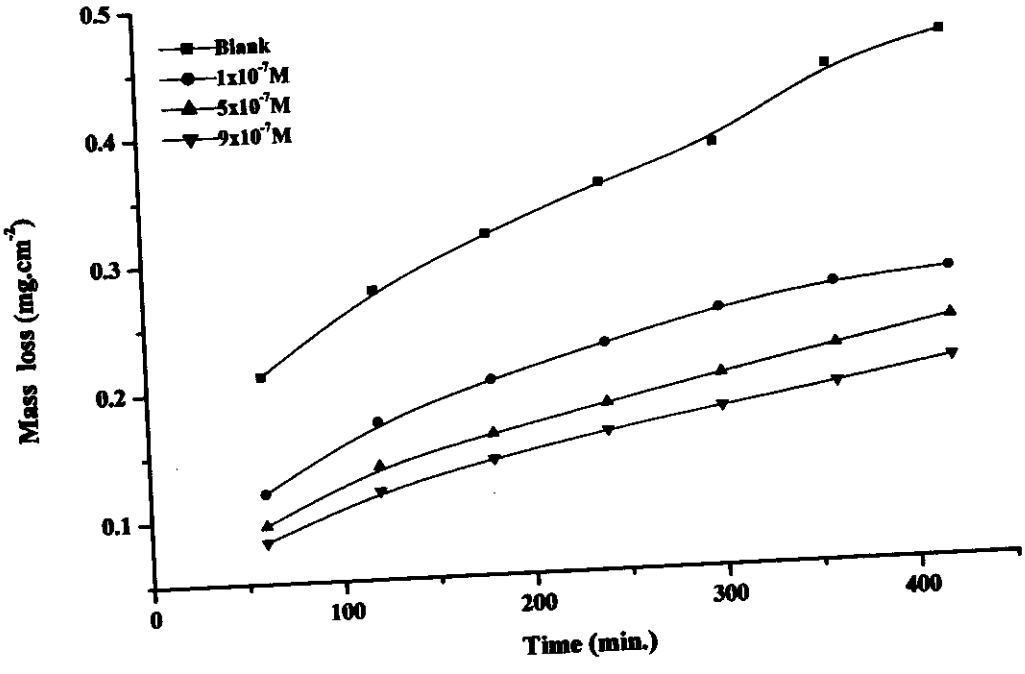

Fig. (3.62): Mass loss-time curves of 304SS in 2M HCl in absence and presence of different concentrations of DB24C8 at 333K.

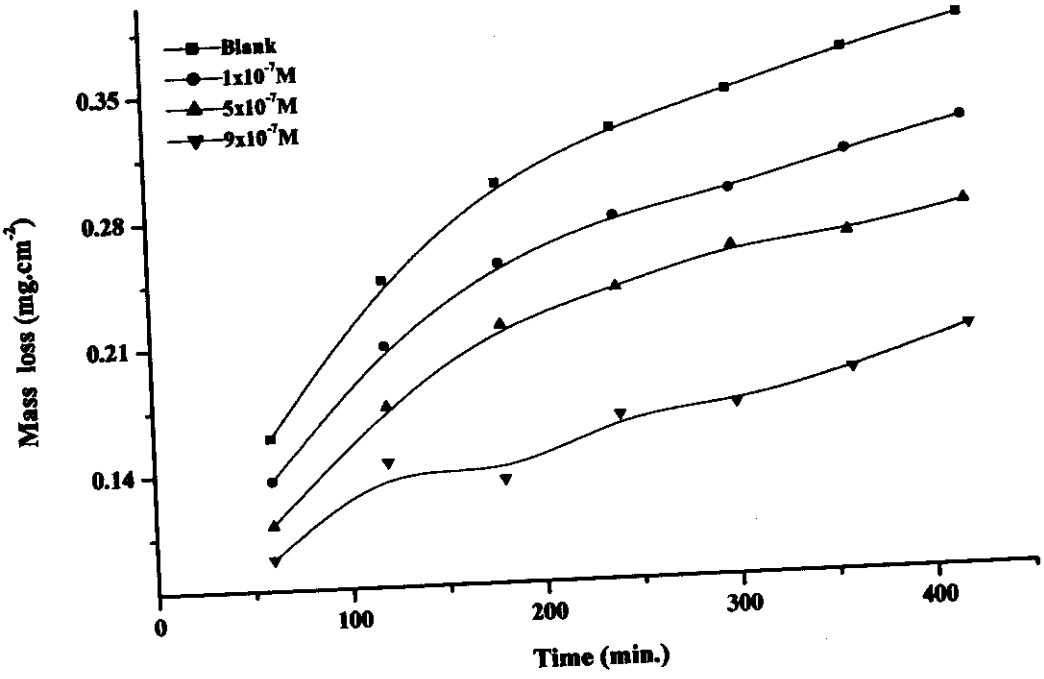

Fig. (3.63): Mass loss-time curves of 316SS in 2M HCl in absence and presence of different concentrations of DB18C6 at 333K.

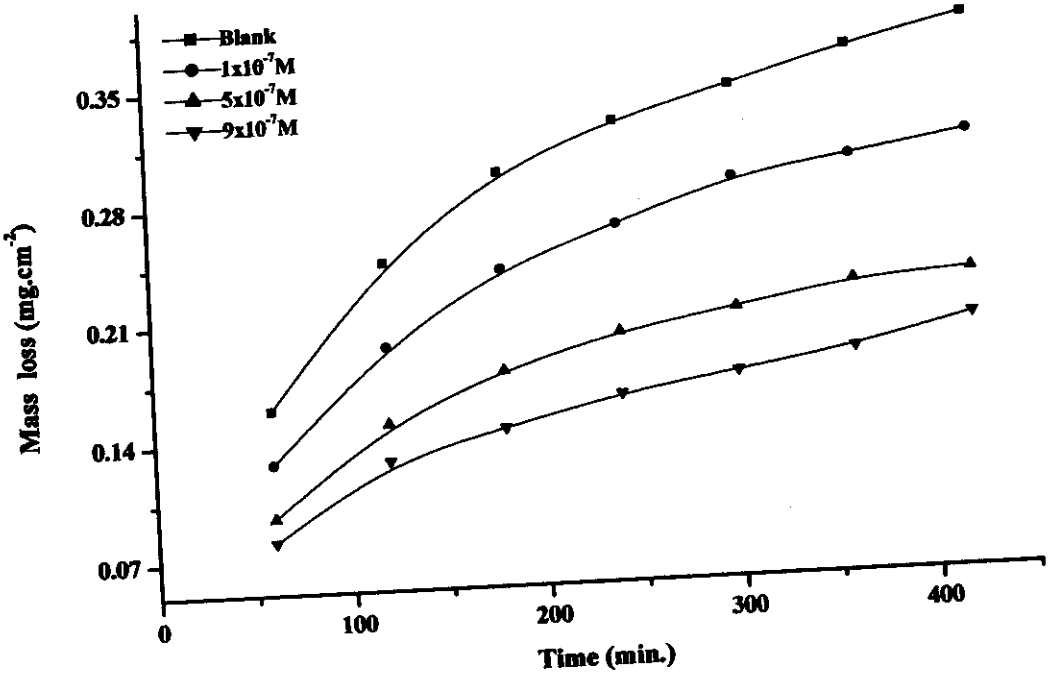

Fig. (3.64): Mass loss-time curves of 316SS in 2M HCl in absence and presence of different concentrations of Kry-22DD at 333K.

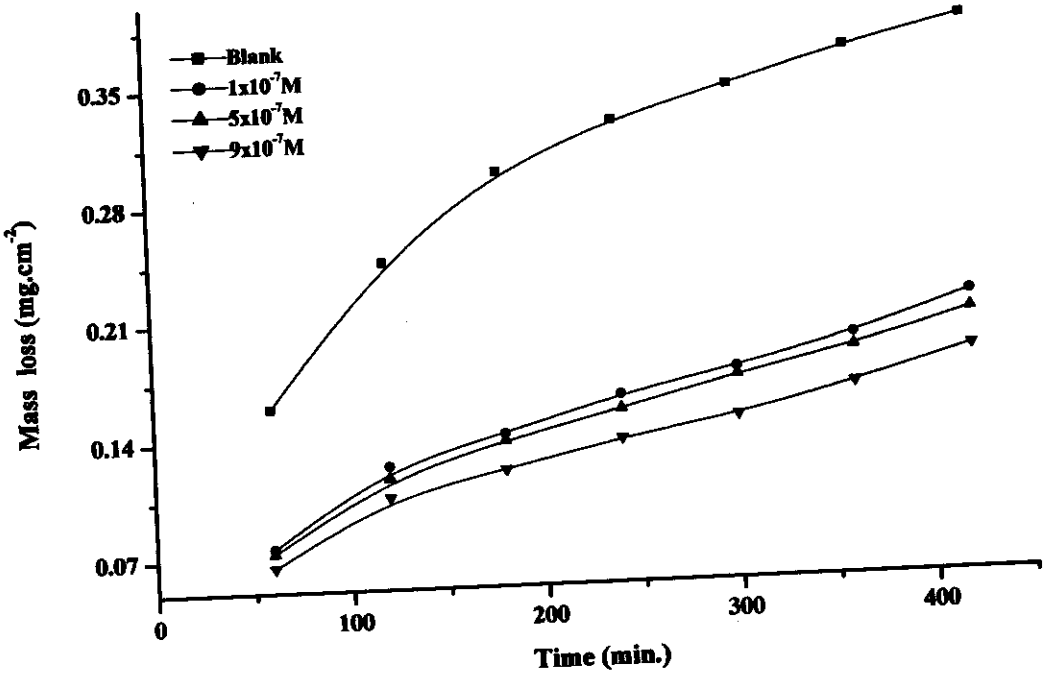

Fig. (3.65): Mass loss-time curves of 316SS in 2M HCl in absence and presence of different concentrations of Kry-222 at 333K.

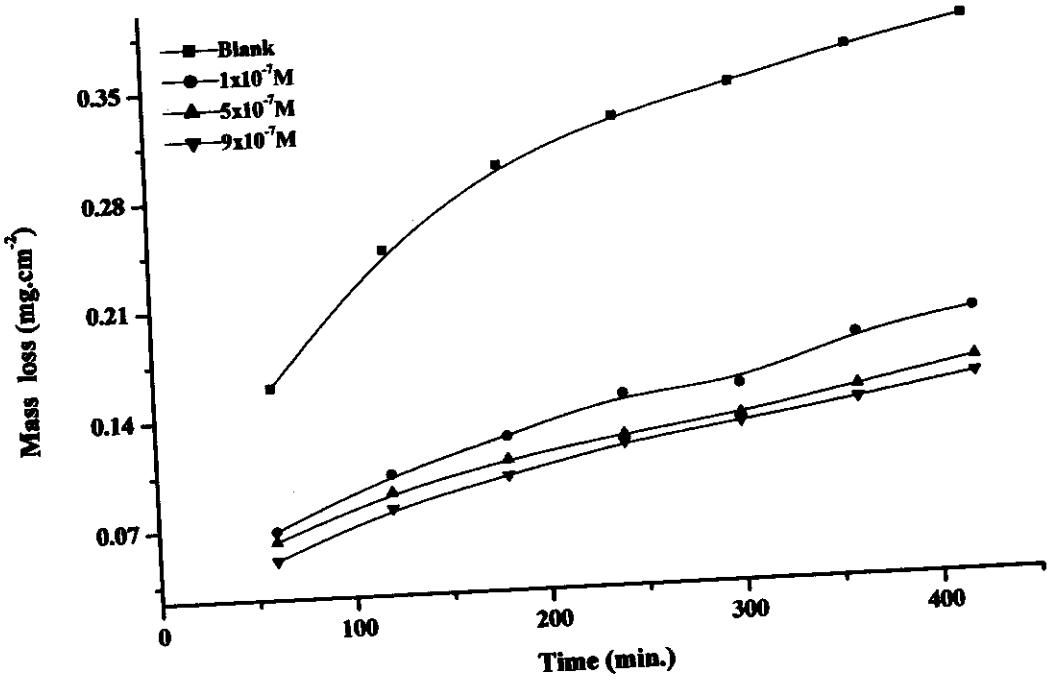

Fig. (3.66): Mass loss-time curves of 316SS in 2M HCl in absence and presence of different concentrations of DB24C8 at 333K.

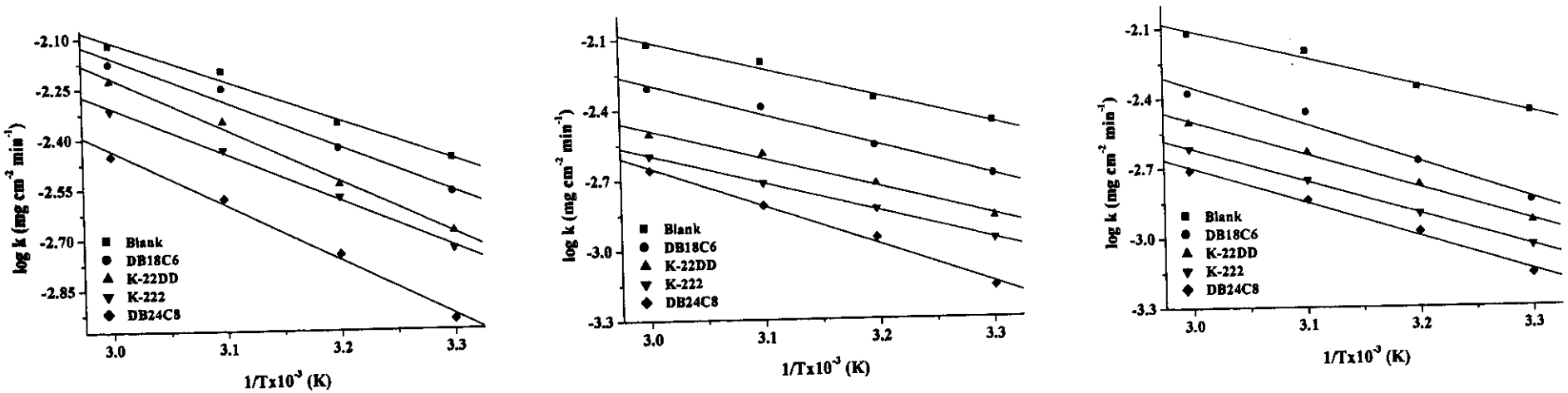

Fig. (3.67): log. corrosion rate vs. 1/T of 430SS in 2M HCl in absence and presence of 10^{-7} M (I), $5x10^{-7}$ M (II) and $9x10^{-7}$ M (III) of different types of crown ethers.

Table (3.5): Thermodynamic activation parameters (ΔG^*, ΔH^* in KJ mol^{-1} & ΔS^* in J mol^{-1}) of 430SS dissolution in 2M HCl in presence of different concentrations of crown ethers at different temperatures.

(I) DB18C6									
Temperature (K)	$1x10^{-7}$ M			$5x10^{-7}$ M			$9x10^{-7}$ M		
	ΔG^*	ΔH^*	$-\Delta S^*$	ΔG^*	ΔH^*	$-\Delta S^*$	ΔG^*	ΔH^*	$-\Delta S^*$
303	83.27	33.50	164.3	84.24	35.61	160.5	84.69	40.13	147.1
313	85.97	33.42	167.9	86.75	35.53	163.5	87.44	40.05	151.4
323	88.21	33.34	169.9	89.07	35.45	166.0	89.51	39.97	153.4
333	90.96	33.25	173.3	91.80	35.36	169.5	92.25	39.88	157.3
(II) Kry-22DD									
Temperature (K)	$1x10^{-7}$ M			$5x10^{-7}$ M			$9x10^{-7}$ M		
	ΔG^*	ΔH^*	$-\Delta S^*$	ΔG^*	ΔH^*	$-\Delta S^*$	ΔG^*	ΔH^*	$-\Delta S^*$
303	83.99	43.76	132.8	85.18	42.77	140.0	85.71	47.81	125.1
313	86.61	43.68	137.2	87.51	42.69	143.2	88.03	47.73	128.8
323	89.00	43.60	140.6	89.97	42.61	146.6	90.74	47.65	133.4
333	91.27	43.51	143.4	92.44	42.52	149.9	92.77	47.56	135.8
(III) Kry-222									
Temperature (K)	$1x10^{-7}$ M			$5x10^{-7}$ M			$9x10^{-7}$ M		
	ΔG^*	ΔH^*	$-\Delta S^*$	ΔG^*	ΔH^*	$-\Delta S^*$	ΔG^*	ΔH^*	$-\Delta S^*$
303	84.54	44.95	130.7	86.08	47.31	128.0	86.62	52.75	111.8
313	87.07	44.87	134.8	88.19	47.23	130.9	88.55	52.67	114.6
323	89.35	44.79	138.0	90.66	47.15	134.7	91.30	52.59	119.9
333	91.82	44.70	141.5	93.19	47.06	138.5	93.53	52.50	123.2
(IV) DB24C8									
Temperature (K)	$1x10^{-7}$ M			$5x10^{-7}$ M			$9x10^{-7}$ M		
	ΔG^*	ΔH^*	$-\Delta S^*$	ΔG^*	ΔH^*	$-\Delta S^*$	ΔG^*	ΔH^*	$-\Delta S^*$
303	85.47	47.07	126.7	86.56	50.47	119.1	87.08	54.68	106.9
313	87.85	46.99	130.6	88.97	50.39	123.3	89.22	54.60	110.6
323	90.22	46.91	134.1	91.21	50.31	126.7	91.51	54.52	114.5
333	92.65	46.82	137.6	93.63	50.22	130.3	94.09	54.43	119.1

SECTION (B)

3.2 Galvanostatic polarization.

Electrochemical techniques are based on current and potential measurements. According to the choice of the technique accurate and confidential data, concerning the corrosion process can be obtained. Addition of inhibitor modifies the changes of the response obtained in the test solution.

In this method, corrosion current ($I_{corr.}$) can be determined from polarization curves by intercept method based on anodic and/or cathodic Tafel curves. The corrosion rate of the system involves the measurements of potential of the working electrode for various applied current densities.

Figures (3.70-3.81) represent the galvanostatic polarization curves (Tafel plots) of the investigated stainless steels in 2M HCl in absence and presence of different concentrations of crown ethers at 303K. The intercept of anodic and cathodic Tafel lines provides the corrosion current ($I_{corr.}$) and their slopes give anodic (β_a) and cathodic (β_c) Tafel constants. The degree of surface coverage (θ) and percentage inhibition efficiency (%IE) are given by using the following equations: [16]

$$\theta = 1 - \frac{I_{inh.}}{I_{free}} \qquad (3.13)$$

$$\%IE = \left(1 - \frac{I_{inh.}}{I_{free}}\right) x\,100 \qquad (3.14)$$

where, $I_{inh.}$ and I_{free} are the corrosion current densities in presence and absence of crown ethers, respectively.

The numerical values of the variation of corrosion current density ($I_{corr.}$), corrosion potential ($E_{corr.}$), Tafel slopes (β_a & β_c), degree of surface coverage (θ) and percentage inhibition efficiency (%IE) of different types of stainless steels in 2M HCl at 303K in absence and presence of different concentrations of crown ethers can be depicted from Tables (3.8-3.19).

The values of corrosion potential, for 430SS, 304SS and 316SS stainless steels in 2M HCl at 303K in absence of crown ethers (Tables: 3.8-3.16), are found to be, (-473) mV, (-462) mV and (-449) mV successively. Firstly, the above mentioned values indicated that the corrosion potential depends upon the composition of stainless steels. Moreover, the above mentioned values agree with the work of Cheng et. al. [99], who found that the corrosion potential ($E_{corr.}$), of 430SS in 0.5 M H_2SO_4 is (-565) mV, and by Sozhan [24], who found that the values of corrosion potential, for 304SS are (-292) mV, (-241) mV, (-261) mV and (-264) mV in 15% NaCl, 45% $NaClO_3$, 0.3% NaOCl and in synthetic cell liquor, respectively. Also, the same author found that the (E_{corr}) values for 316SS are (-279) mV, (-238) mV, (-261) mV and (-267) mV in the same above mentioned aqueous solutions, respectively. So, one conclude that E_{corr} depends upon the type and the concentration of the corrosive medium. Wholly, all the results achieved in Tables (3.8-3.19) are permitted to conclude that:

1) Galvanostatic anodic and cathodic polarization curves for all types of stainless steel exhibit Tafel behavior.

2) Addition of crown ethers caused a shift in both cathodic and anodic polarization curves towards the lower current density region.

3) It is obvious that, by increasing the concentration of crown ethers, both the cathodic and anodic overvoltages were increased and parallel displacement to the more negative and positive values were obtained, respectively. Thus Tafel plots suggested that the crown ethers enhance both anodic and cathodic reactions and are mixed type inhibitors, but the cathode is more polarized when the external current was applied.

4) The corrosion current density values ($I_{corr.}$) decrease with increasing the concentration of crown ethers, while the corrosion potential ($E_{corr.}$) values shift in positive direction. This indicated that the presence of these compounds retards the dissolution of the investigated stainless steels.

5) The Tafel slope values do not change significantly in acidic solutions in presence of these compounds, suggesting that these compounds inhibit the

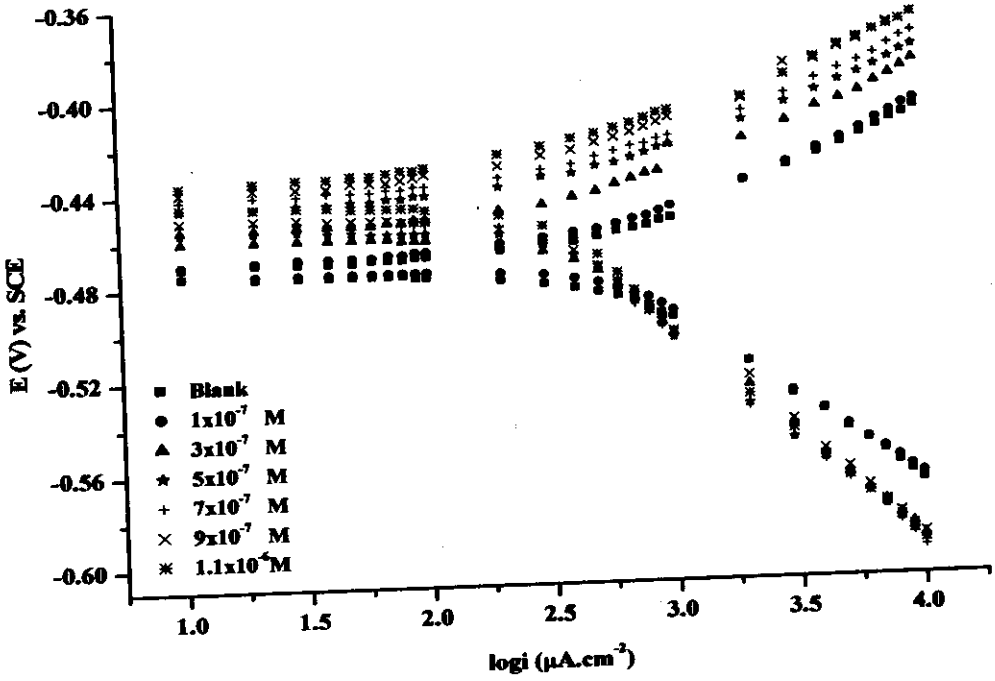

Fig. (3.70): Tafel plot of 430SS in 2MHCl in absence and presence of different concentrations of DB18C6 at 303K.

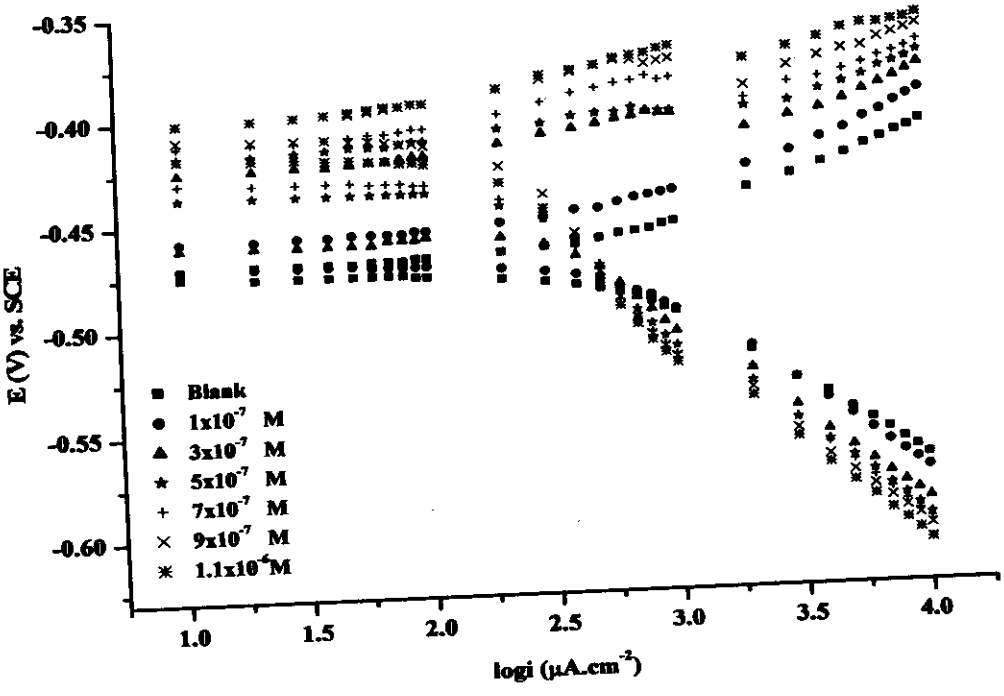

Fig. (3.71): Tafel plot of 430SS in 2MHCl in absence and presence of different concentrations of K-22DD at 303K.

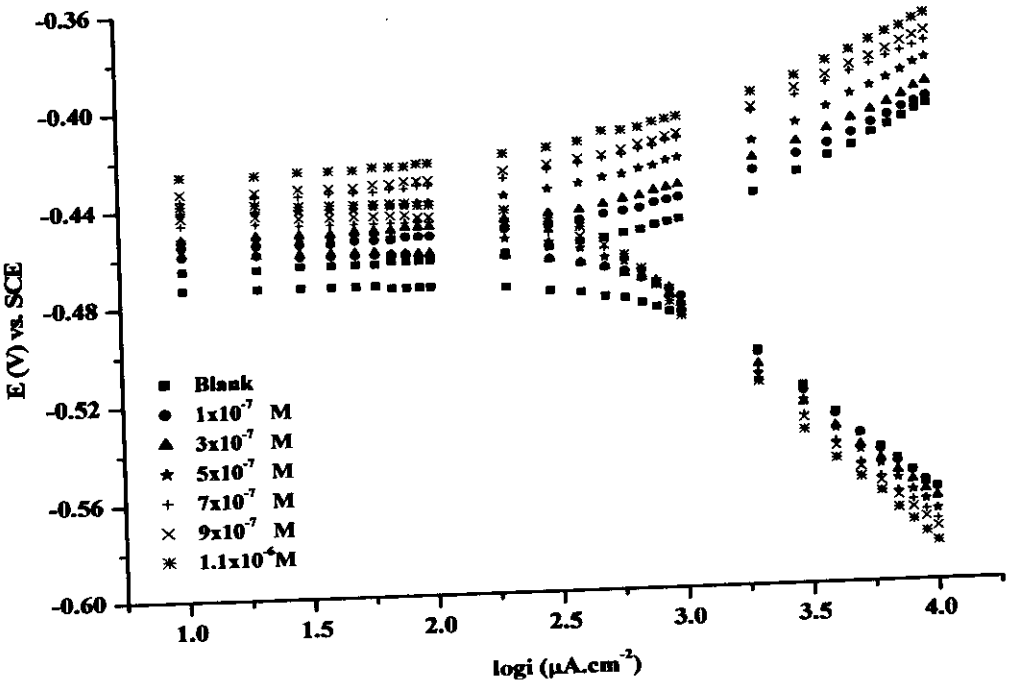

Fig. (3.74): Tafel plot of 304SS in 2MHCl in absence and presence of different concentrations of DB18C6 at 303K.

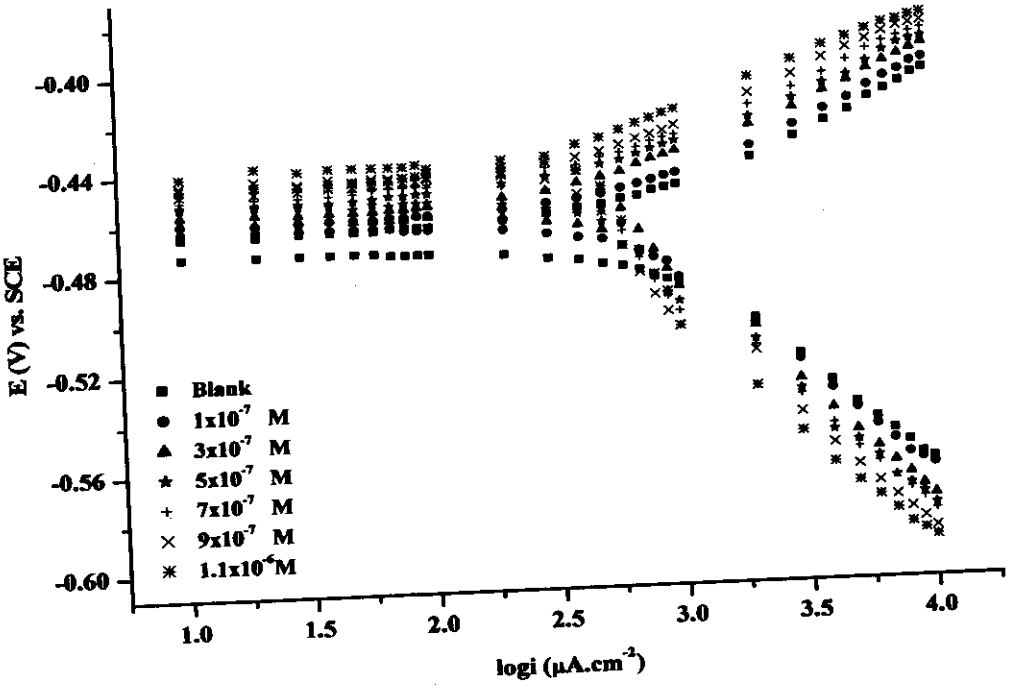

Fig. (3.75): Tafel plot of 304SS in 2MHCl in absence and presence of different concentrations of K-22DD at 303K.

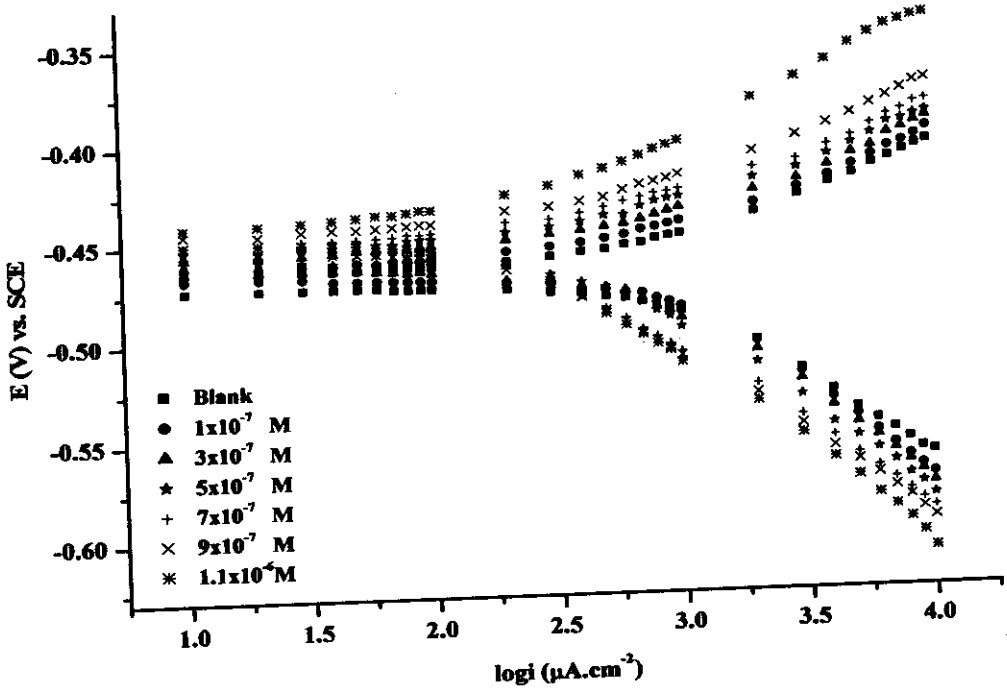

Fig. (3.76): Tafel plot of 304SS in 2MHCl in absence and presence of different concentrations of K-222 at 303K.

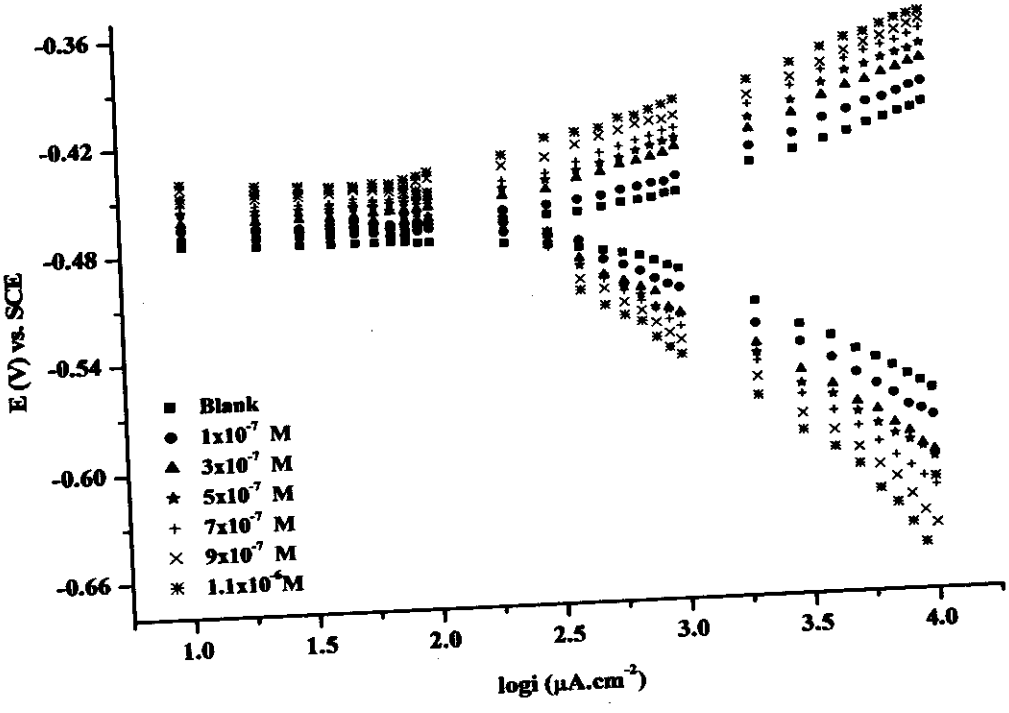

Fig. (3.77): Tafel plot of 304SS in 2MHCl in absence and presence of different concentrations of DB24C8 at 303K.

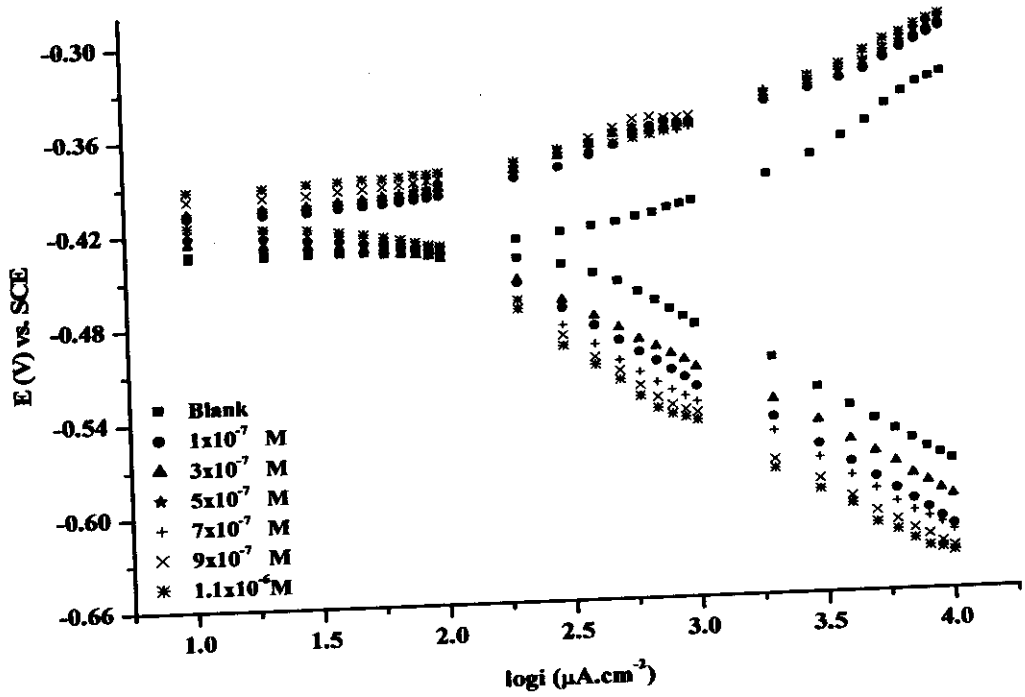

Fig. (3.80): Tafel plot of 316SS in 2MHCl in absence and presence of different concentrations of K-222 at 303K.

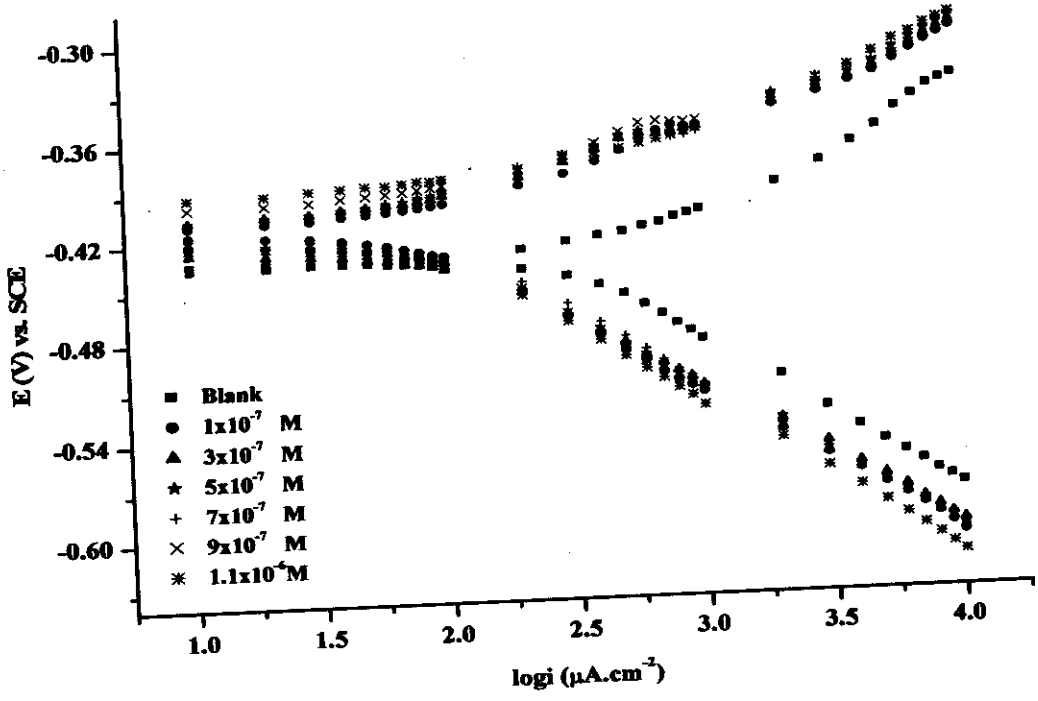

Fig. (3.81): Tafel plot of 316SS in 2MHCl in absence and presence of different concentrations of DB24C8 at 303K.

Table (3.10): Effect of K-222 concentrations on the corrosion potential (E_{corr}), corrosion current density ($I_{corr.}$), Tafel slopes (β_a & β_c), degree of surface coverage (θ) and percentage inhibition efficiency (%IE) of 430SS in 2M HCl at 303K.

concentration (M)	$-E_{corr}$ (mV)	$I_{corr.}$ ($\mu A\ cm^{-2}$)	β_a ($mVdec^{-1}$)	β_c ($mVdec^{-1}$)	θ	%IE
Blank	473	560	51	74	---	---
$1x10^{-7}$	449	277	58	95	0.51	50.6
$3x10^{-7}$	444	240	56	95	0.57	57.1
$5x10^{-7}$	443	195	56	93	0.65	65.1
$7x10^{-7}$	444	191	57	94	0.66	65.9
$9x10^{-7}$	444	167	59	94	0.70	70.2
$1.1x10^{-6}$	443	148	56	95	0.74	73.5

Table (3.11): Effect of DB24C8 concentrations on the corrosion potential (E_{corr}), corrosion current density ($I_{corr.}$), Tafel slopes (β_a & β_c), degree of surface coverage (θ) and percentage inhibition efficiency (%IE) of 430SS in 2M HCl at 303K.

concentration (M)	$-E_{corr}$ (mV)	$I_{corr.}$ ($\mu A\ cm^{-2}$)	β_a ($mVdec^{-1}$)	β_c ($mVdec^{-1}$)	θ	%IE
Blank	473	560	51	74	---	---
$1x10^{-7}$	449	237	64	100	0.58	57.6
$3x10^{-7}$	435	188	53	105	0.66	66.4
$5x10^{-7}$	431	134	50	103	0.76	76.1
$7x10^{-7}$	430	119	50	102	0.79	78.8
$9x10^{-7}$	429	97	51	102	0.83	82.7
$1.1x10^{-6}$	249	37	35	163	0.93	93.4

Table (3.12): Effect of DB18C6 concentrations on the corrosion potential (E_{corr}), corrosion current density ($I_{corr.}$), Tafel slopes (β_a & β_c), degree of surface coverage (θ) and percentage inhibition efficiency (%IE) of 304SS in 2M HCl at 303K.

concentration (M)	$-E_{corr}$ (mV)	$I_{corr.}$ ($\mu A\ cm^{-2}$)	β_a ($mVdec^{-1}$)	β_c ($mVdec^{-1}$)	θ	%IE
Blank	462	731	49	89	---	---
$1x10^{-7}$	458	581	45	86	0.21	20.5
$3x10^{-7}$	454	568	45	91	0.22	22.3
$5x10^{-7}$	451	421	45	87	0.42	42.4
$7x10^{-7}$	443	356	44	91	0.51	51.3
$9x10^{-7}$	441	318	44	93	0.57	56.5
$1.1x10^{-6}$	436	303	45	97	0.59	58.6

Table (3.13): Effect of K-22DD concentrations on the corrosion potential (E_{corr}), corrosion current density ($I_{corr.}$), Tafel slopes (β_a & β_c), degree of surface coverage (θ) and percentage inhibition efficiency (%IE) of 304SS in 2M HCl at 303K.

concentration (M)	$-E_{corr}$ (mV)	$I_{corr.}$ ($\mu A\ cm^{-2}$)	β_a ($mVdec^{-1}$)	β_c ($mVdec^{-1}$)	θ	%IE
Blank	462	731	49	89	---	---
$1x10^{-7}$	460	556	45	84	0.24	23.9
$3x10^{-7}$	454	523	45	95	0.29	28.4
$5x10^{-7}$	452	436	44	95	0.40	40.4
$7x10^{-7}$	448	401	41	97	0.45	45.1
$9x10^{-7}$	445	333	39	98	0.54	54.4
$1.1x10^{-6}$	439	322	38	105	0.56	55.9

Table (3.14): Effect of K-222 concentrations on the corrosion potential (E_{corr}), corrosion current density ($I_{corr.}$), Tafel slopes (β_a & β_c), degree of surface coverage (θ) and percentage inhibition efficiency (%IE) of 304SS in 2M HCl at 303K.

concentration (M)	$-E_{corr}$ (mV)	$I_{corr.}$ ($\mu A\ cm^{-2}$)	β_a ($mVdec^{-1}$)	β_c ($mVdec^{-1}$)	θ	%IE
Blank	462	731	49	89	---	---
$1x10^{-7}$	456	581	43	93	0.21	20.5
$3x10^{-7}$	455	483	44	91	0.34	34.0
$5x10^{-7}$	453	375	45	88	0.49	48.7
$7x10^{-7}$	453	323	45	90	0.56	55.8
$9x10^{-7}$	451	295	48	93	0.60	59.6
$1.1x10^{-6}$	447	172	61	88	0.76	76.4

Table (3.15): Effect of DB24C8 concentrations on the corrosion potential (E_{corr}), corrosion current density ($I_{corr.}$), Tafel slopes (β_a & β_c), degree of surface coverage (θ) and percentage inhibition efficiency (%IE) of 304SS in 2M HCl at 303K.

concentration (M)	$-E_{corr}$ (mV)	$I_{corr.}$ ($\mu A\ cm^{-2}$)	β_a ($mVdec^{-1}$)	β_c ($mVdec^{-1}$)	θ	%IE
Blank	462	731	49	89	---	---
$1x10^{-7}$	462	330	40	82	0.55	54.8
$3x10^{-7}$	461	257	47	88	0.65	64.8
$5x10^{-7}$	459	206	48	87	0.72	71.9
$7x10^{-7}$	451	195	47	100	0.73	73.3
$9x10^{-7}$	447	143	44	100	0.81	80.5
$1.1x10^{-6}$	444	133	45	109	0.82	81.8

Table (3.18): Effect of K-222 concentrations on the corrosion potential (E_{corr}), corrosion current density ($I_{corr.}$), Tafel slopes (β_a & β_c), degree of surface coverage (θ) and percentage inhibition efficiency (%IE) of 316SS in 2M HCl at 303K.

concentration (M)	$-E_{corr}$ (mV)	$I_{corr.}$ ($\mu A\ cm^{-2}$)	β_a ($mVdec^{-1}$)	β_c ($mVdec^{-1}$)	θ	%IE
Blank	449	552	97	97	---	---
$1x10^{-7}$	428	111	62	83	0.80	79.9
$3x10^{-7}$	422	93	58	86	0.83	83.2
$5x10^{-7}$	419	69	54	91	0.88	87.5
$7x10^{-7}$	417	58	52	92	0.89	89.4
$9x10^{-7}$	414	46	50	94	0.92	91.6
$1.1x10^{-6}$	440	38	60	82	0.93	93.2

Table (3.19): Effect of DB24C8 concentrations on the corrosion potential (E_{corr}), corrosion current density ($I_{corr.}$), Tafel slopes (β_a & β_c), degree of surface coverage (θ) and percentage inhibition efficiency (%IE) of 316SS in 2M HCl at 303K.

concentration (M)	$-E_{corr}$ (mV)	$I_{corr.}$ ($\mu A\ cm^{-2}$)	β_a ($mVdec^{-1}$)	β_c ($mVdec^{-1}$)	θ	%IE
Blank	449	552	97	97	---	---
$1x10^{-7}$	425	114	61	87	0.79	79.4
$3x10^{-7}$	422	94	58	89	0.83	82.9
$5x10^{-7}$	421	77	58	86	0.86	86.1
$7x10^{-7}$	407	74	51	93	0.87	86.5
$9x10^{-7}$	407	59	49	89	0.89	89.3
$1.1x10^{-6}$	407	57	50	93	0.90	89.8

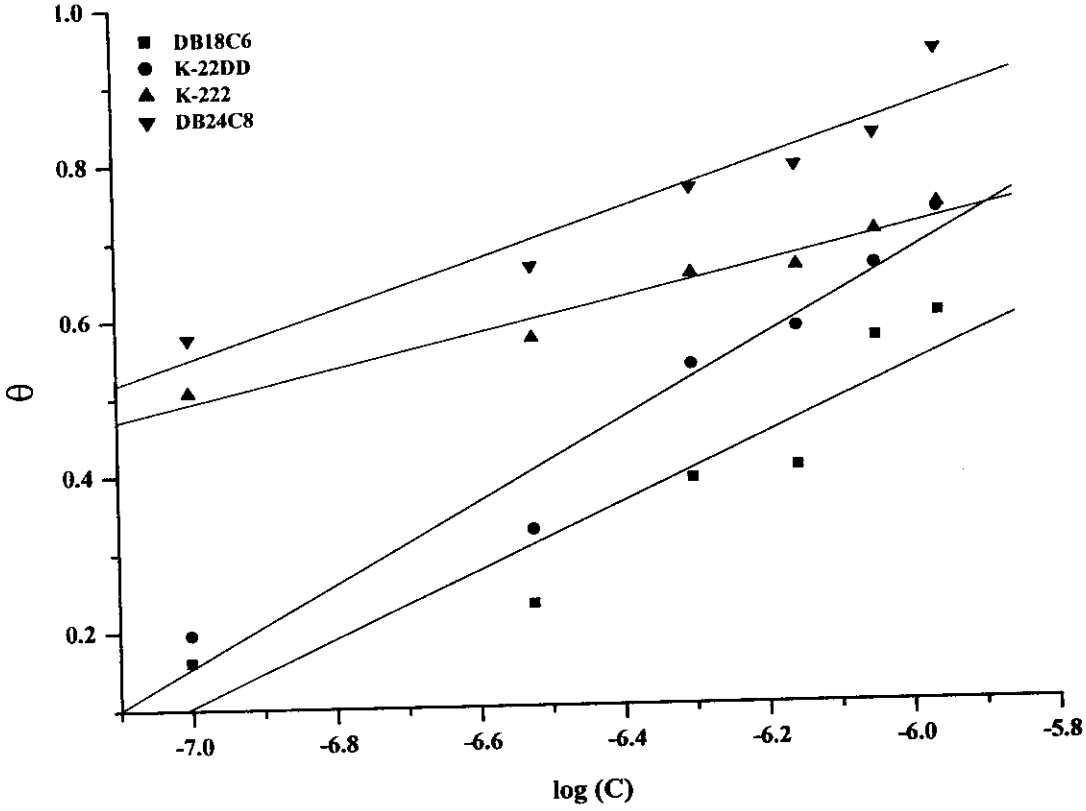

Fig. (3.82): Curve fitting of corrosion data for 430SS in 2M HCl in presence of different concentrations of crown ethers to the Temkin's adsorption isotherm at 303K.

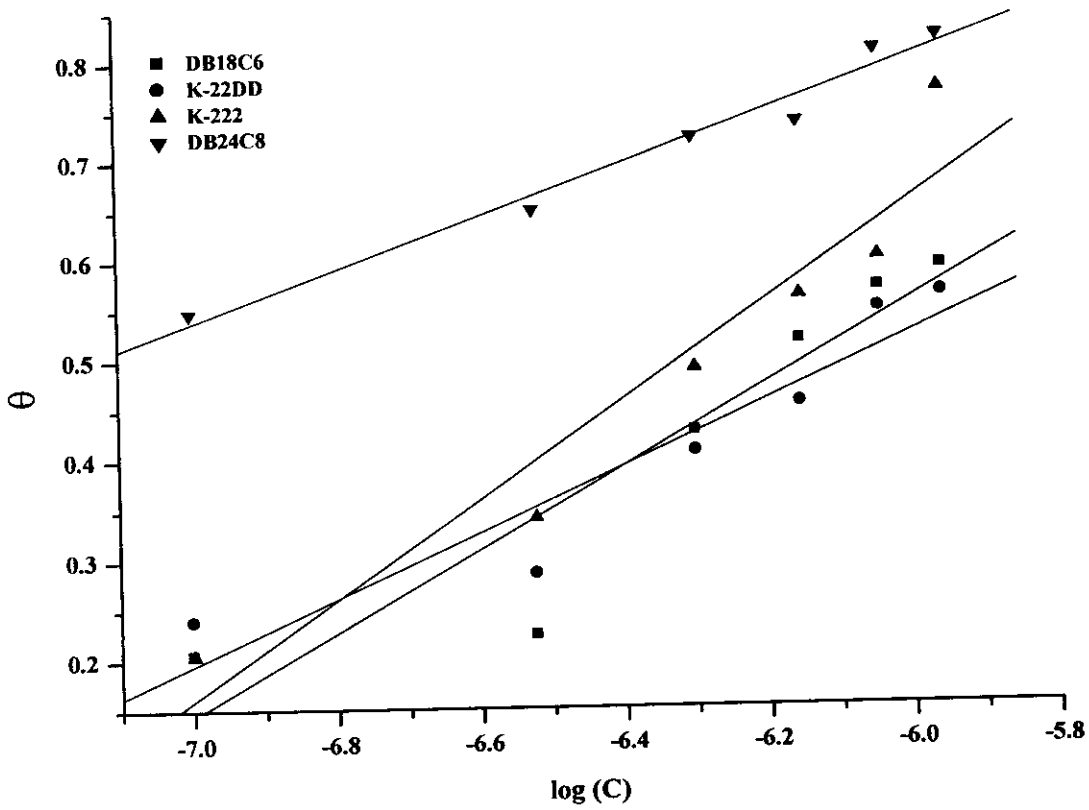

Fig. (3.83): Curve fitting of corrosion data for 304SS in 2M HCl in presence of different concentrations of crown ethers to the Temkin's adsorption isotherm at 303K.

SECTION (C)

3.3 Scanning electron microscopy (SEM).

The morphology of the corroded surface of each specimen was studied using scanning electron microscope (SEM). All micrographs of corroded specimens were taken at a magnification of (x500). All the investigated specimens had been naturally immersed for seven hours in the test solutions.

Scanning electron micrographs [Figs: (3.85-3.99)] are achieved for different types of stainless steel surfaces immersed for seven hours in 2M HCl solution in absence and presence of ($5x10^{-7}$) M and ($9x10^{-7}$ M) of different types of the investigated crown ethers.

Figures (3.85, 3.90 & 3.95) represent the micrographs for 430SS, 304SS and 316SS respectively, in 2M HCl in absence of inhibitors. These micrographs show an extensive etching composed of greenish and dark areas in presence of some white areas. The greenish areas reflect the part of protective film which contains mainly chromium and its oxides, where the white areas represent the ferrite phase and the dark areas represent the pearlite, [mixture of ferrite and cementite (Fe_3C) in a lamellar form].

For example Fig. (3.86-I), reveals that the surface was damaged appreciably owing to the corrosion in the presence of $5x10^{-7}$ M of DB18C6 but is still in better conditions than the specimen exposed to the corrosive medium in the absence of inhibitors (Fig. 3.85). When the concentration of DB18C6 was increased to $9x10^{-7}$ M, there was much less damage to the surface presumably as a result of the protective film of the inhibitor on the surface of 430 stainless steel, (Fig. 3.86-II).

Another example is Fig. (3.87), which represents the conditions of 430SS surface in the presence of $5x10^{-7}$ M (I) and $9x10^{-7}$ M (II) of Kry-22DD. From the given micrographs it is clear that, Kry-22DD provided good protection at the two different concentrations.

The protective film presented on the surface of 430SS at a concentration of $9x10^{-7}$ M of DB24C8, Fig. (3.89-II), appears to be very smooth and to cover the whole surface without any flows. This confirms the observed high percentage inhibition efficiency (%IE) of DB24C8 at $9x10^{-7}$ M as it was discussed in the previous sections (A) and (B).

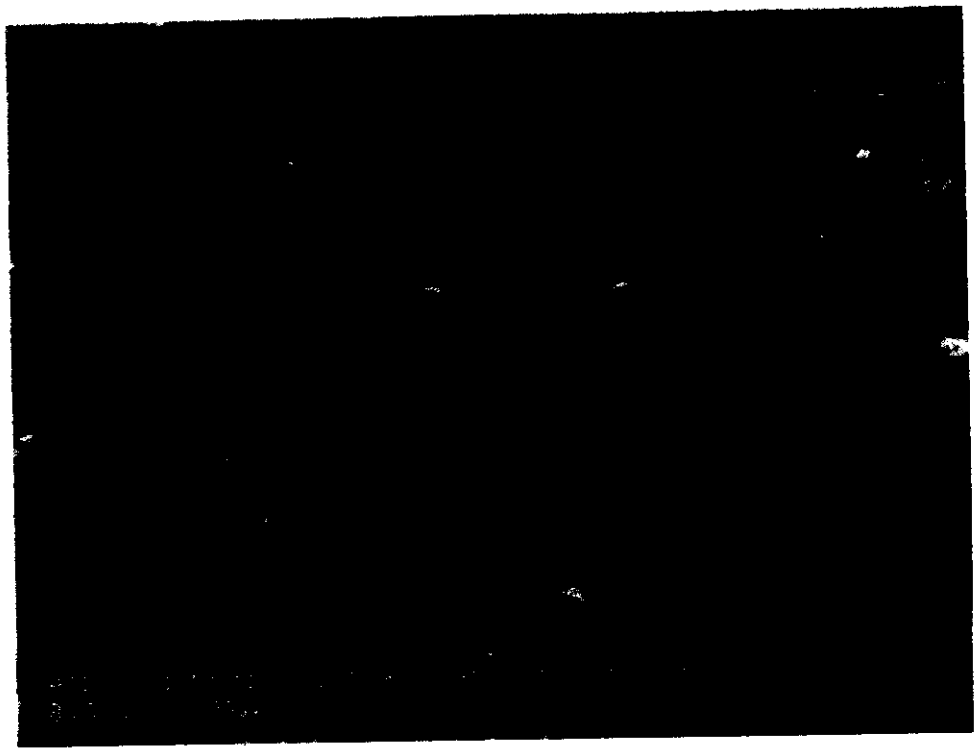

Fig. (3.85): SEM. micrograph (x500) of 430SS immersed in 2M HCl at 303K.

(I)

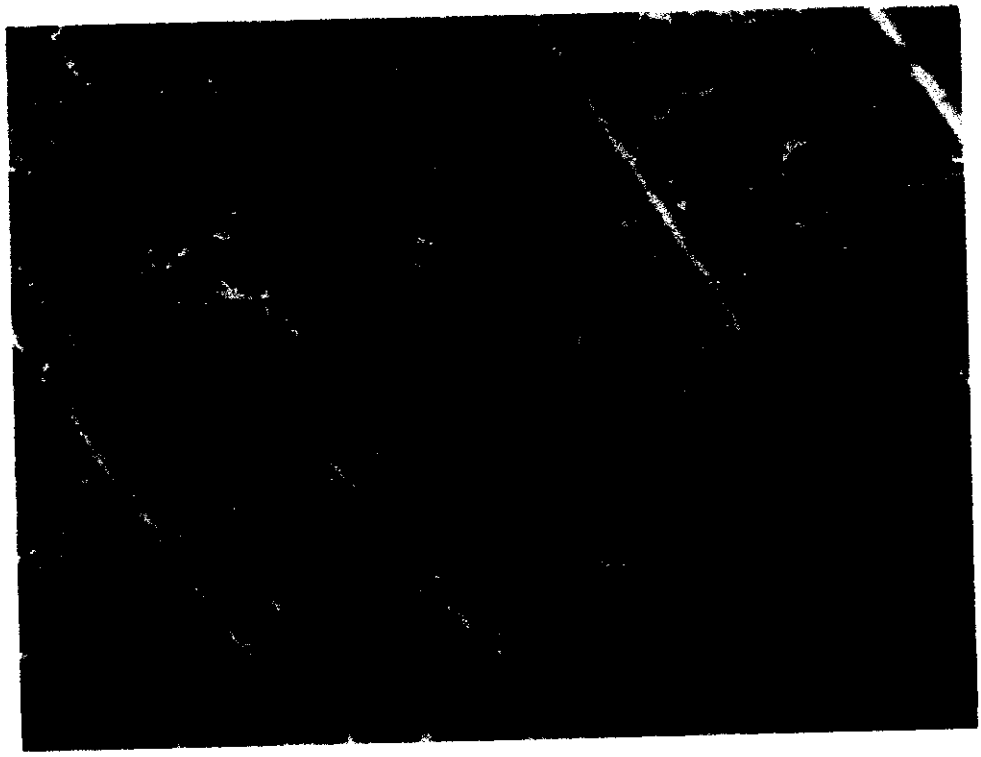

(II)

Fig. (3.86): SEM. micrograph (x500) of 430SS immersed in 2M HCl at 303K in presence of DB18C6 of concentration $5x10^{-7}$M (I) and $9x10^{-7}$M (II).

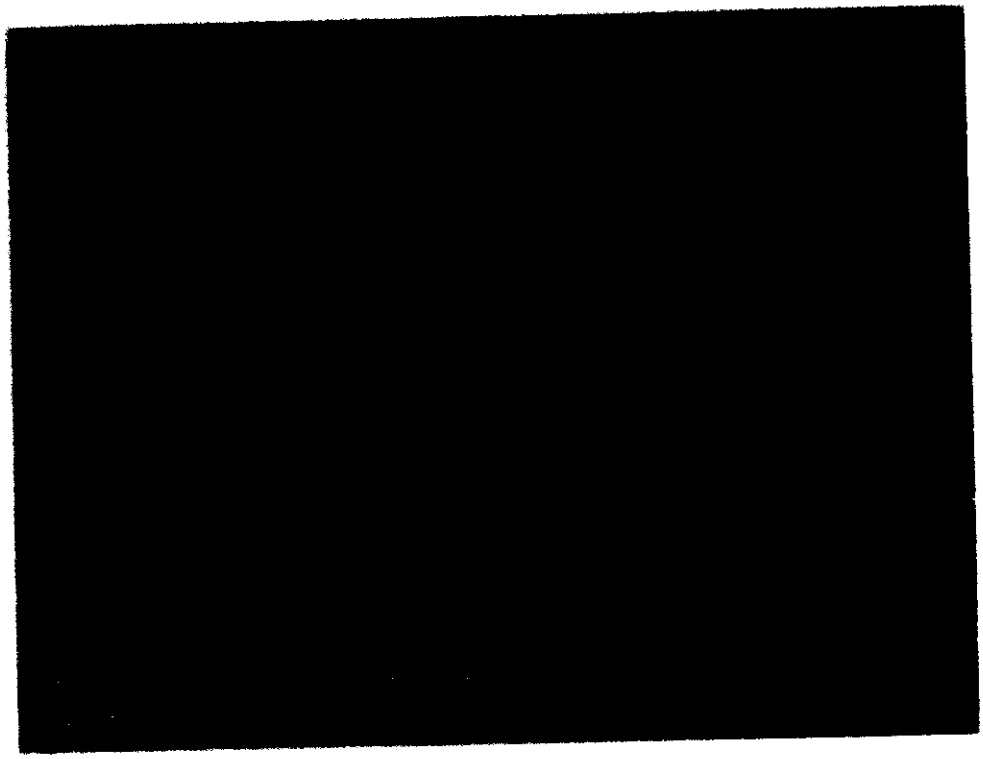

(I)

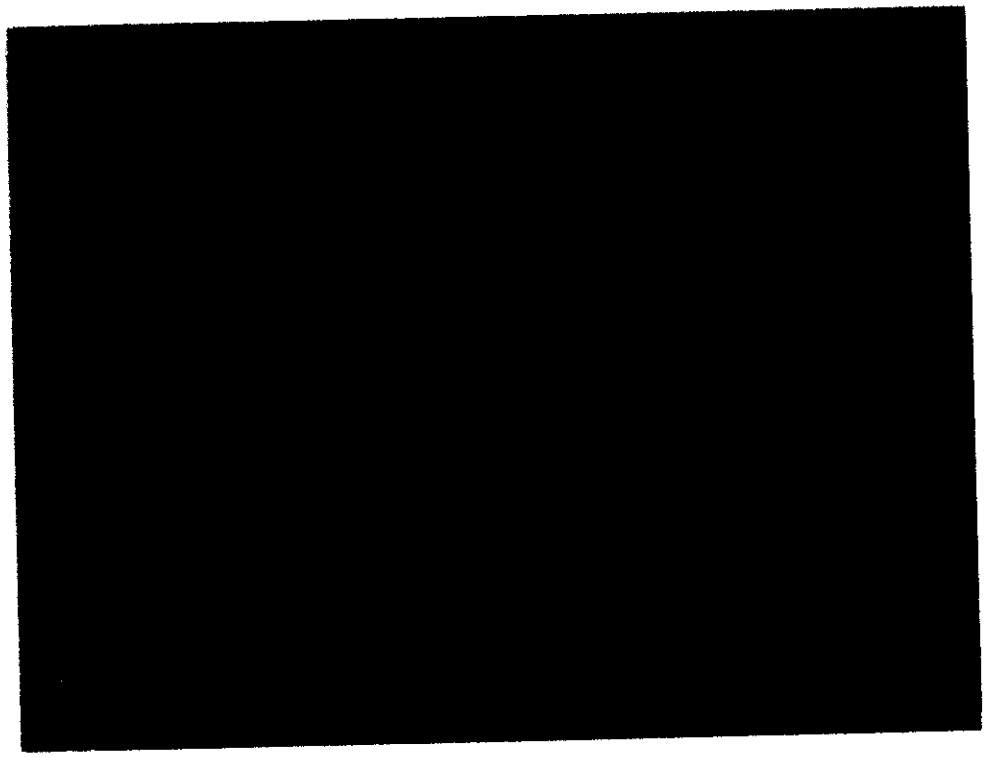

(II)

Fig. (3.87): SEM. micrograph (x500) of 430SS immersed in 2M HCl at 303K in presence of Kry-22DD of concentration $5x10^{-7}$M (I) and $9x10^{-7}$M (II).

(I)

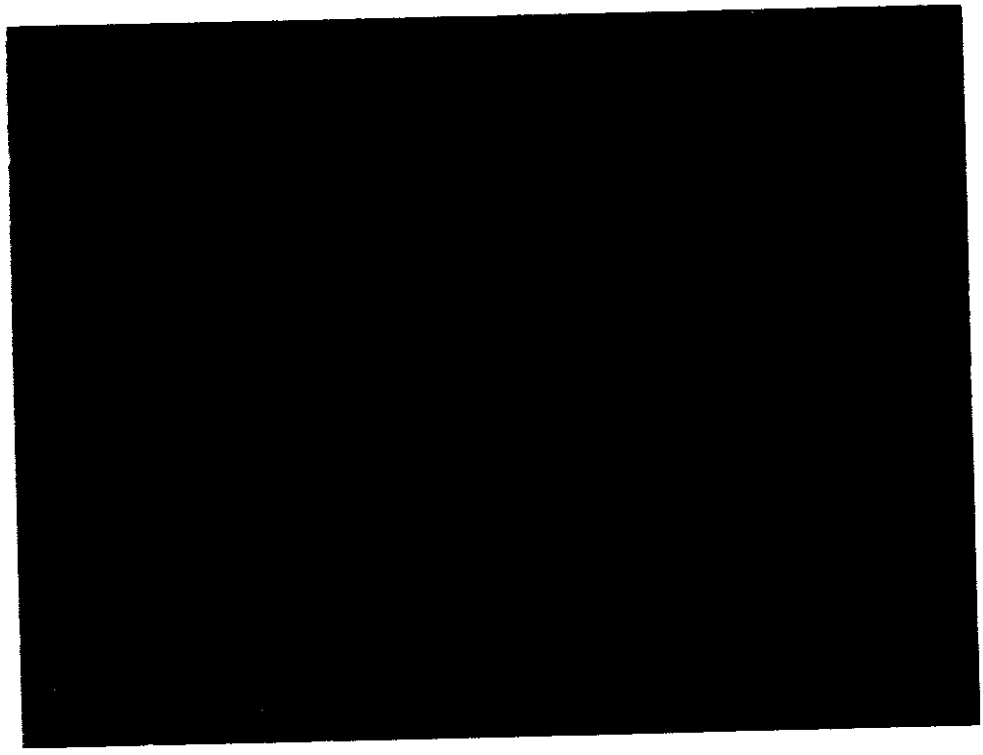

(II)

Fig. (3.88): SEM. micrograph (x500) of 430SS immersed in 2M HCl at 303K in presence of Kry-222 of concentration $5x10^{-7}$M (I) and $9x10^{-7}$M (II).

(I)

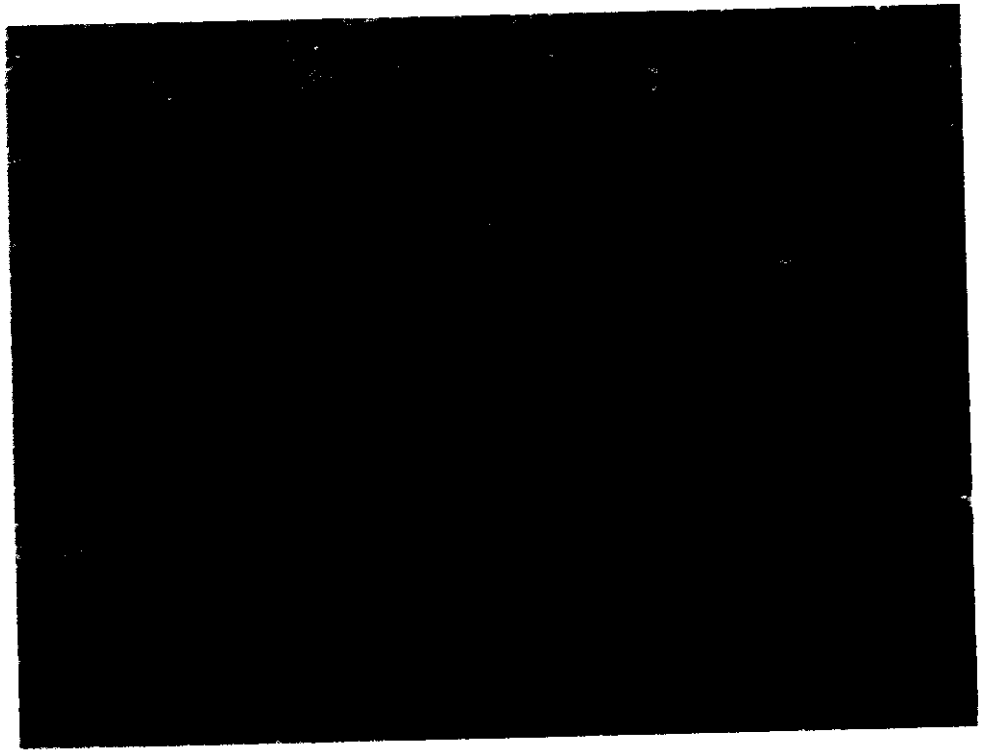

(II)

Fig. (3.89): SEM. micrograph (x500) of 430SS immersed in 2M HCl at 303K in presence of DB24C8 of concentration $5x10^{-7}$M (I) and $9x10^{-7}$M (II).

Fig. (3.90): SEM. micrograph (x500) of 304SS immersed in 2M HCl at 303K.

(I)

(II)

Fig. (3.91): SEM. micrograph (x500) of 304SS immersed in 2M HCl at 303K in presence of DB18C6 of concentration $5x10^{-7}$M (I) and $9x10^{-7}$M (II).

(I)

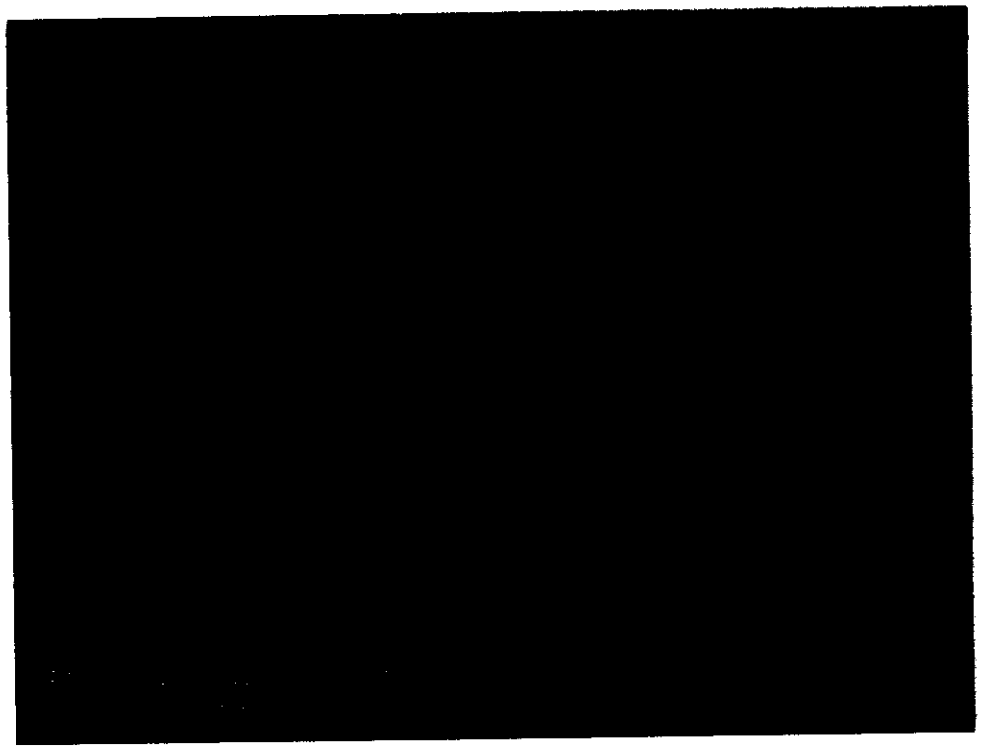

(II)

Fig. (3.92): SEM. micrograph (x500) of 304SS immersed in 2M HCl at 303K in presence of Kry-22DD of concentration $5x10^{-7}$M (I) and $9x10^{-7}$M (II).

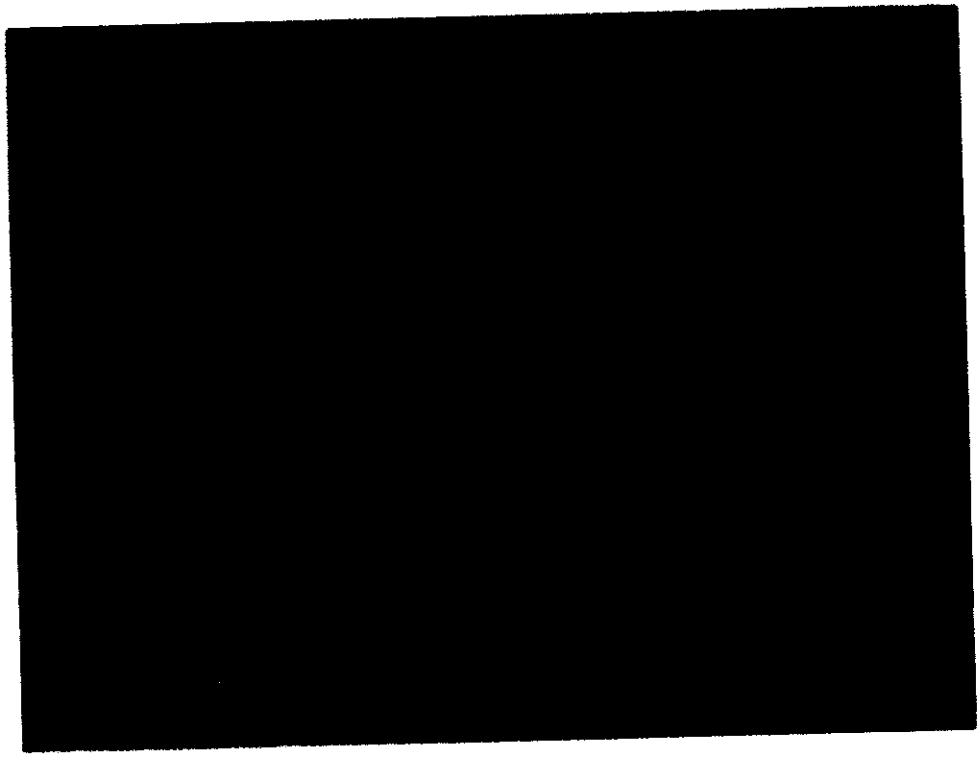

(I)

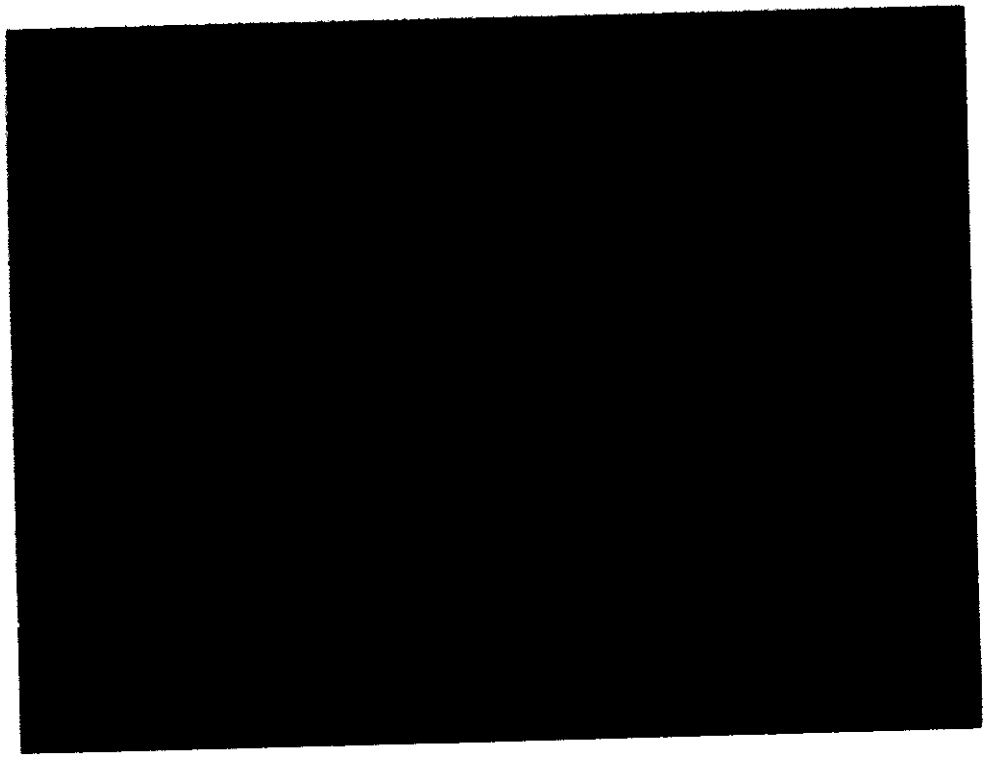

(II)

Fig. (3.93): SEM. micrograph (x500) of 304SS immersed in 2M HCl at 303K in presence of Kry-222 of concentration $5x10^{-7}$M (I) and $9x10^{-7}$M (II).

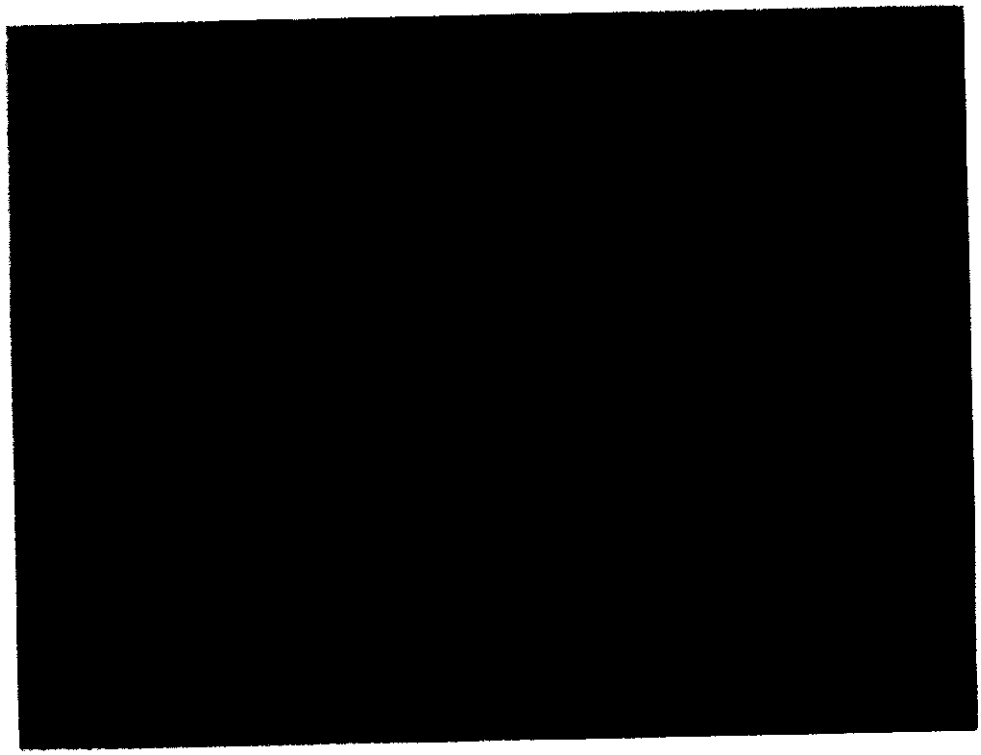

(I)

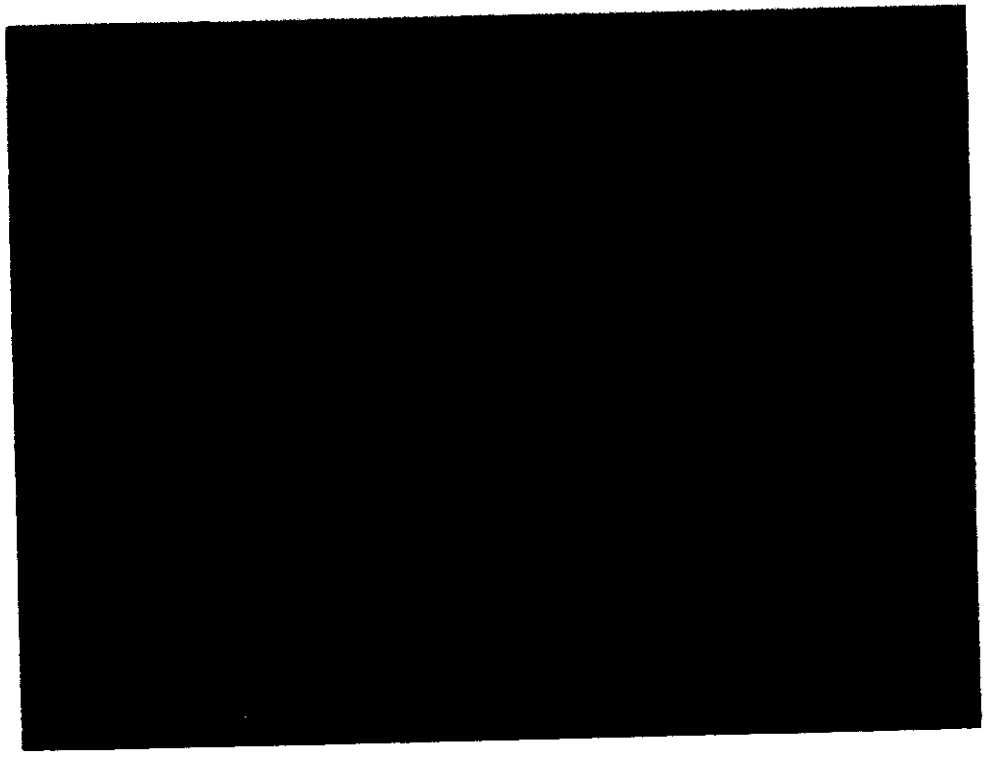

(II)

Fig. (3.94): SEM. micrograph (x500) of 304SS immersed in 2M HCl at 303K in presence of DB24C8 of concentration $5x10^{-7}$M (I) and $9x10^{-7}$M (II).

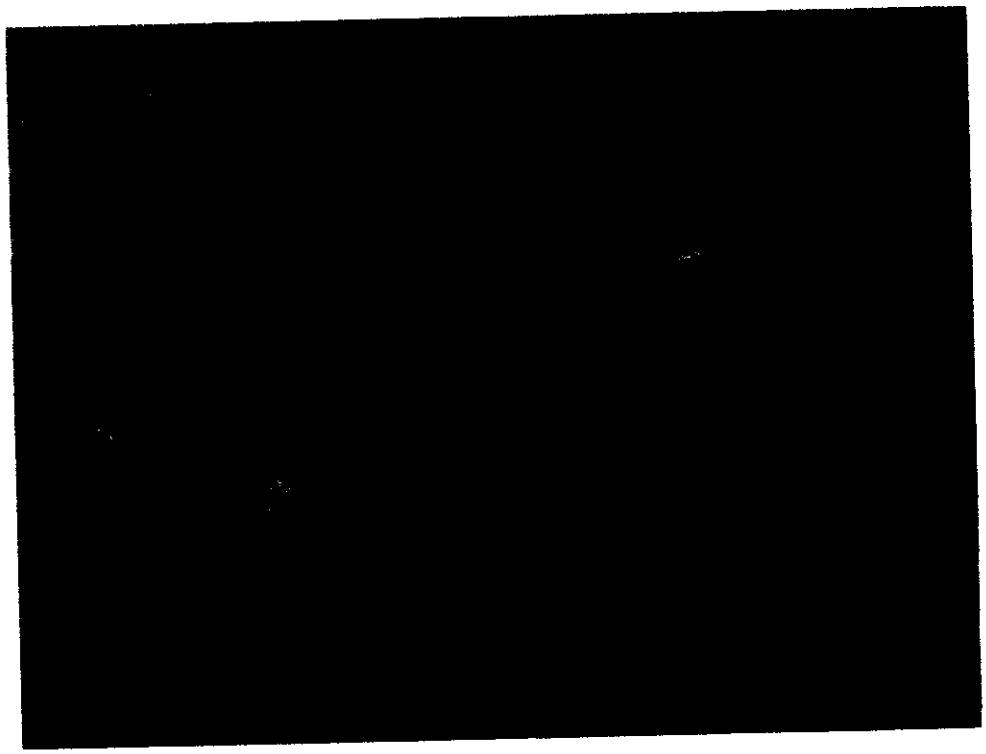

Fig. (3.95): SEM. micrograph (x500) of 316SS immersed in 2M HCl at 303K.

(I)

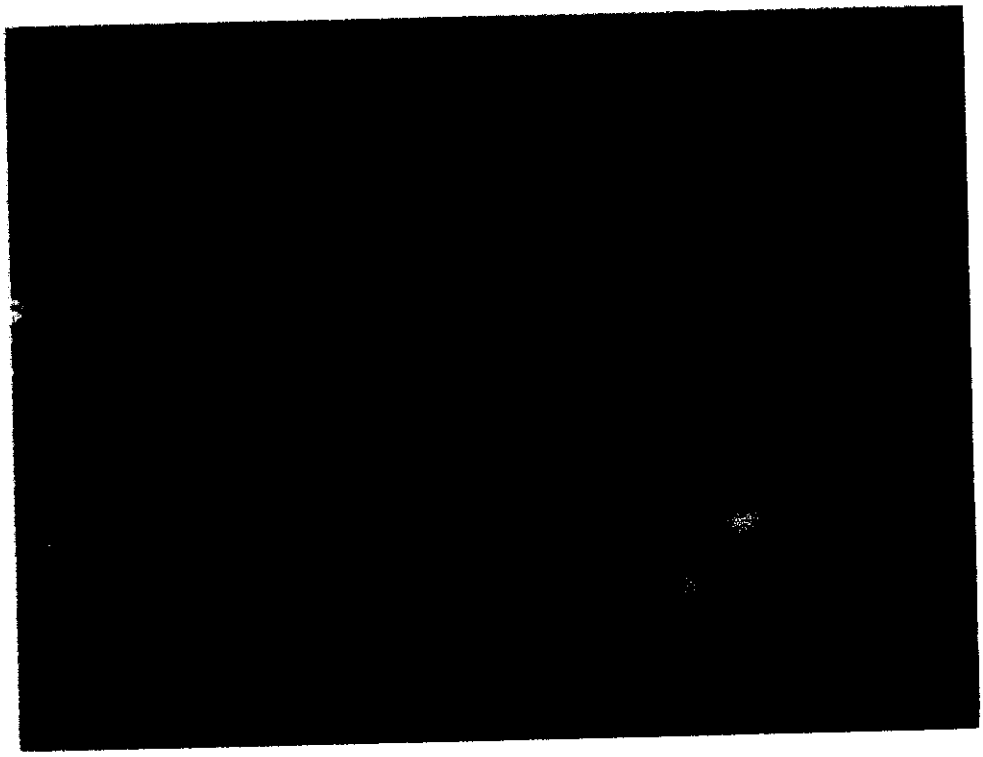

(II)

Fig. (3.96): SEM. micrograph (x500) of 316SS immersed in 2M HCl at 303K in presence of DB18C6 of concentration $5x10^{-7}$M (I) and $9x10^{-7}$M (II).

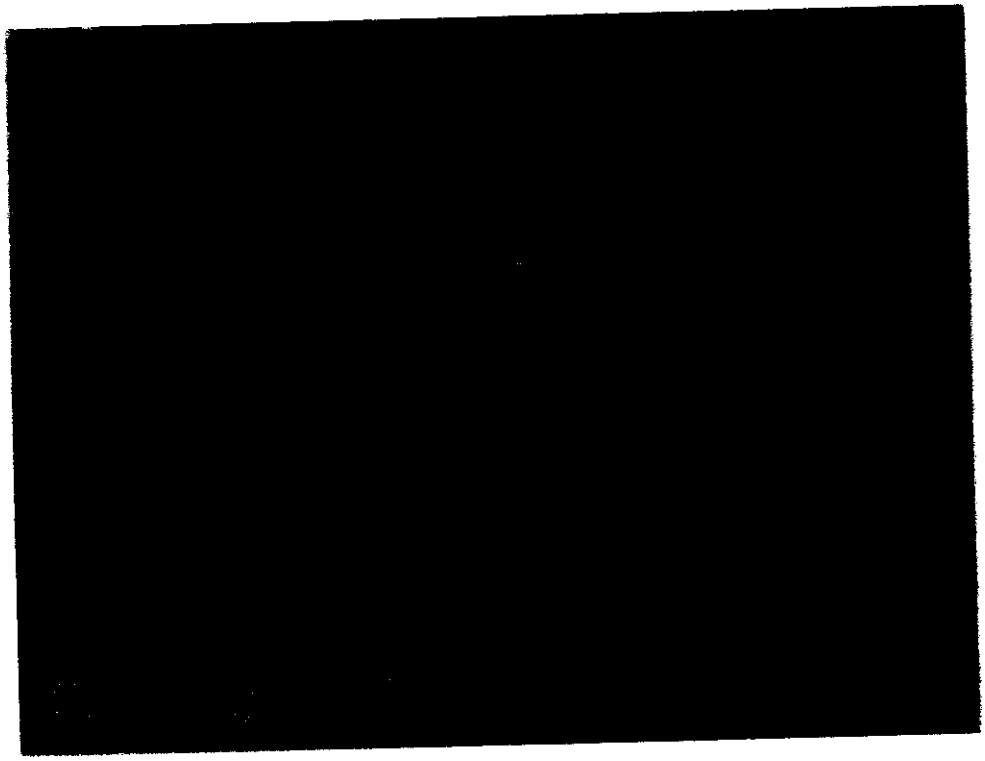

(I)

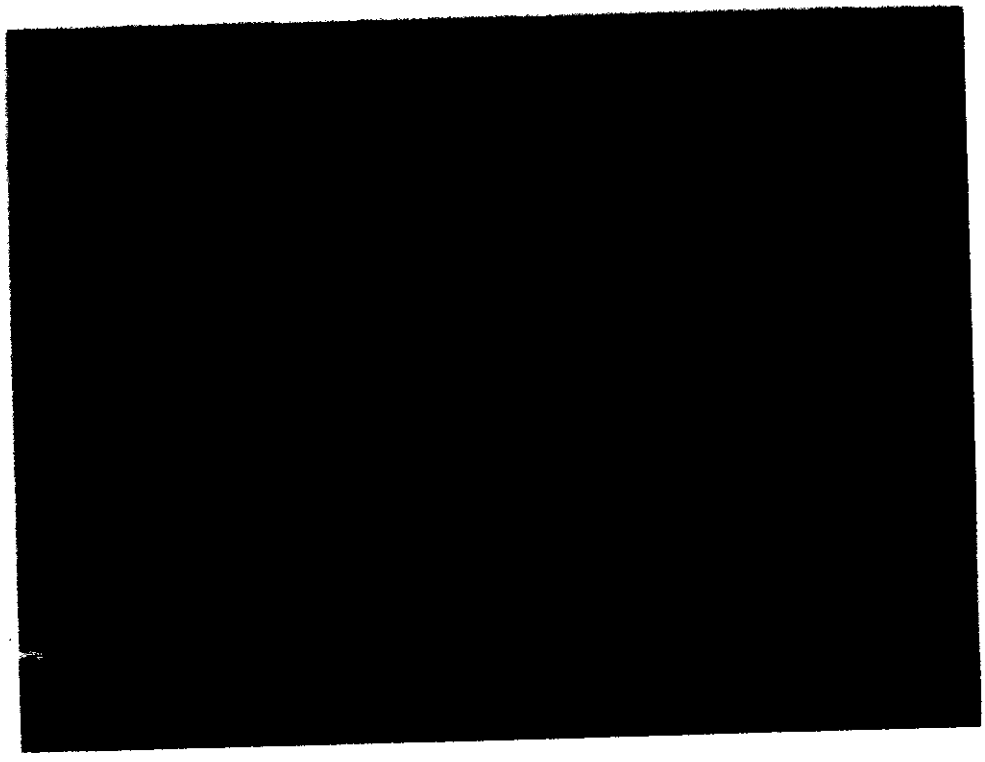

(II)

Fig. (3.97): SEM. micrograph (x500) of 316SS immersed in 2M HCl at 303K in presence of Kry-22DD of concentration $5x10^{-7}$M (I) and $9x10^{-7}$M (II).

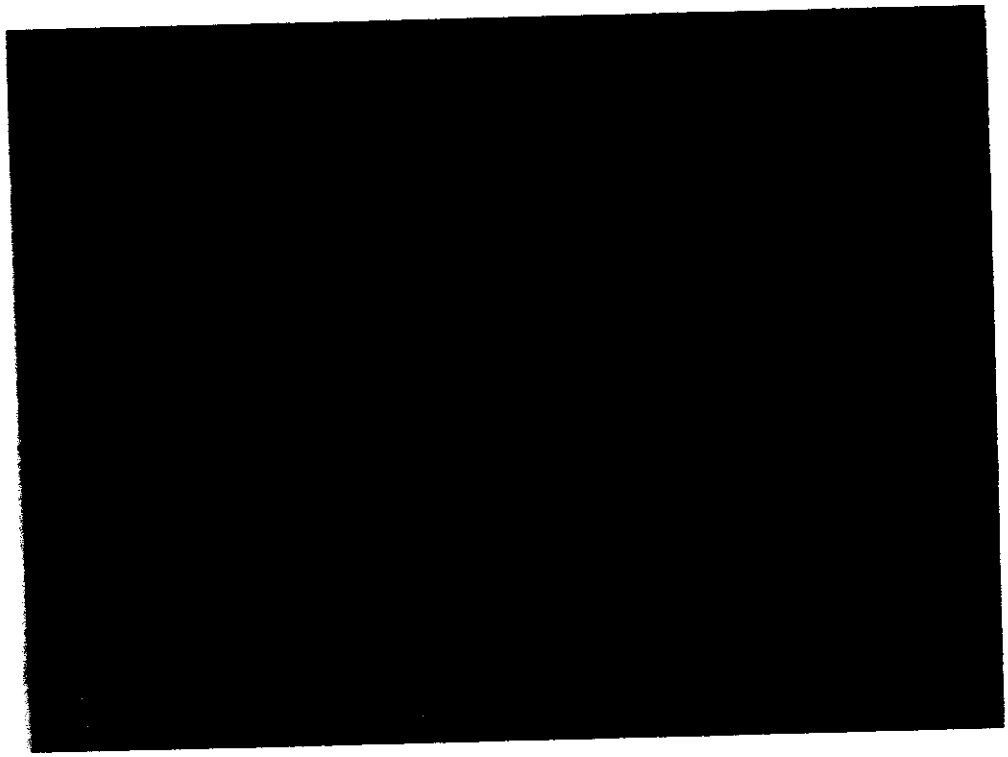

(I)

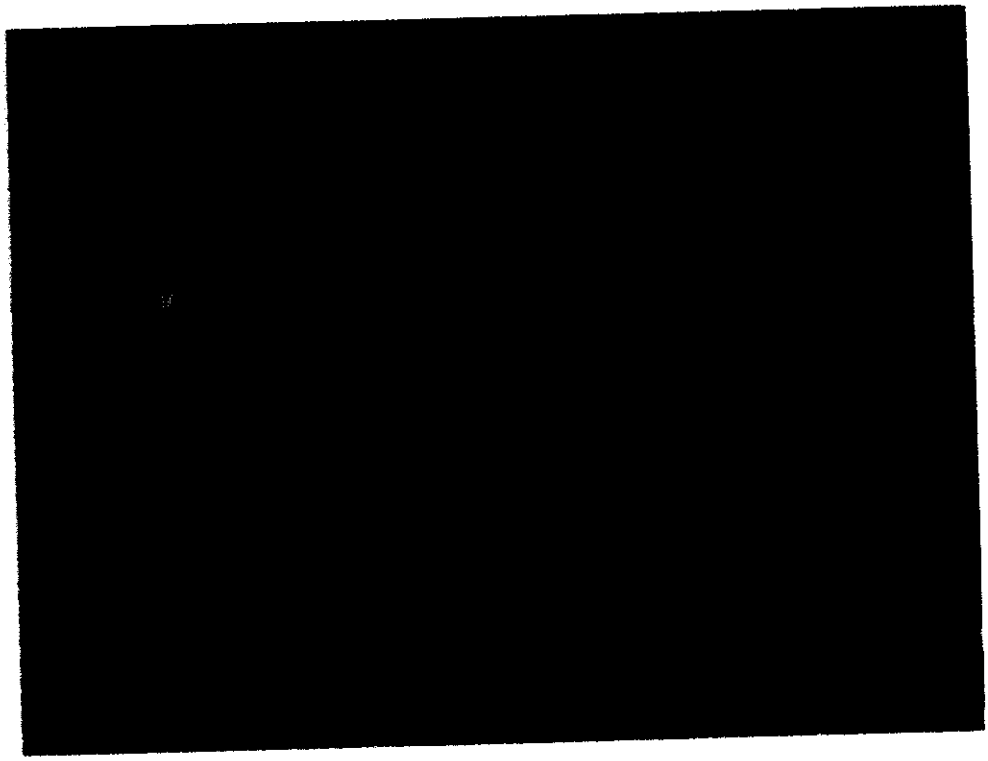

(II)

Fig. (3.98): SEM. micrograph (x500) of 316SS immersed in 2M HCl at 303K in presence of Kry-222 of concentration $5x10^{-7}$M (I) and $9x10^{-7}$M (II).

SECTION (D)

3.4 x-ray photoelectron spectroscopic analysis (XPS).

Surface analyses of different types of stainless steel were carried out using x-ray photoelectron spectroscopic analysis (XPS). The results were plotted on a graph of dN/dE v. electron energy, as shown in figures (3.100-3.114) represent the various peaks owing to different elements.

The x-ray photoelectron spectroscopic analysis (XPS) was achieved for different types of stainless steel surfaces immersed for seven hours in 2M HCl solution in absence and presence of ($5x10^{-7}$) M and ($9x10^{-7}$ M) of different types of the investigated crown ethers.

From all the obtained analysis charts, it was found that the results of (XPS) may be explained and discussed depending on the values of weight percentages (wt %) of carbon and chloride atoms on the surface of different types of stainless steel as follow:

1) In all the charts of (XPS) the carbon atom peak appears around the value of 0.2 KV and the peak of chloride atom appears at 2.6 KV.

2) As the corrosive medium is 2M HCl solution and the organic additives consist mainly of C, O and/or C, O, N atoms, so the variation of chloride and carbon weight percentages on the surface can be used quantitively to explain and discuss the adsorption of crown ethers on the surface of stainless steels.

3) For example, Fig. (3.100) represents XPS of 430SS exposed to 2M HCl at 303K for seven hours, where Fig (3.104) represents the same sample in the presence of $5x10^{-7}$ M of DB24C8. From comparison it is clearly seen that the weight percentage (wt %) of carbon was increased from (2.64%) to (3.55%), on the other hand the weight percentage (wt %) of chloride was decreased in presence of DB24C8 from (2.16%) to (0.42%). By other words, the peak of carbon was increased and the peak of chloride was decreased compared with the corresponding peaks in the absence of DB24C8. This is due to the replacement of the firstly adsorbed chloride atoms by C-atoms (crown ethers). These results confirm the adsorption of DB24C8 on the

surface of 430SS. Figures (3.100-3.114) represent (XPS) of different types of stainless steel in 2M HCl in absence and presence of different types of crown ethers at 303K. All these sharts confirm the above mentioned trend.

4) Tables (3.20, 3.21) and Figs. (3.115, 3.116) summarizes the variations of the weight percentages (wt %) of carbon and chloride in the protective films that achieved using (XPS) for the investigated stainless steels in absence and presence of different types of crown ethers. It is Cleary that, in all cases the weight percentage values of carbon on the surface were increased by increasing the concentration of the investigated crown ethers. On the other hand, the weight percentages (wt %) values of chloride were decreased. This confirms the replacement of the chloride atoms which firstly adsorbed (from 2M HCl) by carbon atoms which come from crown ethers. This confirms the increase in the inhibition efficiency in presence of crown ethers.

5) From Figs (3.115, 3.116) we may conclude that, the increase in the weight percentage (wt %) of carbon obeys the following sequence:

DB18C6 < Kry-22DD < Kry-222 < DB24C8

and vice versa in case of chloride atoms and consequently, the rearrangement of crown ethers according to their inhibition efficiencies could be written as follows:

DB18C6 < Kry-22DD < Kry-222 < DB24C8

This is also in agreement with the observed order of corrosion inhibition efficiency which achieved by loss in mass and galvanostatic polarization techniques.

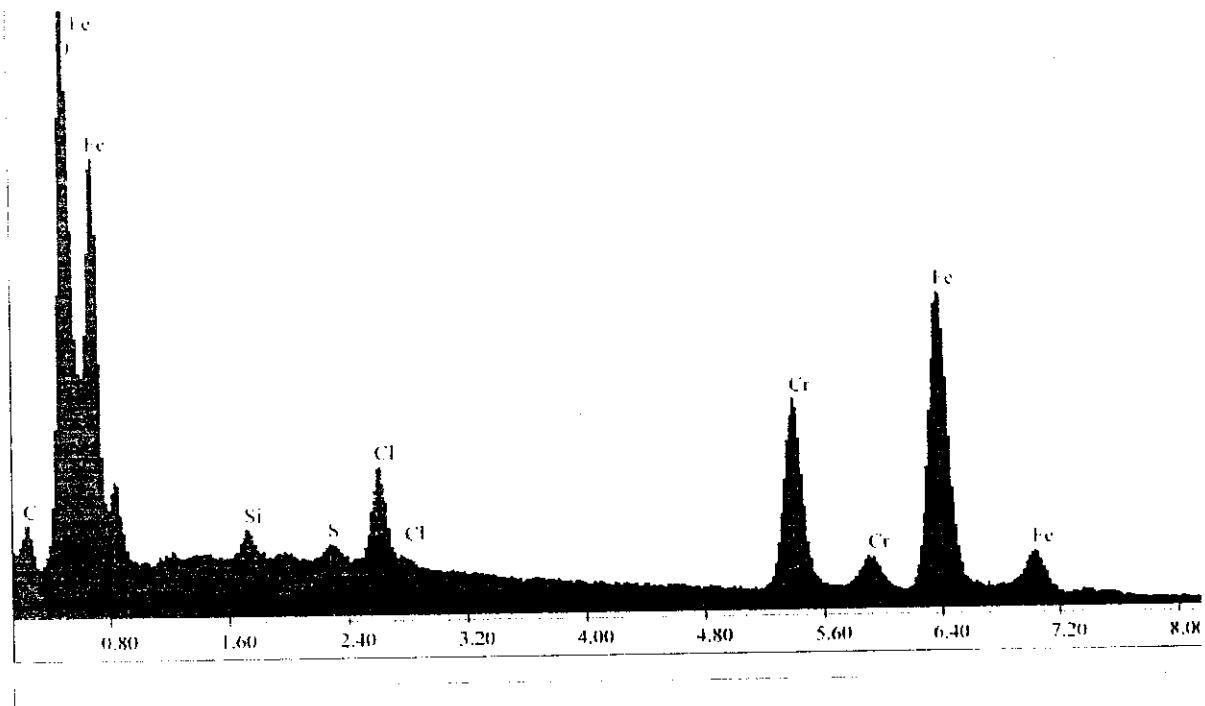

Fig. (3.100): XPS analysis of 430SS surface after immersion in 2M HCl for seven hours at 303K.

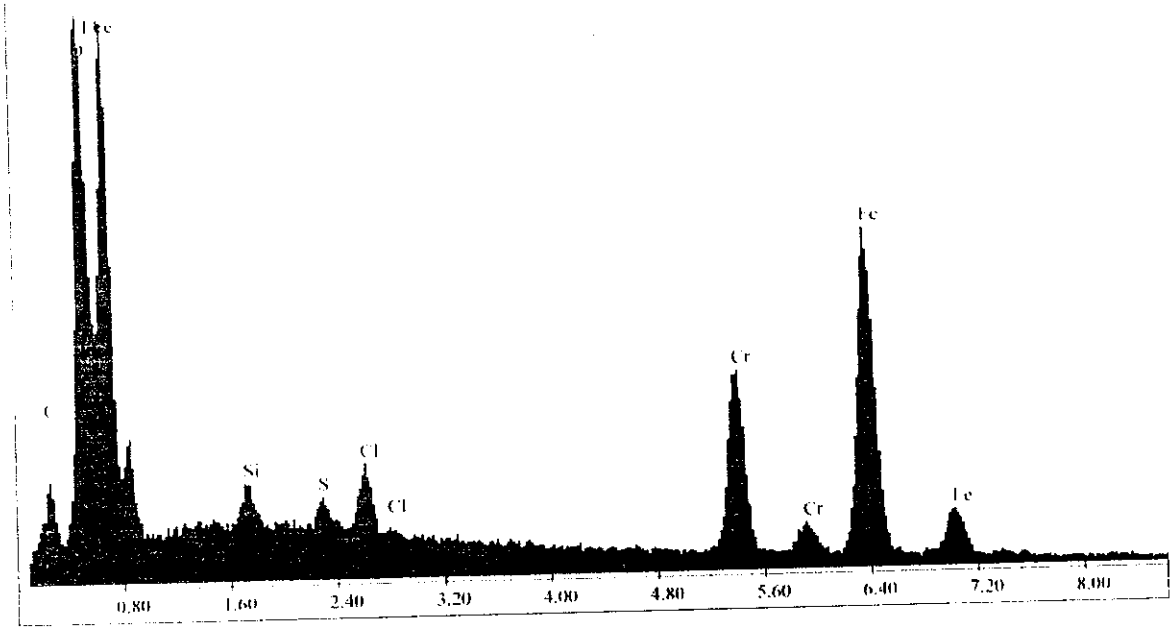

Fig. (3.101): XPS analysis of 430SS surface after immersion in 2M HCl for seven hours at 303K in presence of $5x10^{-7}$ M DB18C6.

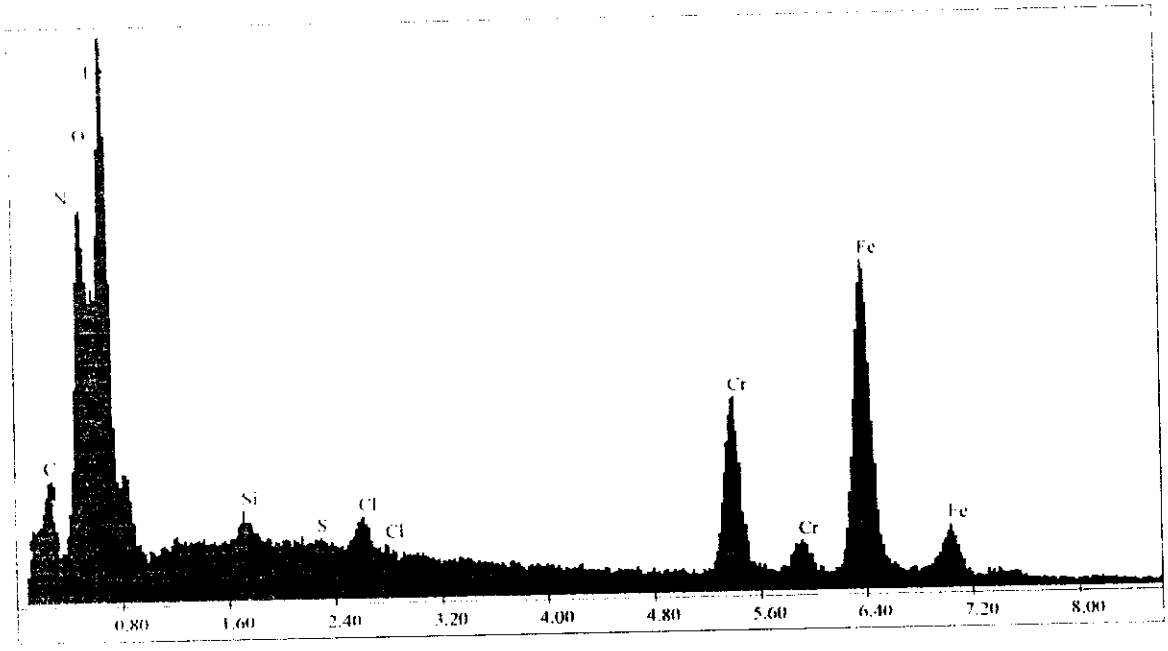

Fig. (3.102): XPS analysis of 430SS surface after immersion in 2M HCl for seven hours at 303K in presence of $5x10^{-7}$ M Kry-22DD.

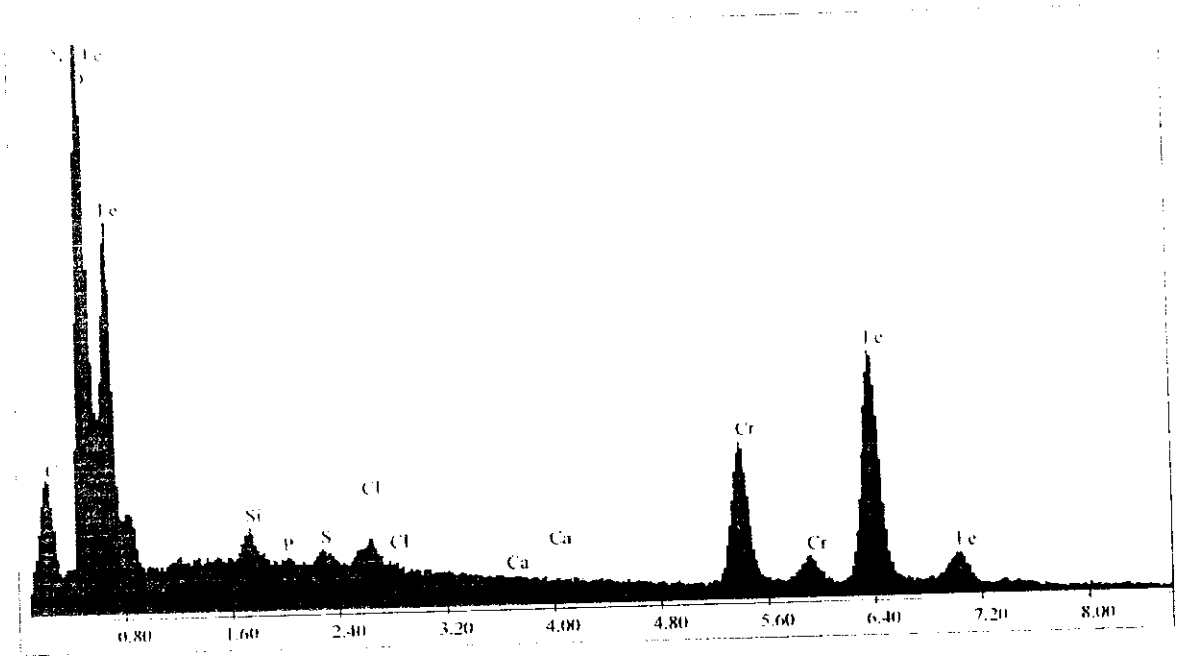

Fig. (3.103): XPS analysis of 430SS surface after immersion in 2M HCl for seven hours at 303K in presence of $5x10^{-7}$ M Kry-222.

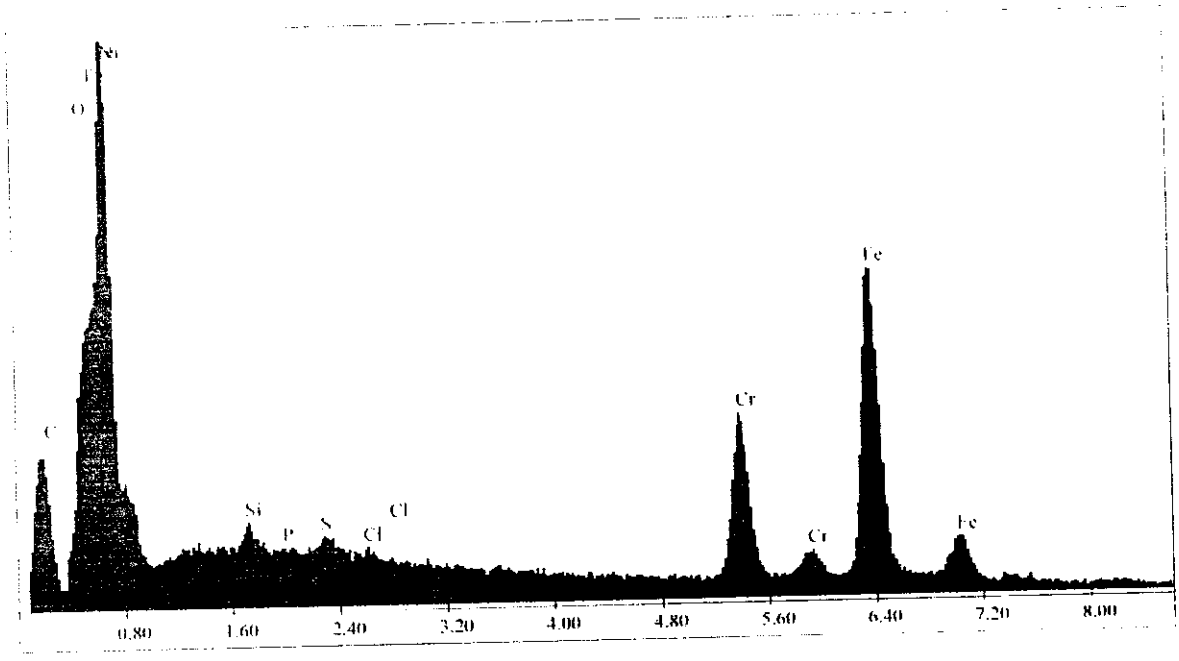

Fig. (3.104): XPS analysis of 430SS surface after immersion in 2M HCl for seven hours at 303K in presence of $5x10^{-7}$ M DB24C8.

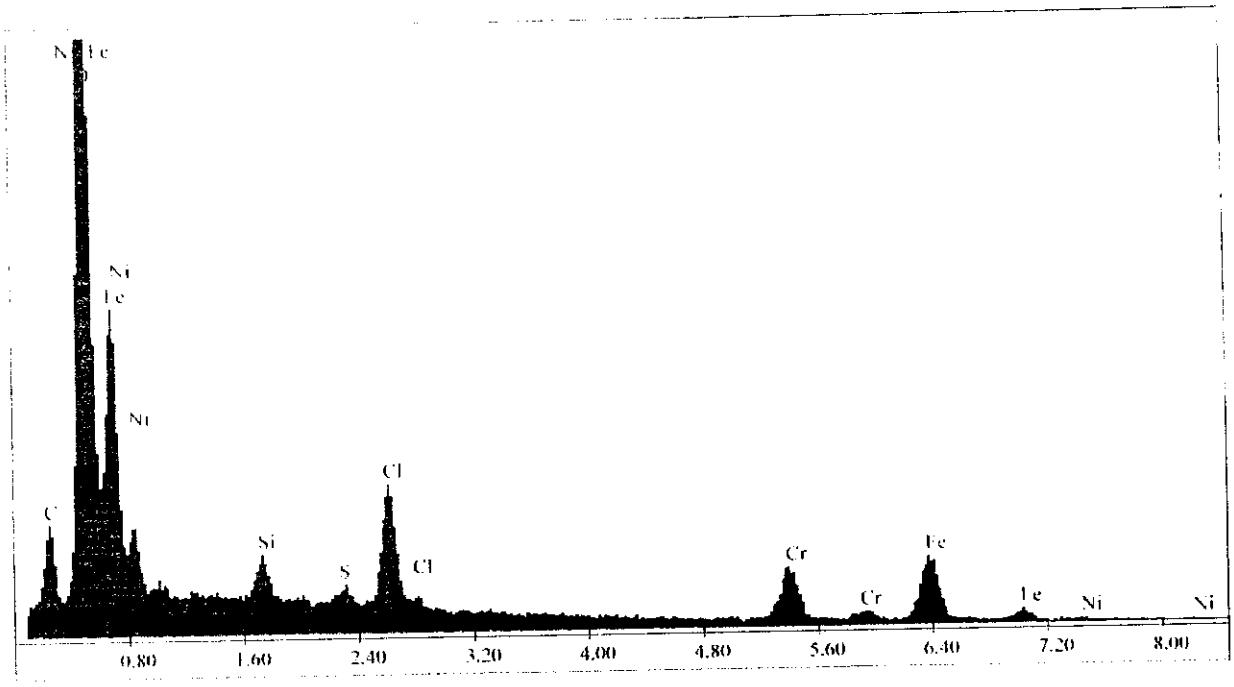

Fig. (3.105): XPS analysis of 304SS surface after immersion in 2M HCl for seven hours at 303K.

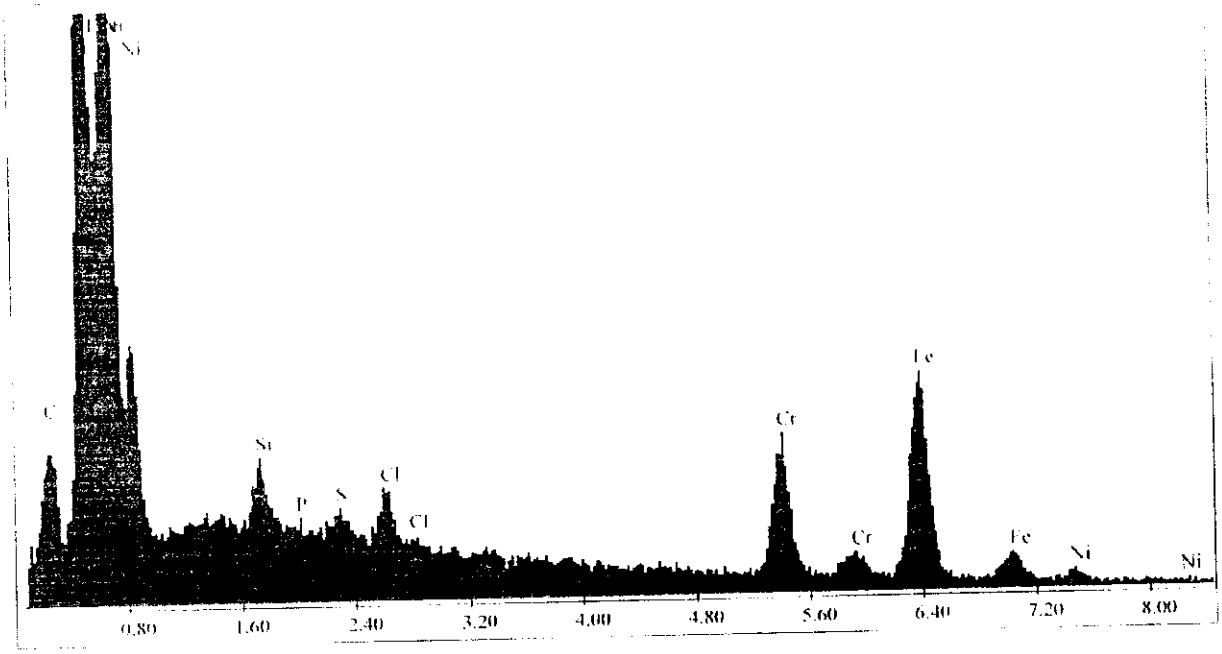

Fig. (3.106): XPS analysis of 304SS surface after immersion in 2M HCl for seven hours at 303K in presence of $5x10^{-7}$ M DB18C6.

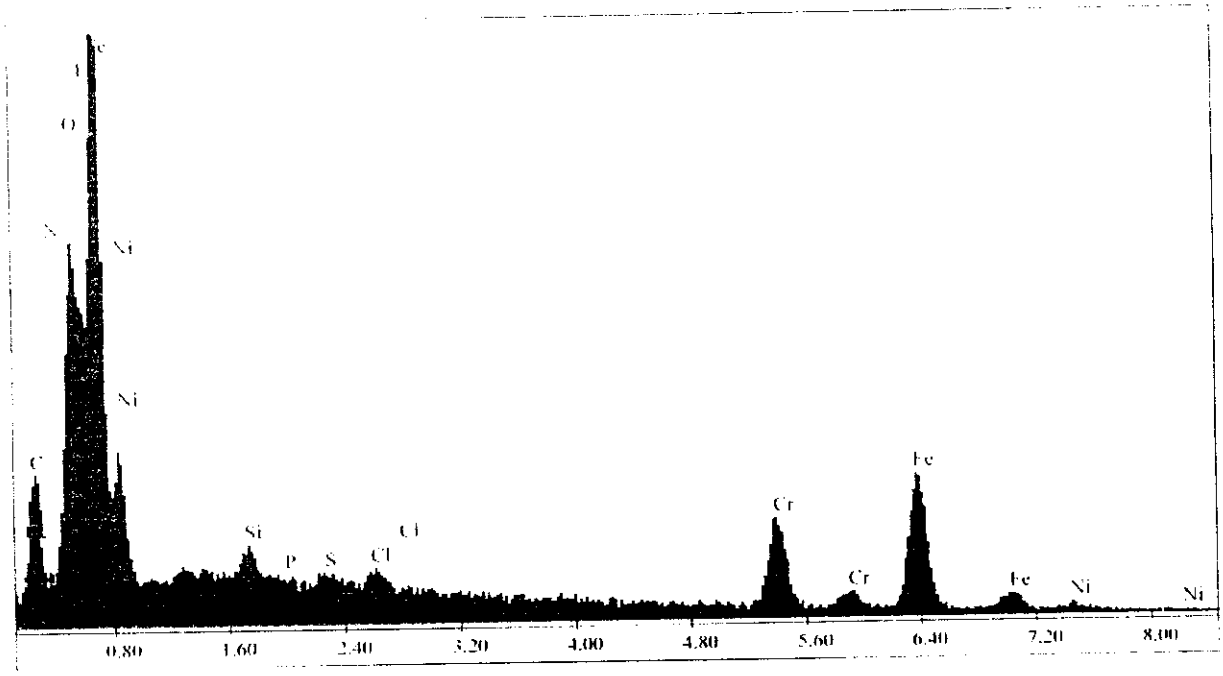

Fig. (3.107): XPS analysis of 304SS surface after immersion in 2M HCl for seven hours at 303K in presence of $5x10^{-7}$ M Kry-22DD.

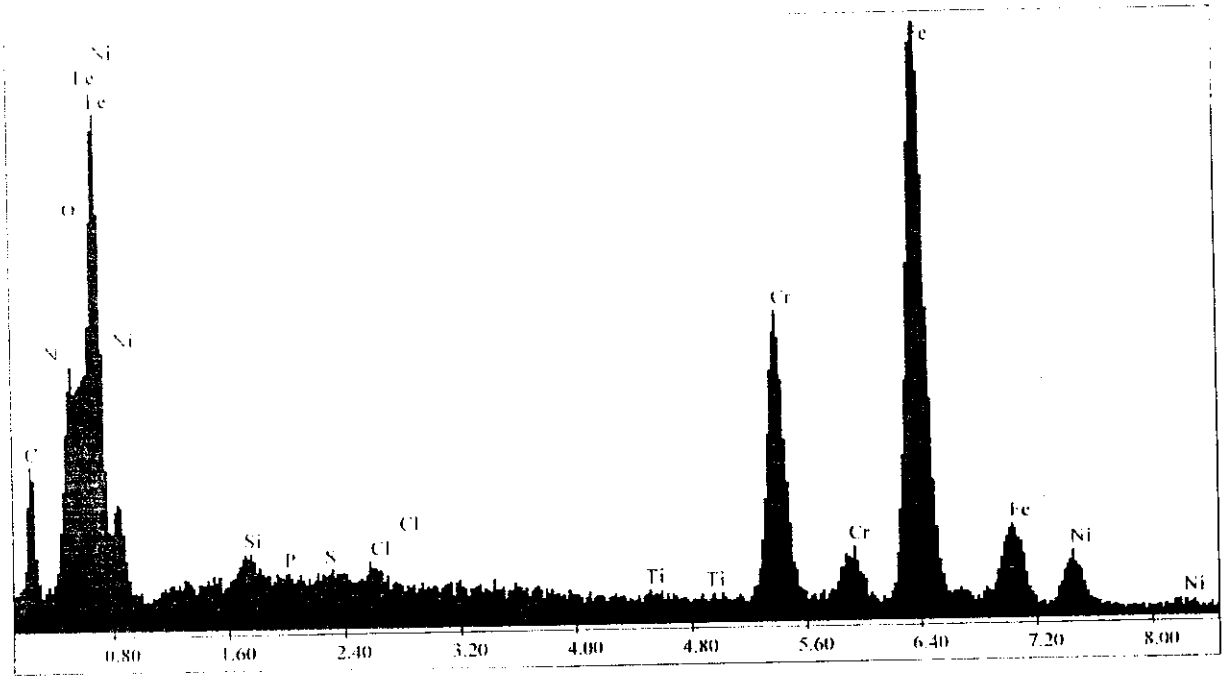

Fig. (3.108): XPS analysis of 304SS surface after immersion in 2M HCl for seven hours at 303K in presence of $5x10^{-7}$ M Kry-222.

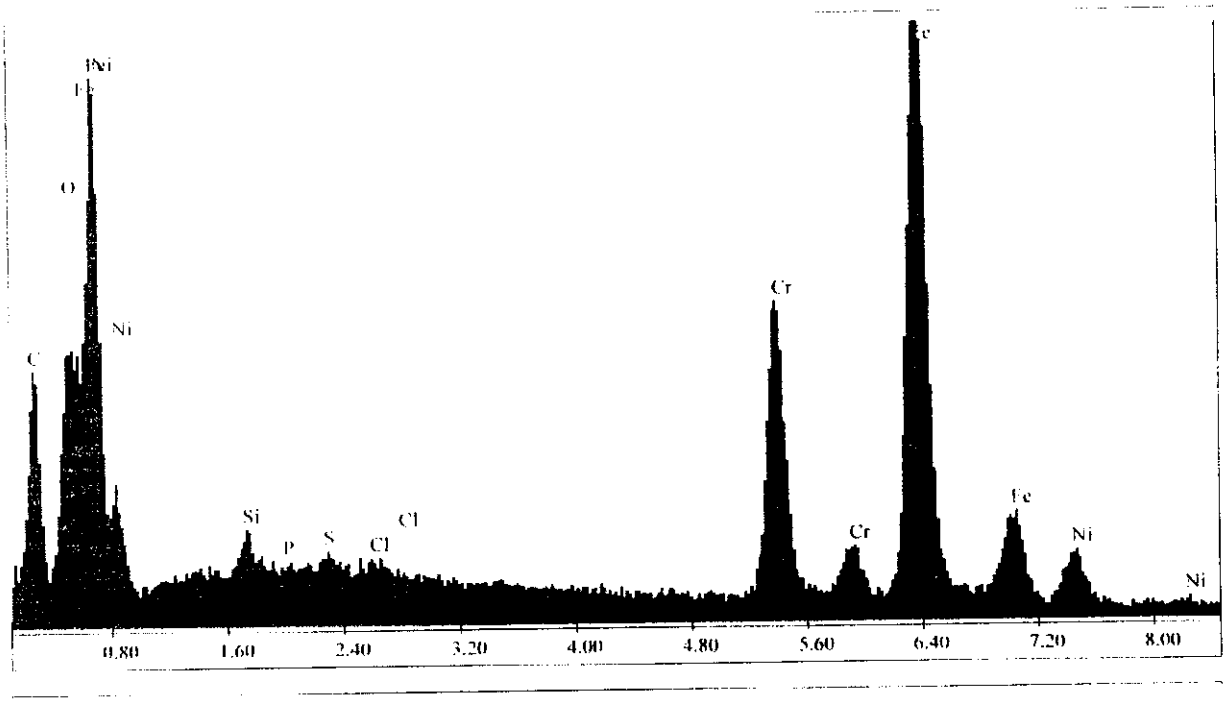

Fig. (3.109): XPS analysis of 304SS surface after immersion in HCl for seven hours at 303K in presence of $5x10^{-7}$ M DB24C8.

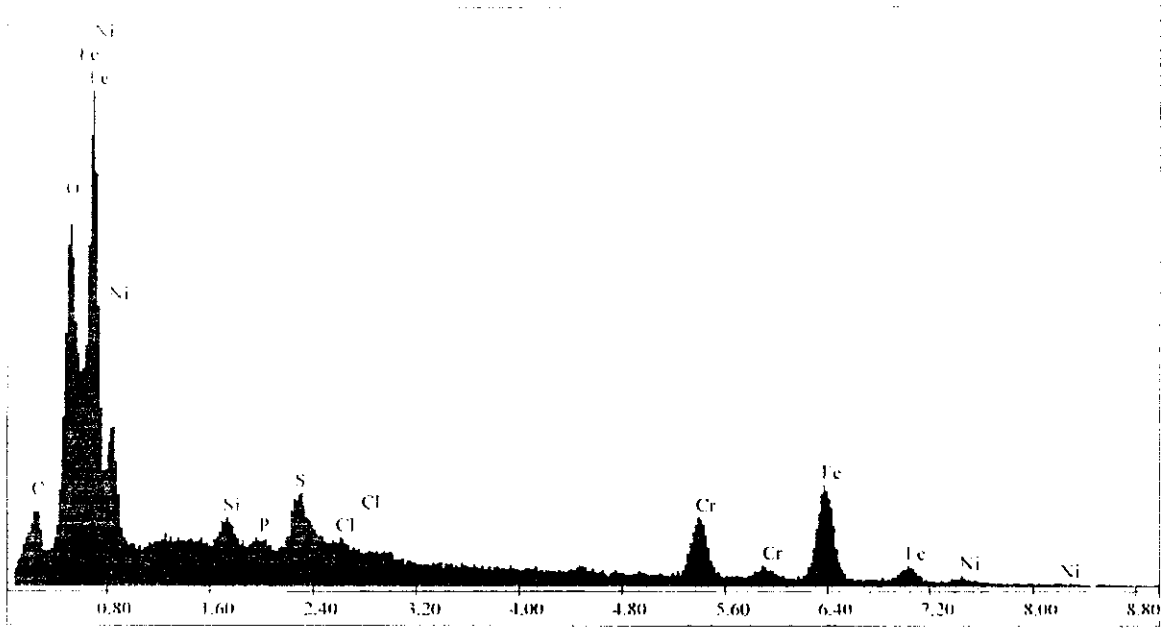

Fig. (3.110): XPS analysis of 316SS surface after immersion in 2M HCl for seven hours at 303K.

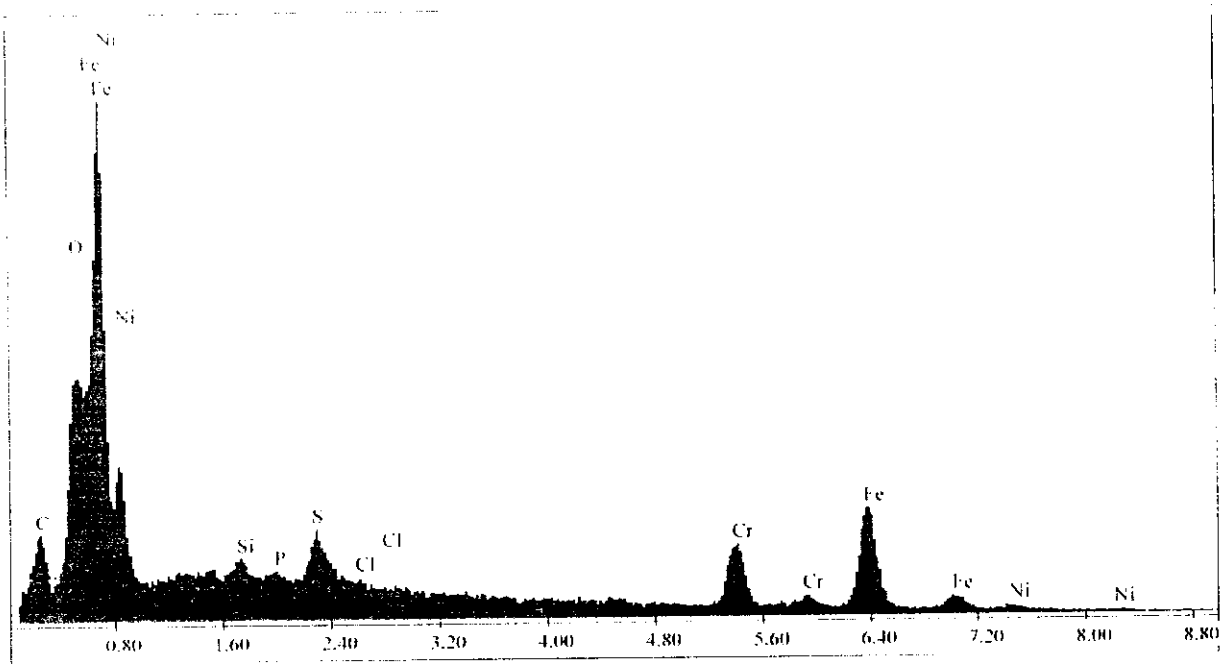

Fig. (3.111): XPS analysis of 316SS surface after immersion in 2M HCl for seven hours at 303K in presence of $5x10^{-7}$ M DB18C6.

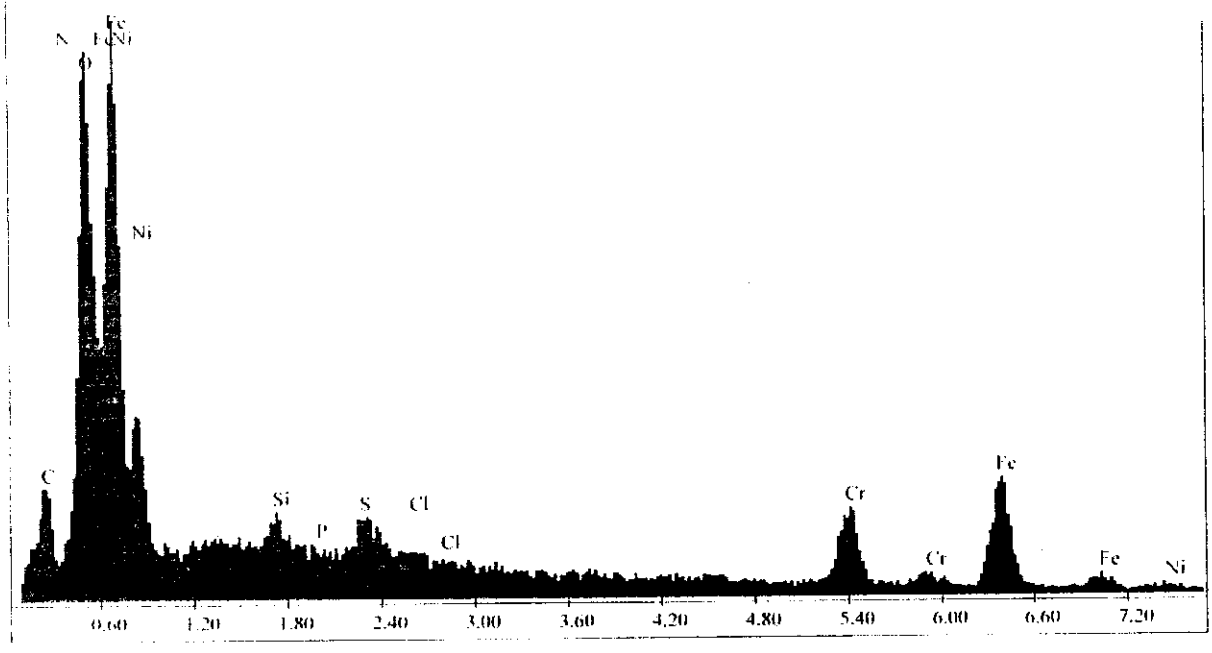

Fig. (3.112): XPS analysis of 316SS surface after immersion in 2M HCl for seven hours at 303K in presence of $5x10^{-7}$ M Kry- 22DD.

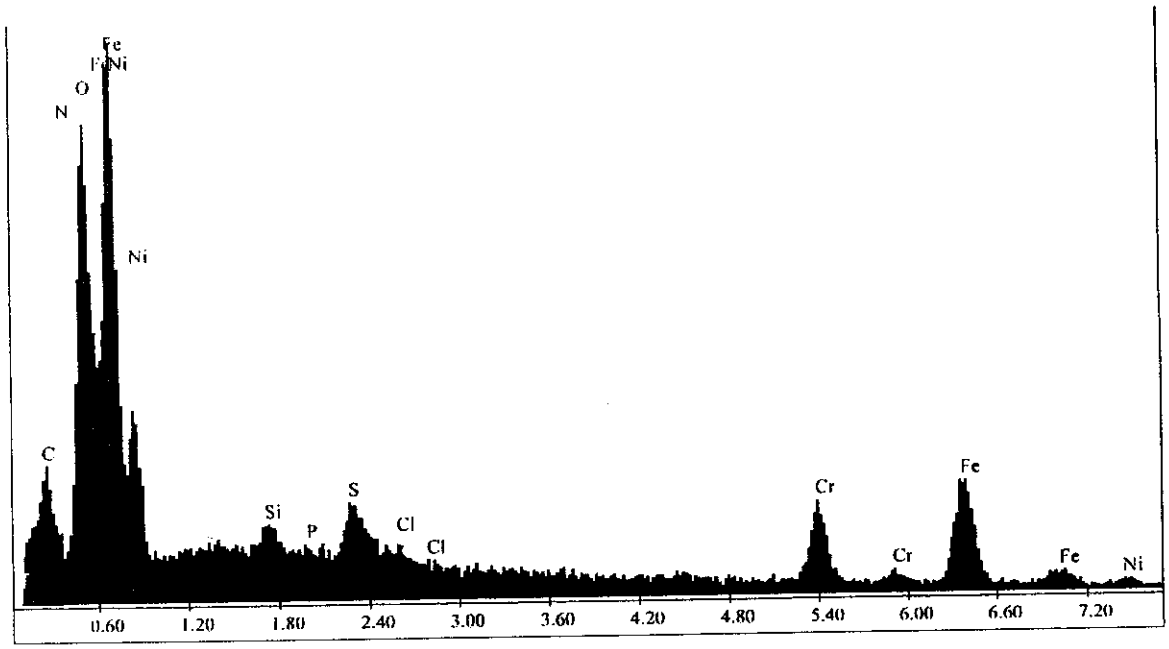

Fig. (3.113): XPS analysis of 316SS surface after immersion in 2M HCl for seven hours at 303K in presence of $5x10^{-7}$ M Kry-222.

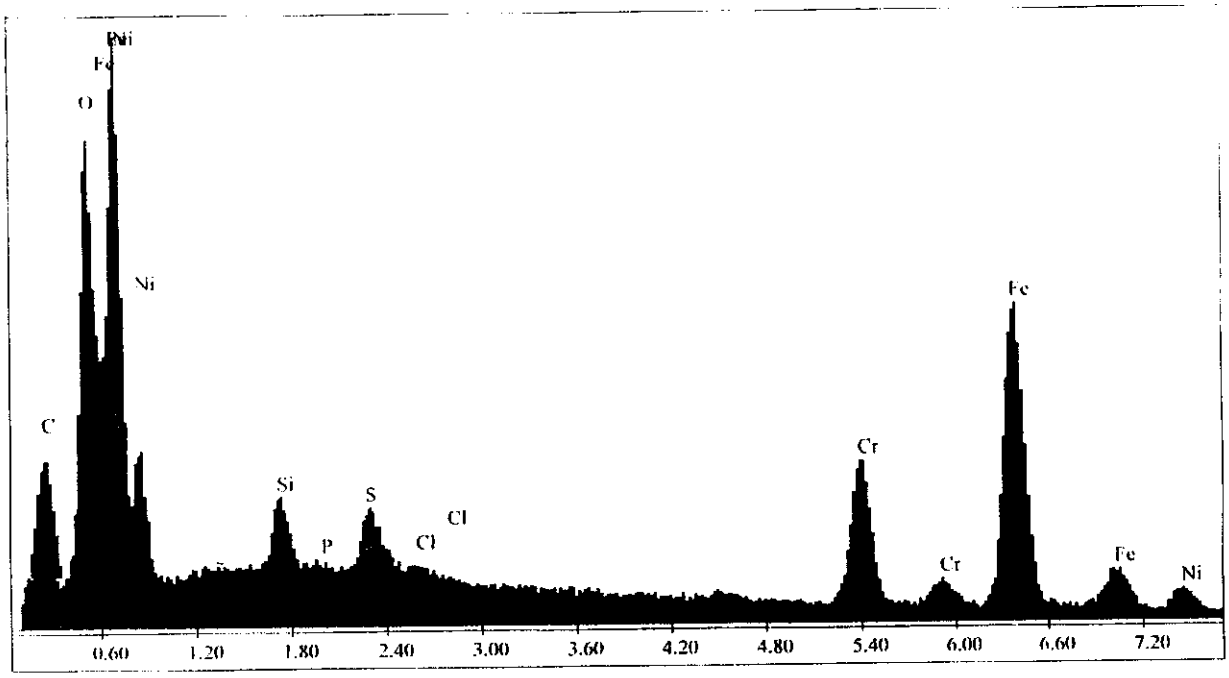

Fig. (3.114): XPS analysis of 316SS surface after immersion in HCl for seven hours at 303K in presence of $5x10^{-7}$ M DB24C8.

Table (3.20): variation of the weight percentage (wt. %) of carbon obtained from (XPS) for different types of stainless steels in absence and presence of crown ethers.

inhibitor	*430SS*		*304SS*		*316SS*	
	$5x10^{-7}$	$9x10^{-7}$	$5x10^{-7}$	$9x10^{-7}$	$5x10^{-7}$	$9x10^{-7}$
Blank	2.64	2.64	2.69	2.69	3.75	3.75
DB18C6	2.72	2.75	2.77	2.85	3.79	3.85
K-22DD	2.79	2.81	2.84	2.88	3.88	3.92
K-222	2.83	2.95	3.11	3.25	3.95	3.99
DB24C8	2.87	3.01	3.55	4.15	4.24	5.16

Table (3.21): variation of the weight percentage (wt. %) of chloride obtained from (XPS) for different types of stainless steels in absence and presence of crown ethers.

inhibitor	*316SS*		*304SS*		*316SS*	
	$5x10^{-7}$	$9x10^{-7}$	$5x10^{-7}$	$9x10^{-7}$	$5x10^{-7}$	$9x10^{-7}$
Blank	4.85	4.85	2.16	2.16	0.56	0.56
DB18C6	2.10	1.96	1.94	1.32	0.51	0.43
K-22DD	1.84	1.67	0.76	0.68	0.48	0.39
K-222	0.74	0.61	0.42	0.39	0.33	0.30
DB24C8	0.42	0.35	0.33	0.31	0.28	0.25

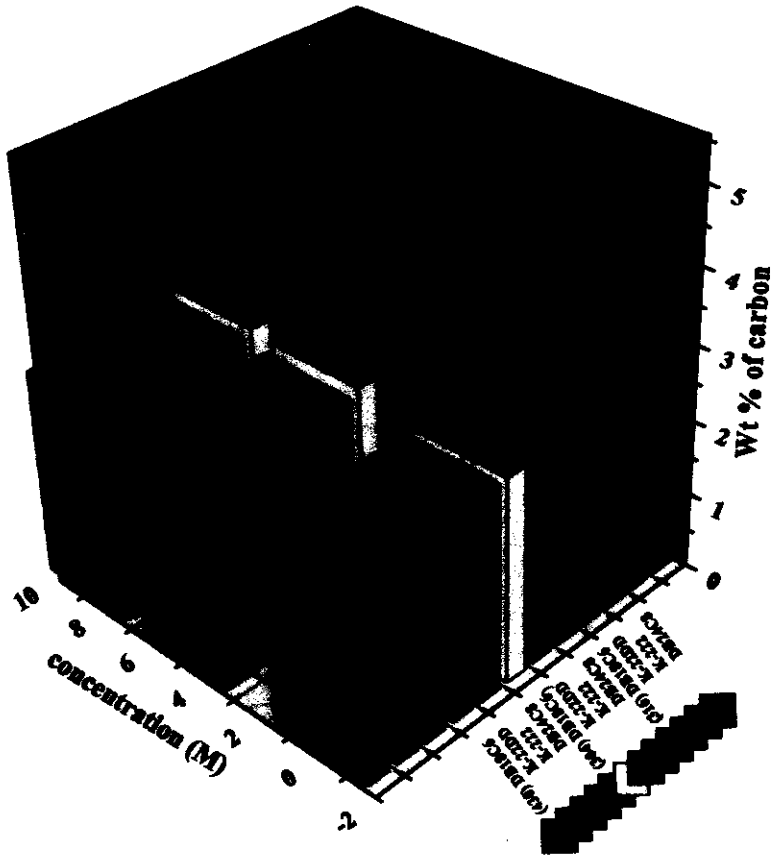

Fig. (3.115): Variation of carbon percentages (Wt %) on the surface of different types of stainless steels immersed in 2M HCl for seven hours in absence and presence of crown ethers.

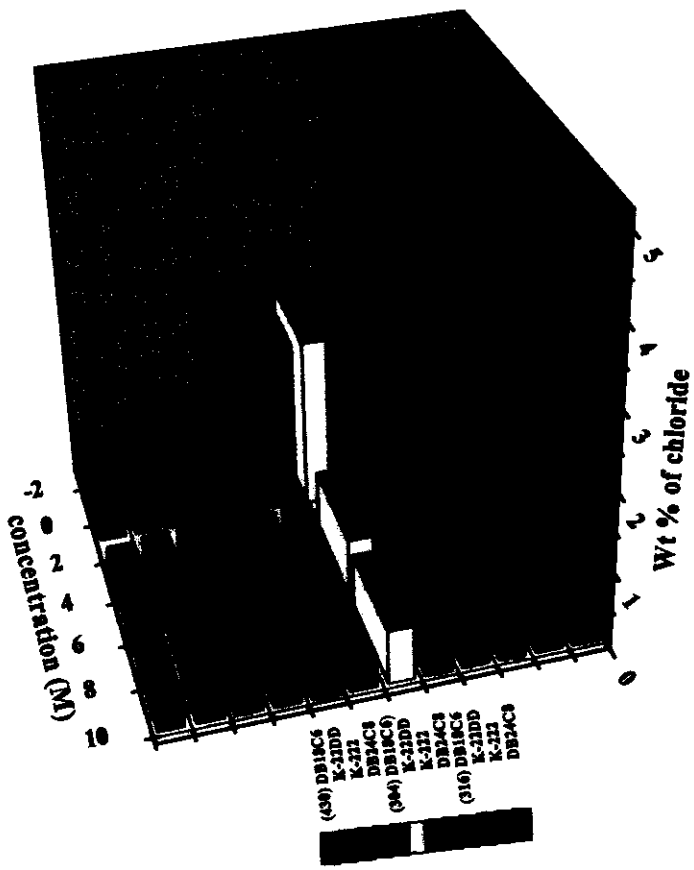

Fig. (3.116): Variation of chloride percentages (Wt %) on the surface of different types of stainless steels immersed in 2M HCl for seven hours in absence and presence of crown ethers.